

**HUMANOID ROBOT OMNIDIRECTIONAL WALKING TRAJECTORY
GENERATION AND CONTROL**

**by
METIN YILMAZ**

**Submitted to the Graduate School of Engineering and Natural Sciences
in partial fulfillment of
the requirements for the degree of
Master of Science**

**Sabanci University
August 2010**

**HUMANOID ROBOT OMNIDIRECTIONAL WALKING TRAJECTORY
GENERATION AND CONTROL**

APPROVED BY:

Assoc. Prof. Dr. Kemalettin ERBATUR
(Thesis Advisor)

.....

Prof. Dr. Asif ŞABANOVIĆ

.....

Assist. Prof. Dr. Ahmet ONAT

.....

Assist. Prof. Dr. Volkan PATOĞLU

.....

Assoc. Prof. Dr. İsmet İnönü KAYA

.....

DATE OF APPROVAL

.....

©Metin Yılmaz

2010

All Rights Reserved

HUMANOID ROBOT OMNIDIRECTIONAL WALKING TRAJECTORY GENERATION AND CONTROL

Metin YILMAZ

ME, MS Thesis, 2010

Thesis Supervisor: Assoc. Prof. Dr. Kemalettin ERBATUR

Keywords: Humanoid, Zero Moment Point, Omnidirectional Walking Trajectory.

ABSTRACT

Walking humanoid machines, once only seen or read in science fiction, became reality with the intensive research of the last four decades. However, there is a long way to go in the direction of technical achievements before humanoid robots can be used widely as human assistants. The design of a controller which can achieve a steady and stable walk is central in humanoid robotics. This control cannot be achieved if the reference trajectories are not generated suitably.

The Zero Moment Point (ZMP) is the most widely used stability criterion for trajectory generation. The Center of Mass (CoM) reference can be obtained from the ZMP reference in a number of ways. A natural ZMP reference trajectory and a Fourier series approximation based method for computing the CoM reference from it, was previously proposed and published for the Sabanci University Robotics ReseArch Laboratory Platform (SURALP), for a straight walk. This thesis improves these techniques by modifying the straight walk reference trajectory into an omnidirectional one.

The second contribution of this thesis is controller designs in order to cope with the changing slopes of the walking surface. The proposed controllers employ the trunk link rotational motion to adapt to the ground surface. A virtual pelvis link is introduced for the robots which do not possess roll and pitch axis in pelvis link.

The proposed reference generation and control algorithms are tested on the humanoid robot SURALP. The experiments indicate that these methods are successful under various floor conditions.

İNSANSI ROBOTLAR İÇİN ÇOK YÖNLÜ YÜRÜME REFERANS YÖRÜNGESİ SENTEZİ VE KONTROLÜ

Metin YILMAZ

ME, Yüksek Lisans Tezi, 2010

Tez Danışmanı: Doç. Dr. Kemalettin ERBATUR

Anahtar Kelimeler: İnsansı Robot, Sıfır Moment Noktası, Çok Yönlü Yürüme Yörüngesi

ÖZET

Bir zamanlar yalnızca bilimkurgu içerisinde görülen yürüyen insansı robotlar, son kırk yıllık araştırmalar sonucunda bir gerçeklik haline gelmişlerdir. Ancak insansı robotların, insanlara yardımcı konuma gelebilmeleri için katedilmesi gereken birçok teknik gelişime hala ihtiyaç duyulmaktadır. Sabit ve kararlı bir yürüyüşün gerçekleştirilebilmesi için tasarlanan bir kontrolör bu anlamda büyük öneme sahiptir. Bu kontrolör, referans yörünge sentezi uygun olarak geliştirilmeden elde edilemez.

Sıfır Moment Noktası (SMN) kriteri, yörünge sentezi için en yaygın olarak kullanılan kararlılık ölçütüdür. Robot Ağırlık Merkezi (RAM) için pozisyon referansları, SMN referansından birden fazla yolla elde edilebilmektedir. Doğal bir SMN referans yörüngesi ve bu referanstan RAM referansının bulunması için kullanılan Fourier serisi yakınsaması temeline dayanan bir metod daha önce önerilmiş ve Sabancı Üniversitesi Robot Araştırmaları Laboratuvar Platformu (SURALP) üzerinde düz bir yürüyüş için yayımlanmıştır. Bu tez, bahsi geçen teknikleri, düz yürüyüş referans yörüngesinden çok yönlü bir yürüyüş referans yörüngesine dönüştürerek geliştirmektedir.

Tezin ikinci katkısı eğimi değişen yürüme yüzeylerinde denge sağlayabilmek amacıyla tasarlanmış kontrolörlerdir. Önerilen kontrolörler üst gövdenin dönüş hareketini kullanarak insansı robotun eğimli yüzeylere uyum sağlamasına yardımcı olmaktadır. Gövdesini bel ekleminden bağımsız olarak hareket ettirebilen bir yunuslama ve yuvarlanma eksenine sahip olmayan robotlar için, sanal bel eklemi tanıtılmıştır.

Önerilen referans sentezi ve kontrol algoritmaları insansı robot SURALP üzerinde test edilmiştir. Deney sonuçları, bu yöntemlerin farklı zemin koşulları altında başarılı olduğunu göstermiştir.

To my family

ACKNOWLEDGEMENTS

First of all, I would like to express my deepest gratitude for my thesis advisor Assoc. Prof. Kemalettin Erbatur. Without his valuable guidance and support, this thesis would not have been possible. Throughout my Master of Science education, he always shed light for my journey with his encouragements, inspirations and teachings. I could not size up the value of his great efforts and company no matter how much I try.

I would like to express my regards and appreciation to my thesis jury members Prof. Dr. Asif Sabanovic, Assist. Prof. Ahmet Onat, Assist. Prof. Volkan Patođlu and Assoc. Prof. İsmet İnönü Kaya for providing their valuable ideas and support for my thesis.

My student colleagues Utku Seven, Evrim Taşkıran and Özer Koca deserve particular thanks for being the best of the best project partners. Without their friendship and support I could not even imagine the realization of this thesis.

Special thanks for my old fellow Osman Koç for being my companion in misfortune and supporting me all times. It is hard to find truly great friends and they are never-to-be-forgotten.

I would like to thank; Kaan Öner, İyad Hashlamon, Hakan Ertaş, Melda Şener, Aykut Cihan Satıcı, Ozan Tokatlı, Cevdet Hançer, Merve Acer, Emrah Deniz Kunt, Teoman Naskalı, Zeynep Temel, Efe Sırımođlu, Serhat Dikyar, Mireia Perez Plius, Tuđba Lelebici, Duruhan Özçelik, Yusuf Sipahi, Sena Ergüllü, Alper Ergin, Çađrı Gürbüz, Can Palaz, Kadir Haspalamutgil and many friends from mechatronics laboratory. I should separately express that I am especially grateful for friendship and support of Ahmetcan Erdoğan who helped me a lot along these two years.

Most importantly, I want to thank my parents, Hüseyin Fikri Yılmaz and Ayşe Selmin Yılmaz, my sister Zeynep Türksoy and her husband Aslan Mert Türksoy, for their invaluable love, caring and support for me along my life. This thesis is dedicated to my beloved family.

TABLE OF CONTENTS

ABSTRACT.....	iv
TABLE OF CONTENTS.....	vii
LIST OF TABLES.....	viii
LIST OF FIGURES.....	ix
1. INTRODUCTION	1
2. LITERATURE SURVEY	4
2.1. Humanoid Robot Terminology	4
2.2. Examples of Humanoid Robots	9
2.3. Reference Generation and Control for the Humanoid Robots	16
3. SURALP: A FULL BODY BIPEDAL HUMANOID ROBOT	25
4. OMNIDIRECTIONAL WALKING REFERENCE TRAJECTORY GENERATION	32
4.1 ZMP Based Walking Reference Generation for a Straight Walk	32
4.2 Central Reference Path (CRP)	41
4.3 Mapping a Linear CRP Walk onto a Circular Arc Shaped CRP Walk	56
5. WALKING CONTROL ON INCLINED PLANES WITH FUZZY PARAMETER ADAPTATION	67
5.1. Straight Walking Control Methods of SURALP	67
5.2. Fuzzy Adaptive Control Methods	69
5.2.1. Fuzzy Adaptive Pitch Tilt Control	70
5.2.2. Fuzzy Adaptive Roll Tilt Control	78
6. EXPERIMENTAL RESULTS	82
7. CONCLUSION	90
REFERENCES	92

LIST OF TABLES

Table 3.1	Denavit Hartenberg table with respect to Figure 3.4	28
Table 3.2	Length and weight parameters	28
Table 3.3	Joint actuation system	29
Table 3.4	Sensors of SURALP	30
Table 5.1	The Fuzzy Rule Base	74
Table 5.2	The Fuzzy Rule Base Roll	80
Table 6.1	Reference Generation Parameters 1	82
Table 6.2	Reference Generation Parameters 2	83
Table 6.3	Rule Strengths and Membership Function Corner Locations Fuzzy Pitch Tilt	87
Table 6.4	Rule Strengths and Membership Function Corner Locations Fuzzy Roll Tilt	88

LIST OF FIGURES

Figure 2.1:	Reference body planes	4
Figure 2.2:	A complete walking cycle	5
Figure 2.3:	An example omnidirectional footstep pattern	6
Figure 2.4:	Step size and swing offset	6
Figure 2.5:	Supporting Polygon	7
Figure 2.6:	CoM and its ground projection	7
Figure 2.7:	Static walking gait and CoM trajectory	8
Figure 2.8:	Waseda University: WL-1, WL-3, WABOT-1 and WL-10RD	9
Figure 2.9:	WABIAN-RII (left) and WABIAN-RIV (right)	10
Figure 2.10:	HONDA humanoid robots family evolution; E0-6 to P1-2	11
Figure 2.11:	P3 and ASIMO of HONDA	11
Figure 2.12:	H5 (left), H6 (center) and H7 (right) of University of Tokyo	12
Figure 2.13:	KHR-1, KHR-2 and KHR-3 (HUBO) of KAIST	13
Figure 2.14:	HRP 2 (left) and HRP-3P (right)	14
Figure 2.15:	The female humanoid robot HRP-4C	14
Figure 2.16:	Aldebaran NAO	15
Figure 2.17:	Soccer playing NAO Robots	15
Figure 2.18:	3D inverted pendulum model	17
Figure 2.19:	A complete walking cycle	18
Figure 2.20:	Online pattern generation architecture	18
Figure 2.21:	A table-cart model	19
Figure 2.22:	A complete walking cycle defined with several stages	21
Figure 2.23:	The architecture of layered omnidirectional walking controller	22
Figure 3.1:	SURALP, side and front views	25

Figure 3.2:	SURALP, dimensions	26
Figure 3.3:	The kinematic arrangement of SURALP	27
Figure 3.4:	Denavit Hartenberg axis assignment for a 6-DOF Leg	27
Figure 3.5:	The bottom view of the final sole design	29
Figure 3.6:	Overall hardware setup of the humanoid robot: SURALP	31
Figure 4.1	The linear inverted pendulum model	33
Figure 4.2	Fixed ZMP references	35
Figure 4.3	Forward moving ZMP reference	35
Figure 4.4	ZMP references with pre-assigned double support phases	35
Figure 4.5	x and y-direction CoM and ZMP references	39
Figure 4.6	x and z-direction foot references as expressed in the world frame.	40
Figure 4.7	Assignment of the body coordinate frame	42
Figure 4.8	The foot pseudo centers	43
Figure 4.9	Ankle frame origins on the on the foot sole	44
Figure 4.10	Foot sole Denavit-Hartenberg frames	45
Figure 4.11	Distance and direction conditions on a central reference path	47
Figure 4.12	Central Reference Path A	49
Figure 4.13	Right foot placement with respect to Central Reference Path A	49
Figure 4.14	Central Reference Path B	50
Figure 4.15	Close up view for CRP A and CRP B	50
Figure 4.16	Normal of foot pseudo center	51
Figure 4.17	Intersection of foot pseudo center normal with CRP A	51
Figure 4.18	Starting point of CRP A	52
Figure 4.19	Distance s travelled on CRP A	52
Figure 4.20	Starting point of CRP B	53
Figure 4.21	Distance s travelled on CRP B	53
Figure 4.22	Marking the end point of the travelled distance on CRP B	54

Figure 4.23	Calculating the normal of CRP B at the end point of s	54
Figure 4.24	σ offset measured on the normal	55
Figure 4.25	Placement of the foot with respect to CRP B	55
Figure 4.26	A central reference path	56
Figure 4.27	The alignment of the world, body right foot pseudo center and left foot pseudo center frames in the initial robot configuration.	57
Figure 4.28	Mapping of foot placement locations of a linear CRP walk onto the foot placement locations of a circular arc shaped CRP walk.	60
Figure 4.29	Geometry of the computation of the body frame origin position on the arc walk.	63
Figure 4.30	Geometry of the computation of the right foot pseudo center position on the arc walk.	64
Figure 4.31	Geometry of the computation of the left foot pseudo center position on the arc walk.	65
Figure 4.32	SURALP CAD model on a circular arc shaped CRP walking trajectory	66
Figure 5.1	Bipedal robot walk on changing slopes	70
Figure 5.2	Legs, pelvis and the upper body	72
Figure 5.3	The membership functions	75
Figure 5.4	Upright upper body posture.	76
Figure 5.5	Legs, pelvis and the upper body in roll axis	79
Figure 5.6	Upright upper body posture leaned right.	81
Figure 6.1	Body Roll and Body Pitch Angles	83
Figure 6.2	Body Roll and Body Pitch Angles for another experiment	84
Figure 6.3	$\bar{\beta}_{pitch}$, Γ_{pitch} , θ_{pitch} and virtual pelvis pitch angle	85
Figure 6.4	$\bar{\beta}_{roll}$, Γ_{roll} , θ_{roll} and virtual pelvis roll angle	86
Figure 6.5	Snapshot taken during an omnidirectional walk	89

Chapter 1

1. INTRODUCTION

The field of humanoid robotics witnessed significant developments in the recent twenty years. The researchers are motivated by the fact that the bipedal structure is suitable for a robot functioning in the human environment. It is expected that humanoid robots can assume human assistive roles. The structure of the humanoid robots allows them to be easily accepted by humans; therefore, enables the realization of the coexistence of bipedal robots and humans in the future. The bipedal kinematic structure helps the humanoid robots to avoid typical obstacles in the human environment. The humanoid robots may provide support to humans, in areas such as elderly care, hospital attendance and many others. These are important motivations for the research concentrated on humanoid robotics.

However, there are numerous technical problems which should be analyzed and solved before the integration of bipedal robots into the human daily environment. The robust balance of the walk is one of the most difficult problems in this field. Due to the many degrees of freedom to be controlled under coupling effects and the non-linear dynamics, control of walking on two legs is a challenging task. The bipedal free-fall manipulator poses a hard stabilization problem. In humanoid robotics research area, balance control techniques are taken into account in conjunction with gait planning. Therefore a stable walking reference trajectory generation is required.

For the legged locomotion, the Zero Moment Point (ZMP) criterion is the most widely accepted and used stability measure. The criterion states that, during the walk, the ZMP should lie within the supporting area - often called the support polygon - of the feet in contact with the ground. The Linear Inverted Pendulum Model (LIPM) is a simple model approximating the bipedal robot dynamics. When the ZMP criterion is applied on the LIPM, a very useful relation between the ZMP reference of the robot and

the robot center of mass (CoM) is obtained. This relation can be used to compute CoM references from predefined stable ZMP references. Once the CoM references are obtained, the joint position references can be computed via inverse kinematics. A number of approaches can be used for the CoM computation from ZMP [1-3]. [4] develops a straight walk ZMP reference and applies the Fourier series approximation technique in [2,3] to compute the reference CoM trajectory. [5] presents experimental results with this reference generation technique on the humanoid robot SURALP (Sabanci University Robotics ReseArch Laboratory Platform).

Although stable reference generation studies for straight walk are very important and motivating, a walking reference generation system will be of limited use if only straight walk is achievable. Generating only straight walking reference is not sufficient for a humanoid robot to adapt into the daily living environment. Omnidirectional walk, however, enhances the obstacle avoidance properties of the bipedal humanoid robot. Humans use their supreme omni-directional walking capabilities for locomotion. By this way, they can avoid obstacles, travel for the shortest paths and perform tasks which require agility. The ability of walking towards any direction desired is a necessity for humanoid robots to fully adapt into human living space.

As its most important contribution, this thesis improves the straight walking reference trajectory in [4,5] into an omnidirectional one, and implements this newly proposed omnidirectional trajectory on SURALP. Principally a projection of the straight walking trajectory on an arc with desired radius is carried out.

One of the most significant problems in the field of humanoid robotics is the balance of the walk not only on even floor but also on surfaces with irregularities and slopes. The changing slopes of the walking surface cause important disturbance effects on the bipedal walker. An inclined plane presents a very typical floor condition encountered in human daily life. Though such planes are mostly part of the city and outdoor environments, since the indoor floors are not perfectly even, the inclined planes can also be found at our homes and offices. In addition to achieving omni-directional walking, the second contribution of this thesis is the design of fuzzy logic parameter adaptation systems for omni-directional walking control on inclined planes.

For the fuzzy logic adaptation system, the mechanical structure of the robot body is assumed to be composed of two rigid bodies. One of them, the lower one is termed in this thesis as the pelvis link. The second one is the upper body (trunk) positioned above the pelvis link. The angle of the upper body with respect to the pelvis link is called

“body pitch angle” and the angle of the pelvis link with respect to a vertical line is called the “pelvis pitch angle”. A measure of the oscillatory behavior of the pelvis pitch motion is introduced. This measure and the average pelvis pitch angle are used as the input of a fuzzy logic system which computes the body pitch angle parameter online, to be applied as a reference position to the robot controller. The rule base is constructed in such a way that it compensates the disturbance effects of changing slopes by shifting the upper body weight forward and backward. The thesis also proposes an inverse kinematics solution for generating the effect of the upper body pitch motion for robots which do not have a pitch joint between the pelvis and upper body, but possess spherical hip joints. We call this approach the “method of the virtual pelvis”.

A similar controller is also applied about the body roll axis to modify upper body orientation references.

In order to test their performance, the proposed walking reference generation and the fuzzy logic parameter adaptation systems are applied on SURALP. Experimental results indicate that the fuzzy logic adaptation system is successful in obtaining a stable walk in the transition from a horizontal plane onto an inclined one with a slope of 5.6 degrees (10 percent). Together with the introduced fuzzy logic control techniques, a stable omni-directional walk is also achieved.

The thesis is organized as follows. The next chapter briefs the humanoid robotics terminology, history of the humanoid robots in the world and presents a survey on reference generation methods and control of biped walking robots. Chapter 3 describes the experimental humanoid robot SURALP on which the designed reference generation algorithms and fuzzy logic control methods are tested. The omni-directional reference trajectory generation method used in this thesis is introduced in Chapter 4. Chapter 5 reviews the flat floor balance control algorithms applied during the biped walking and describes the fuzzy logic parameter adaptation system for walking control on inclined planes. Experimental omni-directional walking results and performances of the employed control algorithms on inclined planes are presented in Chapter 6. Finally, the conclusions and future works are presented in Chapter 7.

Chapter 2

2. LITERATURE SURVEY

2.1. Humanoid Robot Terminology

Humanoid robotics research area appeals many scientists around the world. The fundamentals of bipedal locomotion must be understood in order to gain a perspective on humanoid robotics. First of all, defining the reference planes used in this field is required. In Figure 2.1 three primary reference planes, which facilitate the analysis of basic human movements, are presented. In this thesis, these three reference planes are used to define humanoid motions.

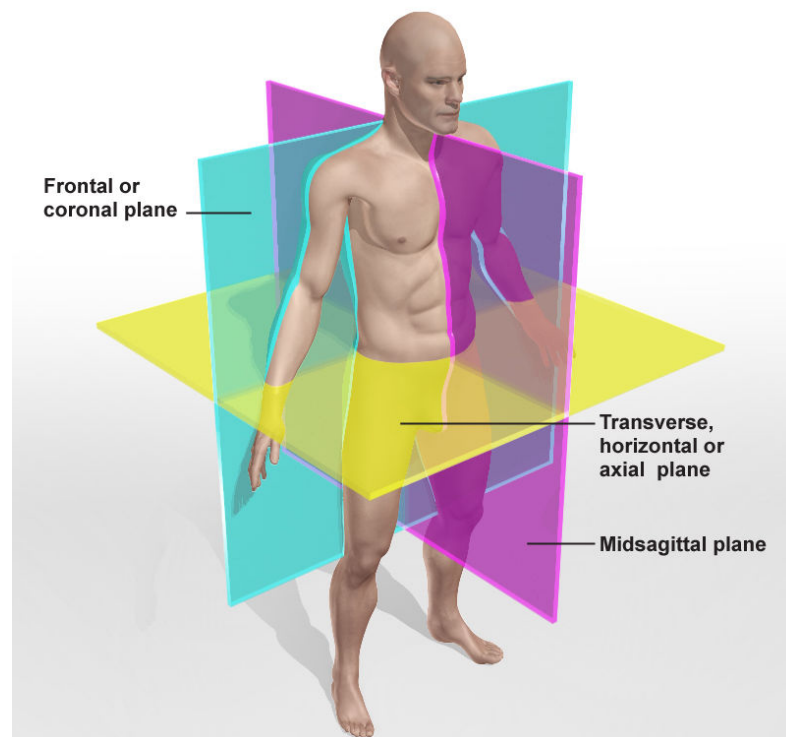


Figure 2.1: Reference body planes [6]

The direction of the straight walking is on the sagittal plane. This sagittal plane cuts the body vertically, into left and right portions. In a number of works, the straight walking reference is achieved by only considering the motions in the sagittal plane [7-10]. Frontal and axial planes are also used in this thesis for the design of robot trunk orientation controllers.

The pattern of steps of a bipedal robot is defined by the term “gait” and periodic motion of this pattern is called “gait cycle”. The gait cycle can be divided into two phases [13], namely “support (stance)” and “swing” phases. Swing phase implies the duration when only one of the legs is in contact with the ground and the other one is moving freely in the air, taking a step. Simultaneously, while this swing phase occurs, the standing leg which is touching the ground is in its support phase. The support phase can also be divided into two subcategories. One is termed “single support phase”, when only one leg is supporting the whole robot body weight. The other one is named “double support phase” implying that both legs are touching the ground and the robot body weight is supported by these two legs at the same time.

To generate stable walking reference trajectories these phases should be clearly identified. To clearly depict the relation between the gait cycle and these phases Figure 2.2 presents a complete walking cycle with several stages.

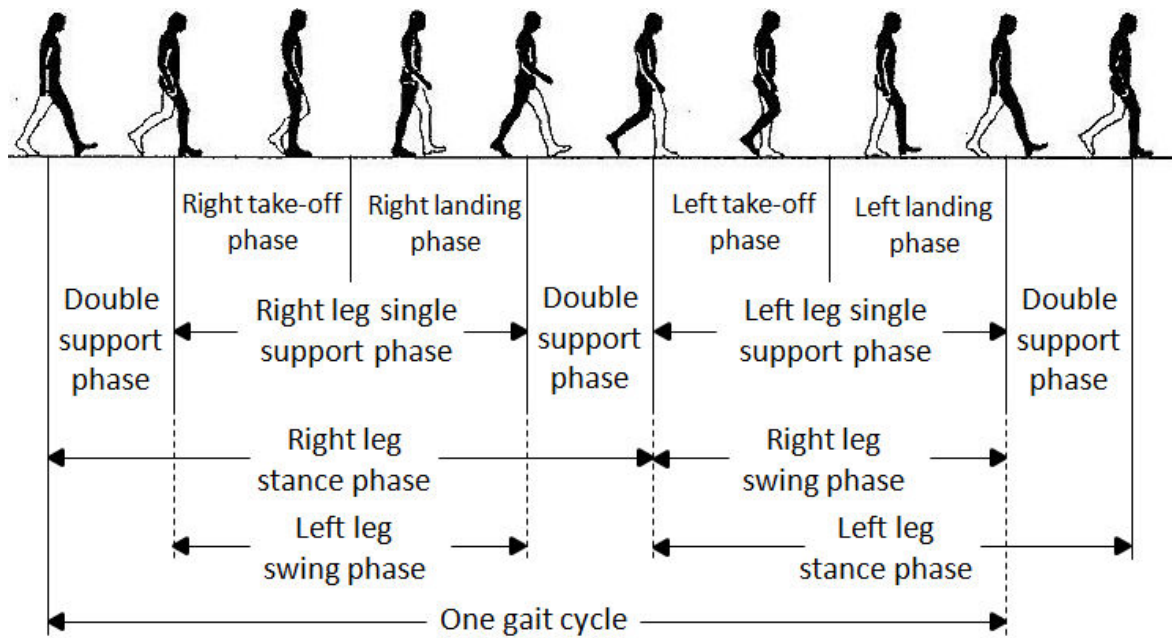


Figure 2.2: A complete walking cycle [11]

The term omnidirectional gait is used to depict a walking pattern which can be directed into any direction. On the other hand, unidirectional gait means that the walking pattern is only able to follow a straight line where the robot is facing. Example of an omnidirectional walking pattern and the corresponding foot placements are shown in Figure 2.3.

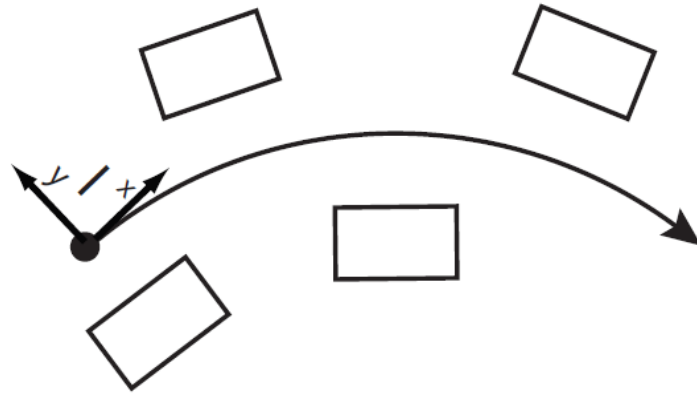


Figure 2.3: An example omnidirectional footstep pattern [43]

Swing foot covers an additional distance during the single support phase relative to the supporting foot. “Step size” is the length of this covered distance. The total distance travelled by the swing foot is called “stride length”. “Swing offset” is the distance between the ankle centers of the feet as shown in Figure 2.4.

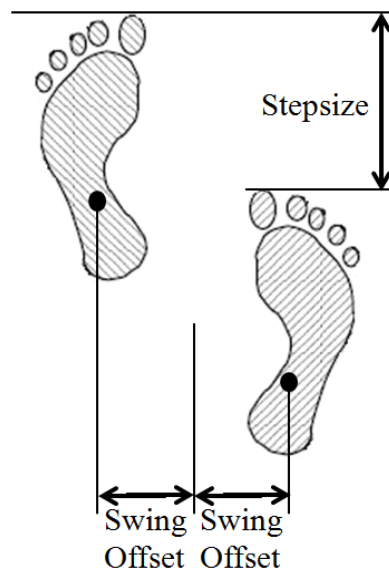


Figure 2.4: Step size and swing offset

Another important term directly related to the stability of the gait cycle is support polygon. In Figure 2.5 the support polygon is shown. It is defined as the area that is enveloped by the supporting foot or feet.

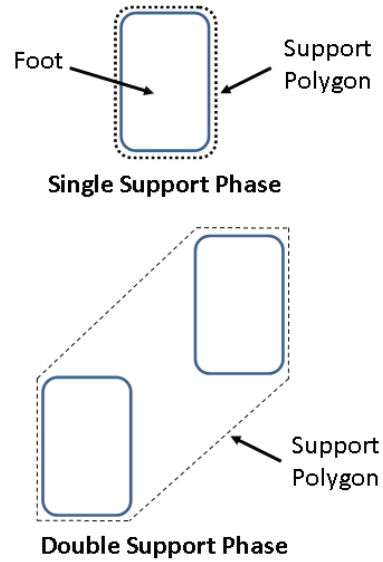


Figure 2.5: Supporting Polygon

Position of the ground projection of Center of Mass (CoM) of a humanoid robot, as shown in Figure 2.6, is closely related with a stable walking reference generation. If the CoM stays in the support polygon during the whole cycle of gait, this is called a static gait. This kind of walking reference is stable but slow.

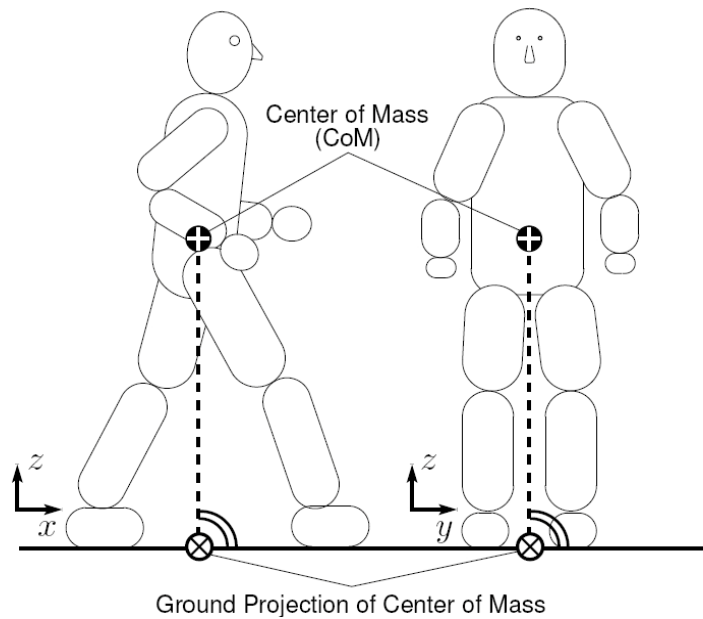


Figure 2.6: CoM and its ground projection [12]

However, the CoM does not have to be restricted into the support polygon during the whole gait. In this way, using the stability provided by the inertial effects, dynamic gait stability is achieved. Realization of dynamic gait stability is more difficult than static gait stability. Nonetheless, a faster gait can be achieved by the adjustment of walking speed in terms of regulating single and double support phase timings. An example of static walking gait and the corresponding CoM trajectory are shown in Figure 2.7.

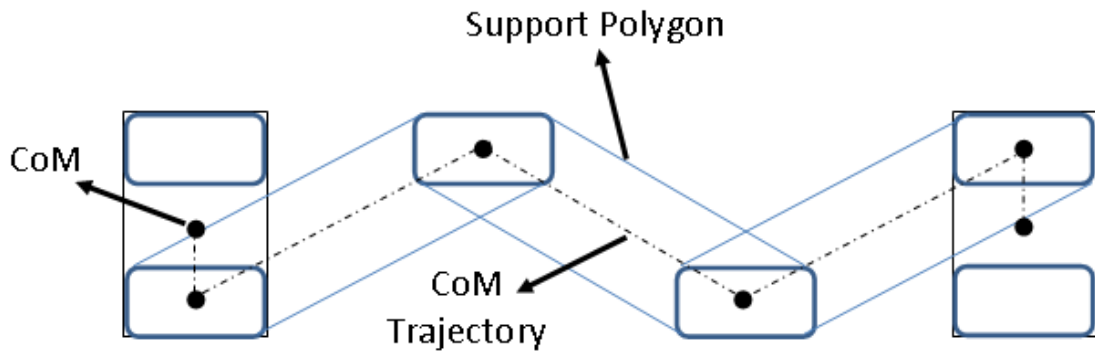


Figure 2.7: Static walking gait and CoM trajectory

The term ZMP was introduced by Vukobratovic [13], as a point on the ground where the sum of all moments of active forces with respect to this point is zero. In the stability analysis of the bipedal robots the ZMP criterion is used frequently. If the ZMP lies in the support polygon of a humanoid robot during gait, this generated walking reference is considered to be stable [1].

2.2. Examples of Humanoid Robots

Even though the interest of humans into the field of bipedal locomotion and biped walking robots was pronounced much earlier, the realization and development of the first humanoid robots corresponds to the late 1960's. During this period, robotic researchers in Japan started investigating human locomotion and finished the design of a biped walker which emerged as a standalone leg module in Waseda University [14]. After this achievement, bipedal locomotion studies gained pace and the studies of walking trajectory generation are followed with a number of different biped walker designs. In Figure 2.8, the first examples of these humanoid robots from Waseda University are shown.

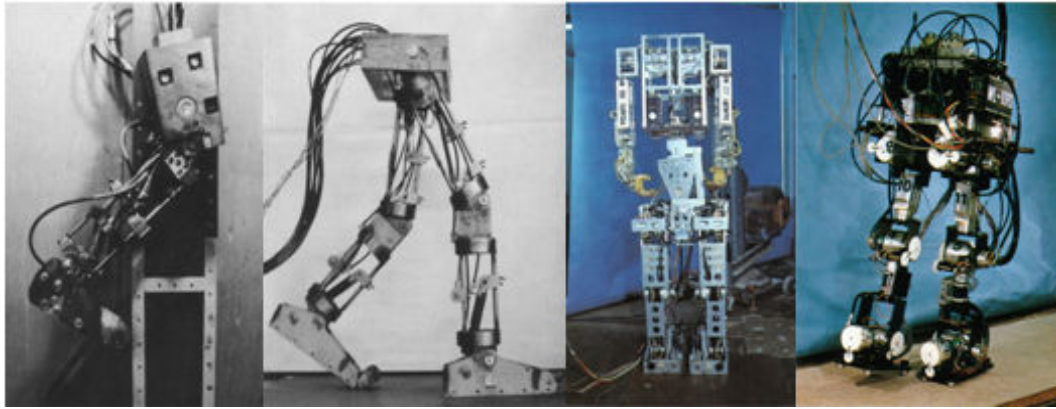


Figure 2.8: Humanoid designs of Waseda University: WL-1, WL-3, WABOT-1 and WL-10RD (from left to right)

The construction of the world's first full scale humanoid robot was accomplished in the year 1973. The humanoid robot WABOT-1 was capable of using a static walking gait and changing the direction of its walk. Using external receptors, it was able to communicate in Japanese and interact with the environment. In 1984 the first dynamic walking gait is achieved by Takanishi *et al* with the WL-10RD prototype. This prototype uses torque feedback from the torque sensors attached to the ankles [15]. During this period in United States, Marc Raibert established the MIT Leg Lab, which was dedicated to research for bipedal locomotion and building robots which employs dynamic stability [16].

Creating a humanoid robot in human proportions and size was the next goal of humanoid robotics researchers in Waseda University. WABIAN humanoid robot, which was using electric motors and consisting of 35 degrees of freedom (D.O.F), was built in

1995. Interaction with the human environment was also another purpose of this project. Waseda University had become well established in humanoid robotics field with consecutive projects. In 1999 WABIAN-RII was introduced. It had the ability to mimic human motions by the parameterization of body motions [17]. In 2004, equipped with vision and voice recognition systems, the prototype WABIAN-RIV was presented. It was also able to mimic human motions with its 43 D.O.F., 1.89 m height and 127 kg weight Figure 2.9 shows WABIAN-RII and WABIAN-RIV of Waseda University.

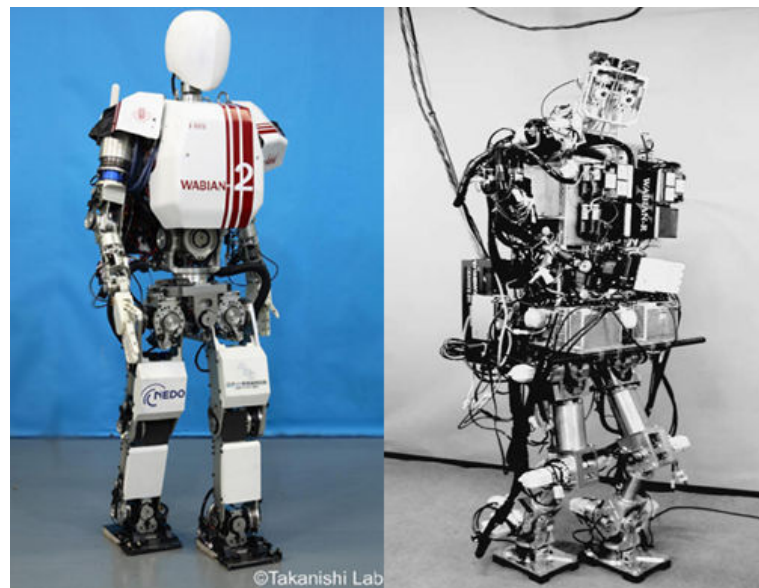


Figure 2.9: WABIAN-RII (left) and WABIAN-RIV (right)

HONDA has been conducting leading research projects in humanoid robotics field since 1986. HONDA's humanoid robot family gained significant interest all around the world. Their humanoid robots still attract attention and considered as the most advanced humanoids of the bipedal robot field. Figure 2.10 presents the evolution of the HONDA humanoid robot family with the initial prototypes E0-6, P1 and P2 [18]. They developed their first human-like model P1 and the next prototype P2 was introduced to the public in 1996. P2 was the first humanoid walking robot which was self-regulated with wireless techniques. It was walking independent of wires, climbing stairs and performing manipulation tasks. This development opened the way for solving the weight and size problems standing before the realization of reliability of humanoid robots of HONDA. With P3 prototype, they reduced the height of the robot from 1.8 meters to 1.6 meters. The weight of the robot is also reduced from 210 kilograms to 130 kilograms. Figure 2.11 shows P3 humanoid robot which enabled the development of a much more advanced humanoid robot generation in HONDA history.

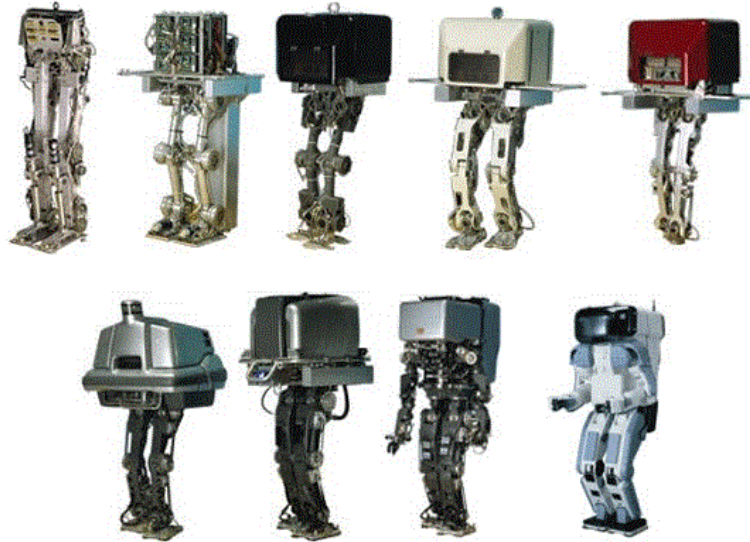


Figure 2.10: HONDA humanoid robots family evolution; E0-6 to P1-2

This latest generation humanoid robot was named ASIMO (Advanced Step in Innovative Mobility). It was introduced in year 2000 and gathered the public attention very quickly. With its more human-friendly and teenage size look, ASIMO became the most popular humanoid robot with smoother human-like motion capabilities. ASIMO is 1.2 meters tall and it weighs 43 kilograms. It is the first humanoid robot which shows harmony with the human living environment by its improved walking technology, wider arm manipulation range and its size. ASIMO has a flexible fast walking and running capability while interacting with its environment with the help of its new walking technology called i-WALK [19]. With ASIMO, researchers all around the world study on the subjects of human-robot interaction, artificial intelligence systems, learning and adaptation control schemes since it has the most advanced walking capabilities among other humanoid robots.



Figure 2.11: P3 and ASIMO of HONDA

In Japan, University of Tokyo also contributed to humanoid robots research field with its humanoid prototypes H5, H6 and H7 which are shown in Figure 2.12. With its 30 D.O.F., H5 was a full body humanoid robot. However, the size of the robot was small weighing only 33 kilograms with 1.27 meter in height [20]. The next generation robot was built with the motivation of research on environment interaction. The humanoid platform H6 was consisting of 35 D.O.F. and it was 1.36 meters tall weighing 51 kilograms. It was manufactured with 3D vision and voice recognition systems. The last prototype H7 was also built in human proportions with 30 D.O.F., 1.47 meters height and 57 kg weight [21]. Today, studies with these prototypes are still conducted in the University of Tokyo.

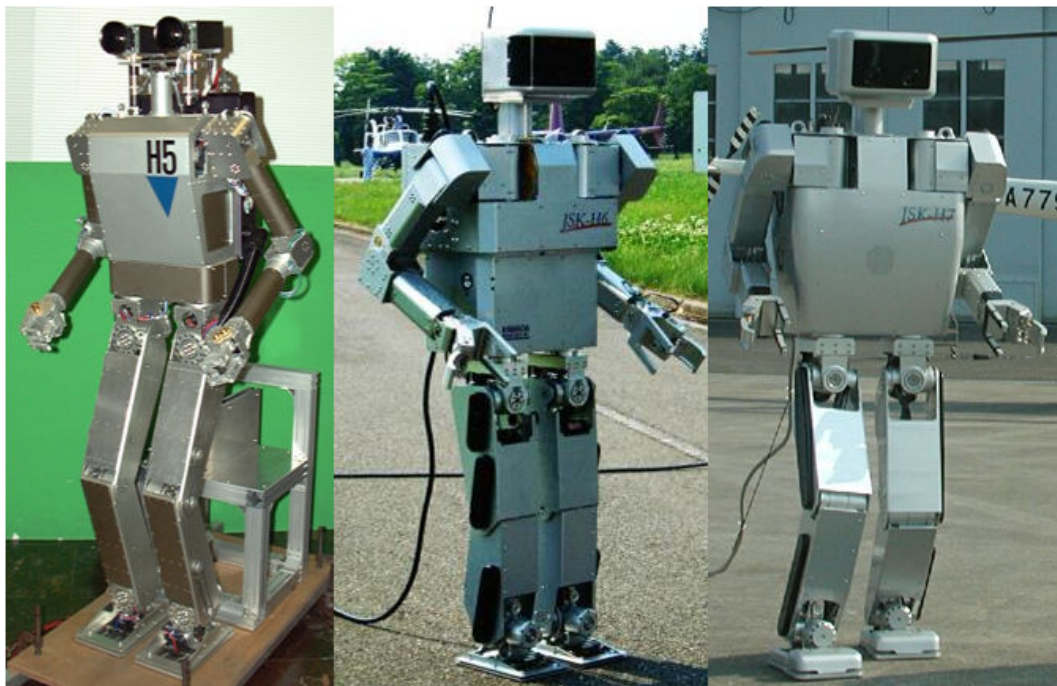


Figure 2.12: H5 (left), H6 (center) and H7 (right) of University of Tokyo

Korea Advanced Institute of Science and Technology announced the humanoid robot platform KHR-1 in 2002. KHR-1 was 48 kilograms in weight and 1.2 meters tall. With its 21 D.O.F, a stable walking performance was successfully employed by using force/torque and inertial sensors [22]. KHR-2 was the second generation with 41 D.O.F. and it achieved vision guided walking and stability of gait on uneven terrains [23]. With the advanced five fingered hand design of the last prototype KHR-3; more human-like properties are carried out like handshaking and object manipulation [24]. These humanoid robots are shown in Figure 2.13.



Figure 2.13: KHR-1, KHR-2 and KHR-3 (HUBO) of KAIST

In 1998, The Ministry of Economy and Industry (METI) of Japan commenced the Humanoid Robot Project (HRP) for the development of humanoid robots which are going to be a part of the labor power of the society. HRP-1 was the first humanoid robot of this project developed by Honda R&D. The robot is designed as a newer generation of the HONDA P3 robot both in shape and controller strategies [25]. National Institute of Advanced Industrial Science and Technology (AIST) developed their own control system in 2001, and achieved to build the second humanoid robot of the project. HRP-2 was a lighter humanoid with 58 kilograms in weight and 1.54 meters in height. The success of this humanoid robot was its compact design with no backpack and a thinner body. Another humanoid robot developed by AIST is HRP-3P. It was designed to perform in rough working conditions like rain and dust [26]. Figure 2.14 presents these humanoid robots. After achievement of human-like walking and manipulation capabilities, researchers of AIST unveiled another humanoid robot named HRP-4C. This female robot, shown in Figure 2.15, was designed with a realistic head and a realistic figure of a human being [27].

Besides these full body human sized robots, the humanoid research field also contains kid size robots. One of the most important of these robots is the NAO robot of Aldebaran Robotics in France [28]. It has 21 D.O.F., 0.6 meters tall and it weighs only 4.3 kilograms. The NAO robot, which is presented in Figure 2.16, has been devised with the concern of cost reduction without sacrificing quality and performance. Affordability of the robot helps it to gain common acceptance in the humanoid robot

research field. In 2007 NAO robot was selected as the platform used in the Robot Soccer World Cup (Robocup) Standard Platform League (SPL), an international robotics competition themed around the idea of football playing robots [29]. Figure 2.17 shows NAO robots playing football as a team, in Robocup.



Figure 2.14: HRP 2 (left) and HRP-3P (right)



Figure 2.15: The female humanoid robot HRP-4C



Figure 2.16: Aldebaran NAO

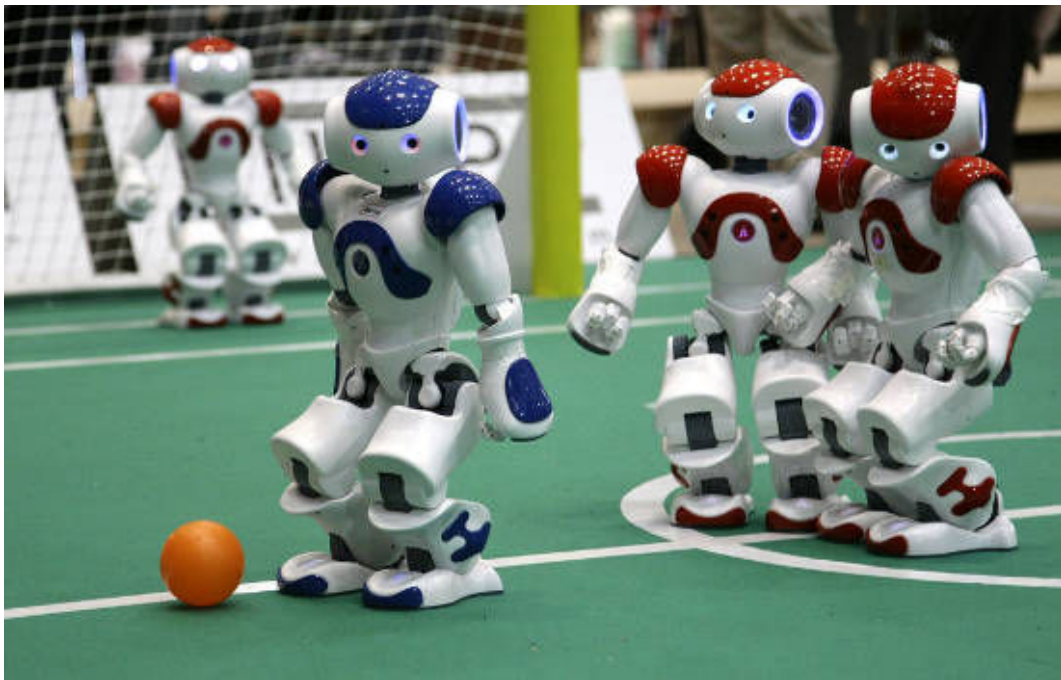


Figure 2.17: Soccer playing NAO Robots

2.3. Reference Generation and Control for the Humanoid Robots

Generation of stable bipedal walking references is one of the key solutions for the bipedal humanoid robots to serve in complex human daily environment. For this purpose, in a number of studies, Linear Inverted Pendulum Model and the Zero Moment Point criterion are applied. In those studies, for the generation of a stable walking reference of the robot center of mass trajectory predefined ZMP trajectories are used. Online modification of the ZMP reference trajectories is another way of generating center of mass trajectory. Using direct or indirect manipulation of the predefined ZMP trajectories is a significant topic for the stable walking of humanoid robots. These methods are presented in this subsection.

In 1995, a Zero Moment Point control algorithm for dynamic bipedal walking is proposed by Lim and Kim [30]. In their work, for the purpose of overcoming the difficulties of analysis of the reaction force created during landing and take-off, a gait is introduced containing only single support phase. In the swing phase, the foot pushes itself forward and also swings itself. By this fashion, the ZMP is made independent of the double support phase. Also the gait is simplified since there are only two different portions of the walk, namely left and right leg supporting phases. Using this technique, the ZMP trajectory does not have to be generated. Putting the ZMP to the center of the supporting foot sole during each step is sufficient.

A new method is proposed by Zhang, Wang, Qiang and Fu in contrast to [30] for the gait generation using the reaction force between the feet and the ground [31]. When the relation between the joint motions and ground reaction force is achieved, using the D'Alembert's principle, the desired joint trajectories of the gait is employed. Desired reaction force for a gait cycle and the joint trajectories are created. It is also stated that the ZMP trajectory is significantly affected by the Center of Mass (CoM) displacement created by the swing leg. Also, it is proposed that in the single support phase the position of the hip joint of support leg should be taken into consideration for ZMP trajectory generation. Fuzzy logic based implementation of the determination for the ZMP trajectory is introduced with the aid of observations made on the human locomotion. These observations suggest that, first strike of the swing foot to the ground is done by the heel, and the last part that touches the ground is the toe of the swing foot. By this way, the ZMP follows a continuous forward moving trajectory on the foot sole.

It is shown that, using this technique, the oscillations of the upper body of a humanoid robot is decreased.

In 2002, Kajita et al. studied on real-time walking control. Using a simplified three-dimensional inverted pendulum model [32], they introduced new walking pattern generation by enabling separate controller designs in both sagittal and frontal planes. In their work, a motion constrained derivation of the three-dimensional inverted pendulum, named Three-Dimensional Linear Inverted Pendulum Model (3D-LIPM), shown in Figure 2.18, is represented. By virtue of this model and using an input device which is a gamepad, experiments carried out for moving straight. Using the projection of the CoM on the walking surface, they enabled omnidirectional walk too. Step size and walking direction can also be adjusted with online modification of the foot placements.

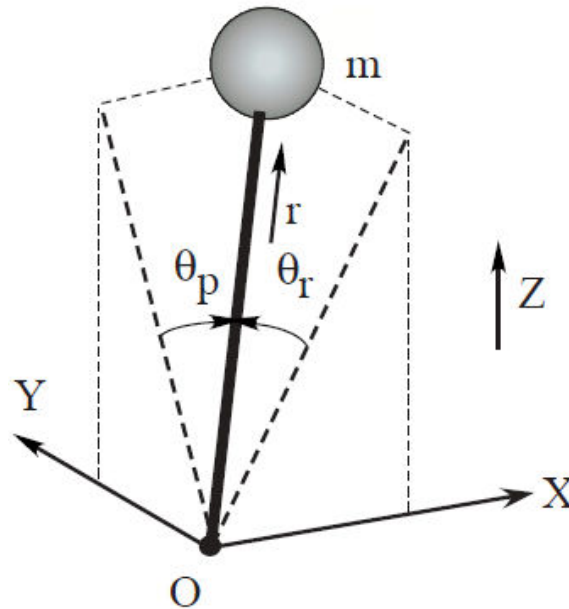


Figure 2.18: 3D inverted pendulum model

In 2002, Lim, Kaneshima and Takanishi introduced an online gait generation method for robots with a trunk [33]. The first part of this pattern generation was updating lower-limb motions and connecting them to the previously generated step pattern for online modification of the gait. With the updated walking command, the second part of the generation method employed waist motions in accordance with the ZMP trajectory to compensate the moments created in the first part. The gait cycle used in this pattern generator is shown in Figure 2.19.

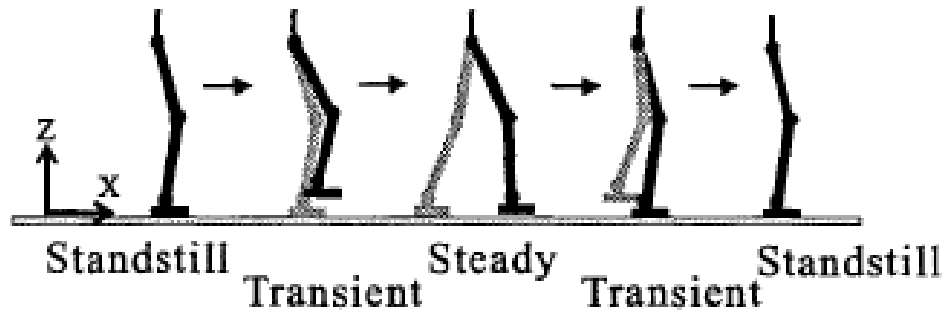


Figure 2.19: A complete walking cycle

The transient and the steady phases are required for the compensation of moments created by the lower-limbs. Online pattern generator which is depicted in Figure 2.20, employs a stable walk with assigned parameters of step length, step height and step direction. These parameters are updated with the first phase of the pattern generator making five steps of lower-limb motion. After these steps, the trunk and waist motion is generated in order to determine the correct ZMP pattern and also compensate for the momentum of the lower-limbs. This final pattern is applied as the gait cycle.

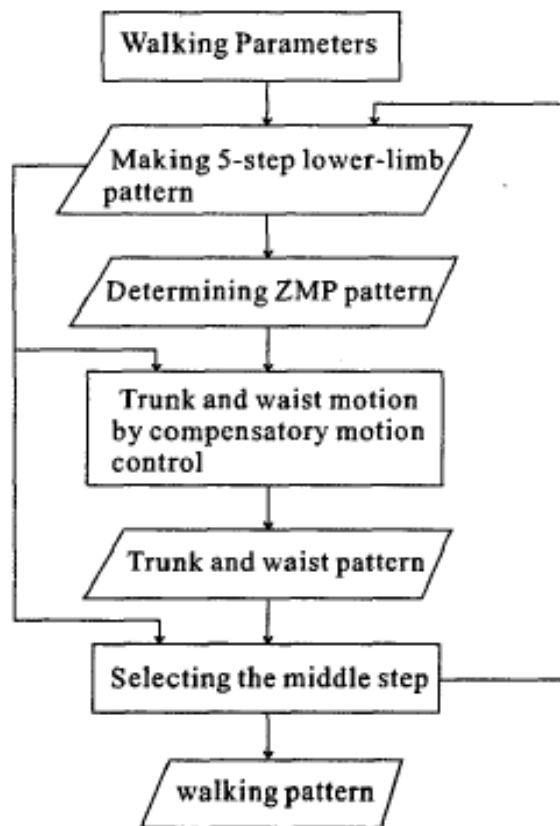


Figure 2.20: Online pattern generation architecture

Sugihara, Nakamura and Inoue, also developed a real-time pattern generator for the control of the Center of Gravity (CoG) by manipulation of the ZMP indirectly, in 2002 [34]. The method contains mainly four parts. The reference planning of the ZMP and the manipulation of ZMP make up the first two parts, while the CoG velocity decomposition for joint angles and local control of joint angles constitute the other two parts. Main advantage of this method arises when higher degrees of freedom humanoid robots used, even if the method is created using a simple LIPM.

In 2004, similar to the work in [34], Harada, Kajita, Kaneko and Hirukawa proposed the generation of CoG and ZMP trajectories simultaneously by a real-time gait planning method [35]. The superior property of this method was the addition of fast and smooth gait transition with respect to the previously calculated gait cycle. This method is called as the quasi-real-time connection method. By virtue of this newly proposed method, if updating of the gait cycle for a step sequence fails to execute in real-time, the regeneration of the gait cycle may be postponed to the next step.

Nishiwaki et al. presented an online walking control system in 2003. This walking control system utilizes layered control architecture. A desired movement, enabling an autonomous locomotion, is followed by the generation of appropriate body trajectories [36]. By this locomotion system, stable walking trajectories on flat surfaces are generated and the gait parameters such as walking speed, direction and upper body posture are satisfied online.

In 2003, Kajita et al. presented a method of gait generation by using a preview control of the Zero Moment Point [1]. There are three main parts of this controller. First part is the integral action on the tracking error of ZMP. The second part can be named as the state feedback phase and the last part is the preview action using the future reference. For the modeling of dynamics of a biped robot a table-cart model shown in Figure 2.21 is used. This model is useful to obtain a suitable representation of ZMP references.

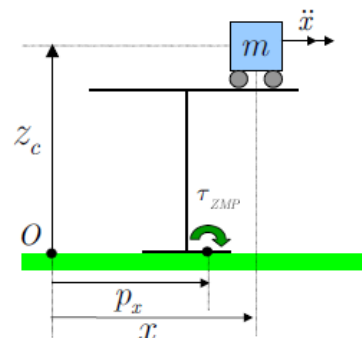


Figure 2.21: A table-cart model

A similar approach to the work in [34] was proposed by Tanaka, Takubo, Inoue and Arai in 2006. The proposed control method was able to change the walking pattern in real-time, which was used to cut the ZMP trajectory, enabling an emergent stop for the robot [37]. A stable gait cycle change is achieved using a relation map between the stop command and the amount of the ZMP modification. The modification amount was calculated using a preview controller and the support polygon. The reliability of the proposed approach was verified by the achievement of an immediate stop to avoid collision, when an unexpected object appears in the walking direction.

Verrelst et al. worked on the subject of stepping over obstacles with humanoid robots in 2006 [38]. The ZMP criterion is used as a stability measurement while stepping over obstacles, which is a dynamic motion. Also preview controller defined in [1] is used for the dynamic balance of the robot. Method is proven to be useful in dynamic motions such as overstretching the knees, reducing reaction force which occurs during the landing of the swing foot and stepping over obstacles.

Nishiwaki and Kagami used a dynamically stable gait generation algorithm that can change the walking pattern at 40 milliseconds [39]. The applied algorithm was used to update the gait cycle in a short time after an input command is received from the wrist force sensor. This idea utilizes the robot to obey to the direction and speed commands of a human holding its hand.

Another model for the gait pattern generation is proposed by Huang et al., for the bipedal robots walking on an uneven plane [40]. Using the Table-Cart model and the known slope gradient, CoM trajectory of the humanoid robot is generated. The desired locations and future ZMP references are found in accordance with the slope of the walking surface. Experiments carried out such as walking up a slope to demonstrate the effectiveness of the proposed algorithm.

Kim, Park and Oh suggested a control scheme for the realization of dynamic gait in 2006 [41]. In the experiments, human locomotion is observed for the design of an appropriate gait cycle. Using these data, the gait is divided into different segments as shown in Figure 2.22. Using the inertial sensor information and control methods which update the walking pattern information a stable reference generation was obtained through this algorithm.

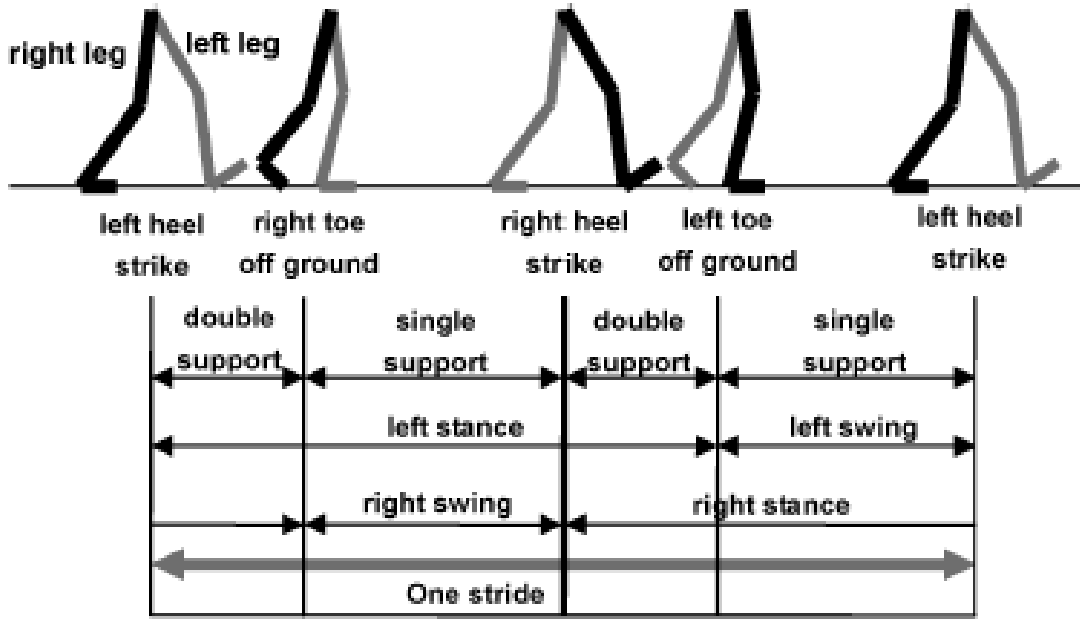


Figure 2.22: A complete walking cycle defined with several stages

In 2006, Behnke proposed an online trajectory generation for omnidirectional walking [42]. When the target walking direction, speed and rotation are specified, the algorithm employs an omnidirectional gait. There are three important ingredients of this approach. The first one is the lateral shifting of the robot CoM. Second ingredient is parameterization of the speed of swing leg into walking direction. The swing leg moves faster than the support leg while the supporting leg is positioned to have maximum extension as a third ingredient.

Another important contribution is presented in [43] by Strom et al. in 2009. Employing the preview control for the control of the ZMP trajectory, a stable omnidirectional walk is achieved. Using a constant motion vector with both forward and rotational components, the stepping sequence foot placements are selected. The ZMP trajectory is computed online from the generated foot places on the walking surface. Experimental results verify the success of the proposed walking pattern algorithm.

Hong et al. introduced a walking pattern generator which is using quartic polynomials to create omnidirectional gait [44]. They proposed a step module for generating stable walking pattern based on ZMP and LIPM model. This step module uses both the characteristics of periodicity and the least square method in order to reduce the fluctuation range of the ZMP trajectory according to various footprints. For the realization of the algorithm, the trajectory of the desired ZMP is designed with the quartic polynomials.

In 2007, Xu and Tan proposed the layered omnidirectional walking controller for humanoid soccer robots [45]. The walking control algorithm of the robot can be parameterized using the destination position and the desired direction. There are multiple layers that are running on different time scales as shown on Figure 2.23. Firstly, the walking path planner takes destination position and desired walking direction and computes the properly needed movement and rotation. Gait primitive generator creates the next gait segment. The limb controller determines the desired joint angles for the realization of desired gait.

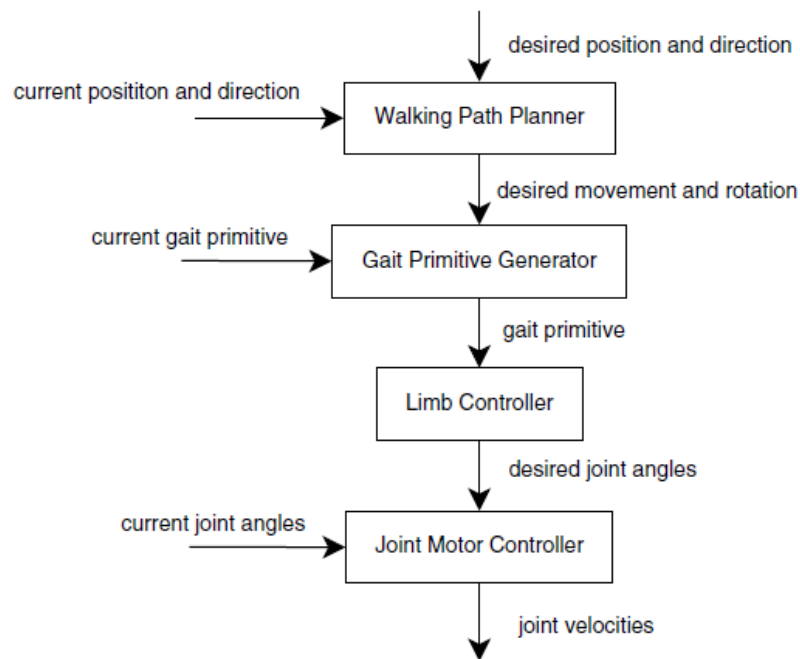


Figure 2.23: The architecture of layered omnidirectional walking controller [45].

As explained the Linear Inverted Pendulum Model and the Zero Moment Point criterion are applied in a number of studies for stable walking reference generation of biped robots. This is also the main route of reference generation in this thesis.

A natural and continuous ZMP reference trajectory is employed for a stable and human-like walk. The ZMP reference trajectories move forward under the sole of the support foot when the robot body is supported by a single leg. Robot center of mass (CoM) trajectory is obtained from predefined ZMP reference trajectories by Fourier series approximation.

The ZMP coordinates are functions of the positions and accelerations of the links and the body of the humanoid robot. It is difficult to use these expressions of many variables in reference generation and control algorithm design. Dynamics equations of the free fall biped robot are also complicated and it is also not straight forward to have

an insight from them to design stable references and stabilizing controllers. This is where an approximate model can prove much more useful than a detailed one. The LIPM [32] is such an approximate model of the legged robot. It consists of a point mass of constant height and a massless rod connecting the point mass with the ground. By virtue of this model, a quite simple relation between the ZMP and the robot CoM coordinates is obtained. There is a freedom in choosing the ZMP reference as long as the criterion above is satisfied. A choice is to keep it fixed at the center of the foot sole when only one foot is supporting the body (single support phase) and interpolating between the foot centers when two feet support it (double support phase) [2]. However, human-like walk can be obtained by ZMP trajectories which move forward when the robot body is supported by a single leg [46-49]. A discussion on the definition of naturalness and performance of the walk can be found in [3].

In [3], Erbatur and Kurt introduce a forward moving discontinuous ZMP reference trajectory for a stable and human-like walk and as in [2] employ Fourier series approximation to obtain CoM reference trajectory from this ZMP trajectory. This method exploits the periodic nature of the steady walk trajectories as is done with Fast Fourier Transforms in an earlier work in [50]. The ZMP reference in the double support phases in [3] is obtained indirectly with a Lanczos smoothing, which also provides smoothing of the Gibbs phenomenon peaks due to Fourier approximation. Although the walk period is defined by the user, the partition of the period into the single and double support phases is due to the smoothing process, and not predefined. [4] use a Fourier series approximation for the computation of the CoM trajectory from a given ZMP reference curve. However, it improves [3] by defining a continuous ZMP reference and the durations of the single and double support phases are fully pre-assigned. This is useful since these parameters play an important role in the parameter tuning in experiments as [51, 52] suggest. The naturalness of the walk is preserved, in that the single support ZMP reference is forward moving. Also, the continuity of the introduced ZMP reference makes smoothing unnecessary.

[5] employs the CoM reference generation method of [4]. However, [4] justifies the applicability of the technique via simulations on a 12-DOF biped robot model, whereas [5] presents experimental walking results obtained with the robot SURALP. In addition to experimental verification, a second contribution of [5] is the introduction of ground push phases in the z-directional foot references before foot take off instances. As a contribution, in this thesis, an omni directional walking pattern generation method is

proposed with the ZMP based reference algorithm in the context of gait generation. The next chapter introduces the experimental robot SURALP on which the designed algorithms are tested.

Chapter 3

3. SURALP: A Full Body Bipedal Humanoid Robot

SURALP (Sabanci University Robotics ReseArch Laboratory Platform) is designed as a test platform for the bipedal robot walking experiments within the framework of a project (106E040) funded by TUBITAK (The Scientific and Technological Research Council of Turkey). The project was successfully concluded at the end of 2009 summer. Built as a research platform on stable bipedal walking and humanoid robot interaction with objects using force and vision control, SURALP serves to this end since the conclusion of the TUBITAK project. This chapter introduces SURALP, presented in Figure 3.1, in terms of its mechanical design, actuation mechanism, controller hardware and sensory system.

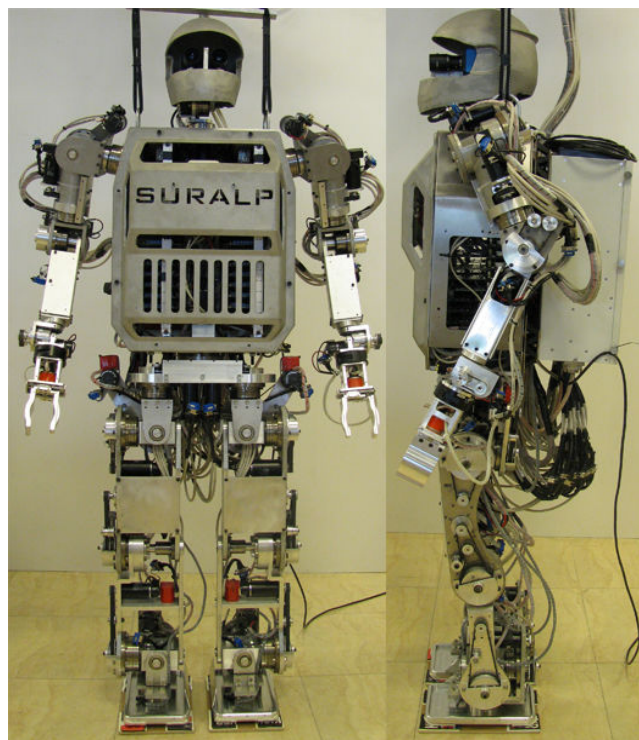


Figure 3.1: SURALP, side and front views

SURALP is a full-body bipedal humanoid robot with 29-DOFs, including leg, arm, hand, neck and waist joints. Leg module of SURALP which consists of 12-DOF was introduced earlier in [51]. The controller hardware of SURALP is attached to its trunk. The robot is designed to be realistic in human proportions and adaptable to human environment. The design and dimensions of the humanoid robot SURALP is presented in Figure 3.2.

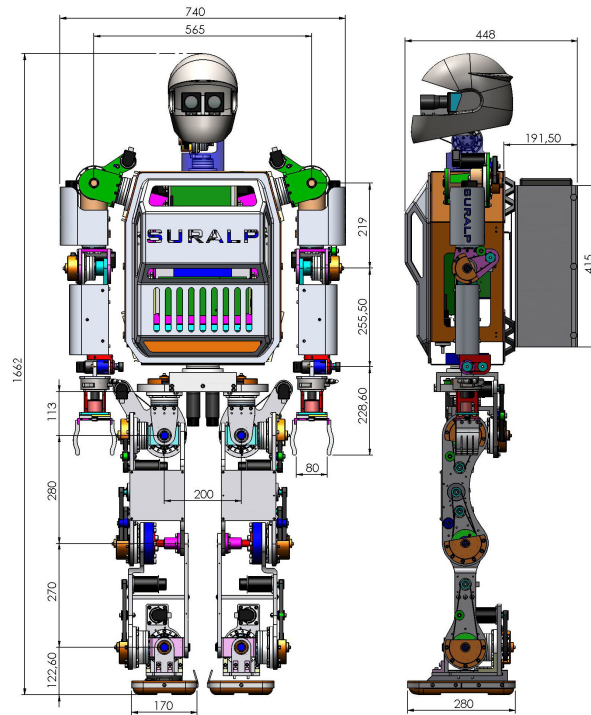


Figure 3.2: SURALP, dimensions

The kinematic arrangement of SURALP is shown in Figure 3.3. Each leg consists of 6-DOF and each arm has 7-DOF. Hips and shoulders are composed of three orthogonal joint axes. These joint axes intersect at a fixed common point. At the legs, the knee axis follows the hip pitch axis. Ankle pitch and ankle roll joints are designed as two orthogonal axes. At the arms, the shoulder motion is utilized by three orthogonal joint axes. The elbow is in a revolute joint configuration. For the actuation of the wrist, a roll and a pitch axis is positioned in the arm of the robot. Hands are actuated by single D.O.F linear motion. There is a waist yaw axis positioned on the pelvis and the neck is composed of two axes in the pan-tilt configuration. The Denavit Hartenberg axis assignment for the 6-DOF leg is presented in Figure 3.4 followed by Table 3.1 which shows the Denavit Hartenberg table of the leg.

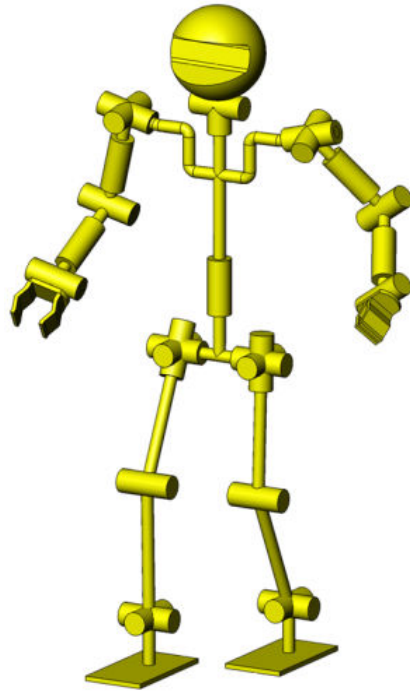


Figure 3.3: The kinematic arrangement of SURALP

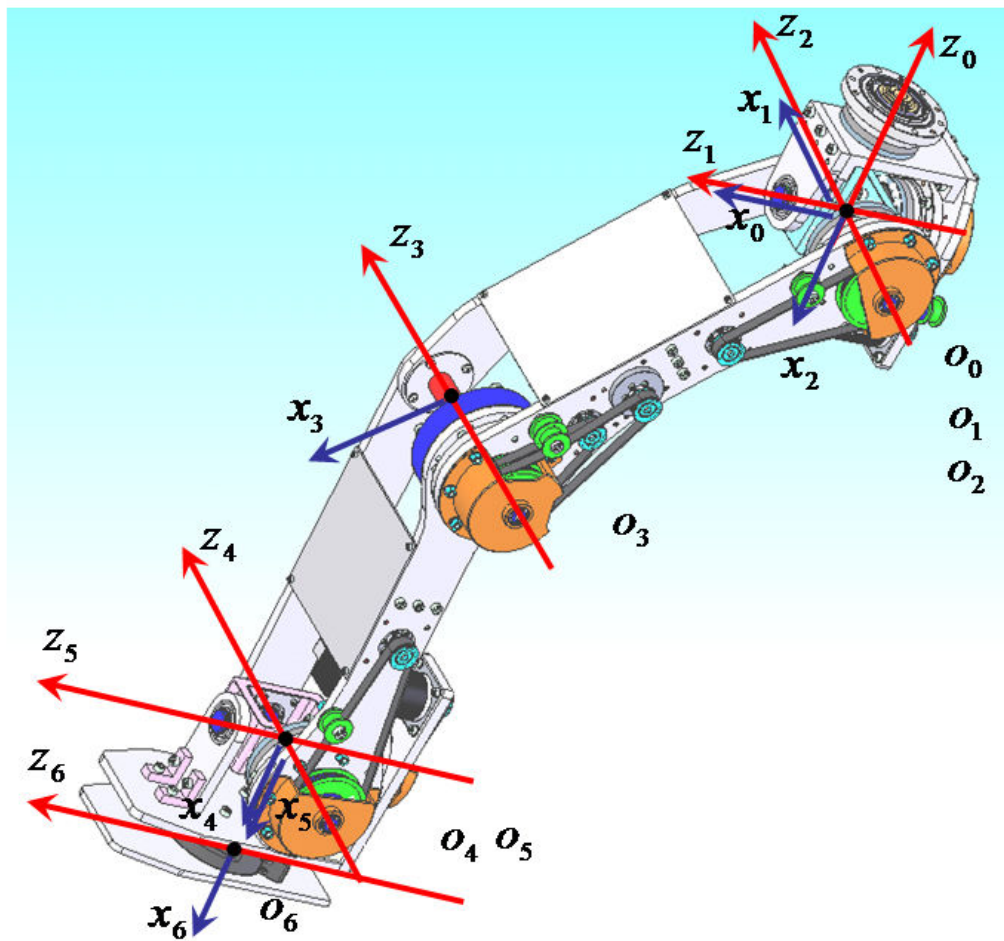


Figure 3.4: Denavit Hartenberg axis assignment for a 6-DOF Leg

Table 3.1: Denavit Hartenberg table with respect to Figure 3.4

	a	α	d	θ
Link 1	0	-90°	0	θ_1^*
Link 2	0	90°	0	θ_2^*
Link 3	L_3	0	0	θ_3^*
Link 4	L_4	0	0	θ_4^*
Link 5	0	-90°	0	θ_5^*
Link 6	L_6	0	0	θ_6^*

The link lengths and weight information are given in Table 3.2. 7000 Series aluminum is chosen as the construction material.

Table 3.2: Length and weight parameters

Upper Leg Length	280mm
Lower Leg Length	270mm
Sole-Ankle Distance	124mm
Foot Dimensions	240mm x 150mm
Upper Arm Length	219mm
Lower Arm Length	255mm
Robot Weight	101 kg

All joints have a single DC motor actuation mechanism except the knee joint. The knee joint is driven by two DC motors for high torque capability. Harmonic Drive reduction gears are selected to obtain very high reduction ratios in a very compact space. Belt-pulley systems transmit the motor rotary motion to Harmonic Drive reduction gears. The joint motor power capabilities, reduction ratios of belt-pulley systems and the Harmonic Drives are displayed in Table 3.3. The working ranges of the joints are set along with the design of the robot. These values are also given in this table.

Table 3.3: Joint actuation system

Joint	Motor Power	Pulley Ratio	HD Ratio	Motor Range
Hip-Yaw	90W	3	120	-50 to 90 deg
Hip-Roll	150W	3	160	-31 to 23 deg
Hip-Pitch	150W	3	120	-128 to 43 deg
Knee 1-2	150W	3	160	-97 to 135 deg
Ankle-Pitch	150W	3	100	-115 to 23 deg
Ankle Roll	150W	3	120	-19 to 31 deg
Shoulder Roll 1	150W	2	160	-180 to 180 deg
Shoulder Pitch	150W	2	160	-23 to 135 deg
Shoulder Roll 2	90W	2	120	-180 to 180 deg
Elbow	150W	2	120	-49 to 110 deg
Wrist Roll	70W	1	74	-180 to 180 deg
Wrist Pitch	90W	1	100	-16 to 90 deg
Gripper	4W	1	689	0 to 80 mm
Neck Pan	90W	1	100	-180 to 180 deg
Neck Tilt	70W	2	100	-24 to 30 deg
Waist	150W	2	160	-40 to 40 deg

During the landing phases of the leg, the feet experience an impact force caused by the floor. Absorbing this impact significantly increases the stability of the gait. With this in mind a mechanical solution is proposed which reduces the affect of the impact force. Various foot designs with soft rubber materials for the sole of the feet are tested. Despite the fact that soft materials reduces an important amount of the impact, very soft designs caused the robot foot to slip on the ground and resulted in a serious loss of stability. The final design of the sole is more human-like and the best walking performances are obtained with this design, shown in Figure 3.5.

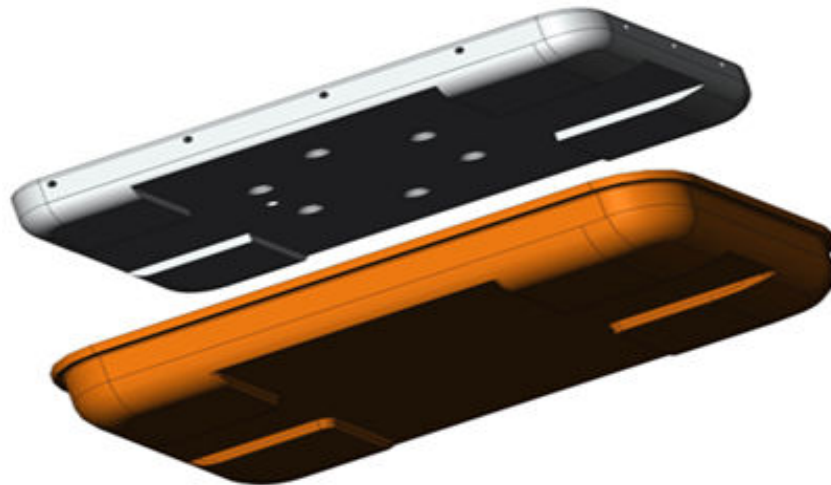


Figure 3.5: The bottom view of the final sole design

For sensory feedback, joint incremental encoders which measure the motor angular positions, force/torque sensors, inertial measurement systems and CCD cameras are employed. The motor angular positions are measured by 500 ppr (pulse per revolution) optic incremental encoders mounted to DC motors. Force and torque measurements are done with 6 axis force/torque sensors which are positioned at the ankle of the robot. The robot is equipped by a rate gyro, an inclinometer, and a linear accelerometer which are mounted at the robot torso too. These sensors are used for the information of roll/pitch angles and angular rates in the roll/pitch/yaw axes. The inclinometer was particularly important for the development of control algorithms presented in this thesis. Two USB cameras are mounted to the robot head for visual information. These sensors are tabulated in Table 3.4 with their working ranges and mounting locations.

Table 3.4: Sensors of SURALP

	Sensor	Number of Channels	Range
All joints	Incremental optic encoders	1 channel per joint	500 pulses/rev
Ankle	F/T sensor	6 channels per ankle	± 660 N (x, y-axes) ± 1980 N (z-axis) ± 60 Nm (all axes)
Torso	Accelerometer	3 channels	± 2 G
	Inclinometer	2 channels	± 30 deg
	Rate gyro	3 channels	± 150 deg/s
Wrist	F/T sensor	6 channels per wrist	± 65 N (x, y-axes) ± 200 N (z-axis) ± 5 Nm (all axes)
Head	CCD camera	2 with motorized zoom	640x480 pixels (30 fps)

The control electronics is based on dSPACE modular hardware. A DS1005 microcontroller board of the dSPACE is used as the central controller. This is the board where all the reference generation and control algorithms are coded. Apart from the μP , seven DS3001 incremental encoder input boards are used to provide the connectivity for 35 joint encoders. Current design of SURALP occupies 31 of these connections. Two 32-inputs DS2002 Multi-Channel A/D Boards are employed for conversion of analog signals from inertial and force/torque sensors. One DS2103 Multi-Channel D/A Board provides 32 parallel D/A channels for the reference signals of the actuators.

The rate gyro, accelerometer, inclinometer and 6-axis force/torque sensors are integrated over the analog inputs. The analog outputs provide torque references for the four-quadrant Maxon & Faulhaber DC motor drivers. The controller and data acquisition boards mentioned above are housed by a dSPACE Tandem AutoBox enclosure, which is mounted in a backpack configuration in the robot assembly. The overall hardware structure is drawn in Figure 3.6. The rate gyro, accelerometer, inclinometer and Maxon & Faulhaber DC motor drivers are located in the torso of the humanoid robot. The power source and a remote user interface computer are placed externally.

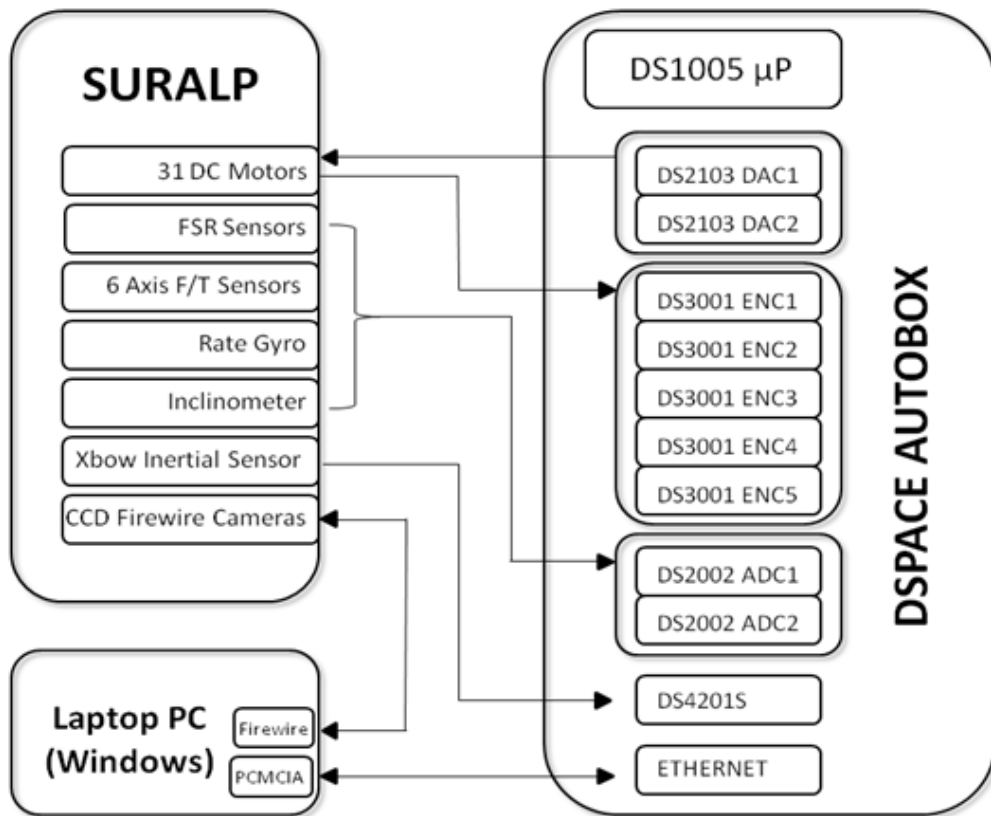


Figure 3.6: Overall hardware setup of the humanoid robot: SURALP

Chapter 4

4. OMNI-DIRECTIONAL WALKING REFERENCE TRAJECTORY GENERATION

This chapter describes a method of omnidirectional walking reference generation based on the ZMP stability criterion. There are a multiplicity of ways for defining and generating omnidirectional walk. Also, it is true that this kind of walk can be linked to the ZMP stability in various ways. The method presented in this thesis “maps” the CoM trajectory obtained from a stable straight walk ZMP reference and associated foot trajectories onto CoM and foot trajectories about a circular arc.

The mapping method, which is at the heart of the proposed omnidirectional walking reference generation, does not depend on the specific shape of the straight walk ZMP reference employed. It is also independent of the way how the CoM reference is obtained from the ZMP reference. However, in the implementations on the robot SURALP presented in Chapter 6, the method in [5] is used for the straight walk reference generation. As many parameters and variables of this straight walk reference trajectory are used for the design of the circular arc reference too, this straight walk reference generation method is reviewed in the next section. This is followed in Section 4.2 by the definition of a “central reference path,” which is very useful for the development of the mapping method presented in Section 4.3.

4.1. ZMP Based Walking Reference Generation for a Straight Walk

The ZMP based CoM reference trajectory generation method as in [5] is discussed in this section for the sake of completeness. The foot reference generation is

also presented.

In place of using complex full dynamics models, the simple LIPM is more suitable for controller synthesis. In this model, a point mass is assigned to the CoM of the robot and it represents the body (trunk) of the robot. The point mass is linked to a stable (not sliding) contact point on the ground via a massless rod, which is idealized model of a supporting leg. In the same manner, the swing leg is assumed to be massless too. With the assumption of a fixed height for the robot CoM a linear system which is decoupled in the x and y directions is obtained. The system described above is shown in Figure 4.1. $c = (c_x \ c_y \ c_z)^T$ is position of the point mass in this figure. The ZMP is defined as the point on the x - y plane on which no horizontal torque components exist. For the structure shown in this figure, the expressions for the ZMP coordinates p_x and p_y are [1]

$$p_x = c_x - (z_c/g) \ddot{c}_x \quad (4.1)$$

$$p_y = c_y - (z_c/g) \ddot{c}_y \quad (4.2)$$

where z_c is the height of the plane, the motion of the point mass is constrained and g is the gravity constant. A suitable ZMP trajectory can be generated without difficulty for reference generation purposes:

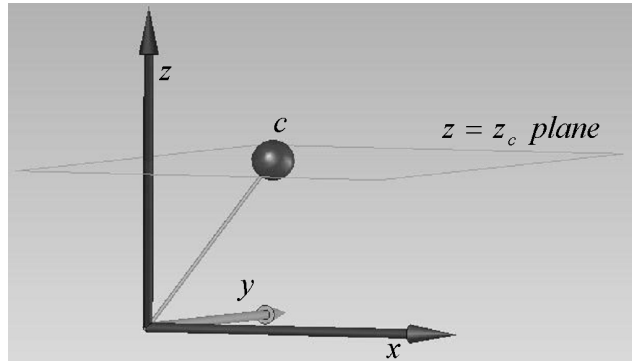


Figure 4.1: The linear inverted pendulum model

As the only stability constraint, the ZMP should always lie in the supporting polygon defined by the foot or feet touching the ground. The ZMP location is generally chosen as the middle point of the supporting foot sole. In [2], the reference ZMP

trajectory shown in Figure 4.2 is created with this idea. Firstly, support foot locations are chosen. A in the figure is the distance between the foot centers in the y direction, B is the step size and T is the half of the walking period. The selection of support foot locations and the half period T defines the staircase-like p_x and the square-wave structured p_y curves. However, in [2], the naturalness of the walk is not considered. As mentioned above, in that work ZMP stays at a fixed point under the foot sole, although investigations in [47-49] show that the human ZMP moves forward under the foot sole. Figure 4.2 also shows that the transition from left single support phase to the right single support phase is instantaneous. There exists no double support phase. In order to address the naturalness issue, the p_x reference (p_x^{ref}) curve shown in Figure 4.3 is employed in [3]. In this figure, b defines the range of the ZMP motion under the sole. A trajectory symmetric in the x -direction, centered at the foot frame origin is assumed.

Having defined the curves, and hence the mathematical functions for $p_x^{ref}(t)$ and $p_y^{ref}(t)$, the next step is obtaining CoM reference curves $c_x^{ref}(t)$ and $c_y^{ref}(t)$ from $p_x^{ref}(t)$ and $p_y^{ref}(t)$, respectively. Position control schemes for the robot joints with joint references obtained by inverse kinematics from the CoM locations can be employed once the CoM trajectory is computed.

The computation of CoM trajectory from the given ZMP trajectory can be carried out in a number of ways [1, 2]. [2], for the reference ZMP trajectories in Figure 4.2, propose an approximate solution with the use of Fourier series representation to obtain CoM references. Taking an approach similar to the one in [2], [3] develops an approximate solution for the c_x and c_y references corresponding to the moving ZMP references in Figure 4.3. In this process Fourier series approximations of the ZMP references $p_x^{ref}(t)$ and $p_y^{ref}(t)$ and of the CoM references are obtained. Although the ZMP reference in the x -direction in Figure 4.3 is forward moving and hence natural as desired, it is not continuous. So is the ZMP reference of Figure 4.3 in the y -direction. The y -direction reference is in the form of a square wave as in Figure 2. This discontinuous function corresponds to an instantaneous switching of the support foot, from right to left and from left to right foot, without an intermediate double support phase. [3] uses Lanczos sigma factor smoothing for i) suppressing the Gibbs phenomenon, ii) introducing double support phases. This approach, however, introduces problems too: Gibbs suppression and double support period determination are coupled.

However, having the single and double support periods as freely adjustable parameters plays a vital role in tuning of the walking pattern.

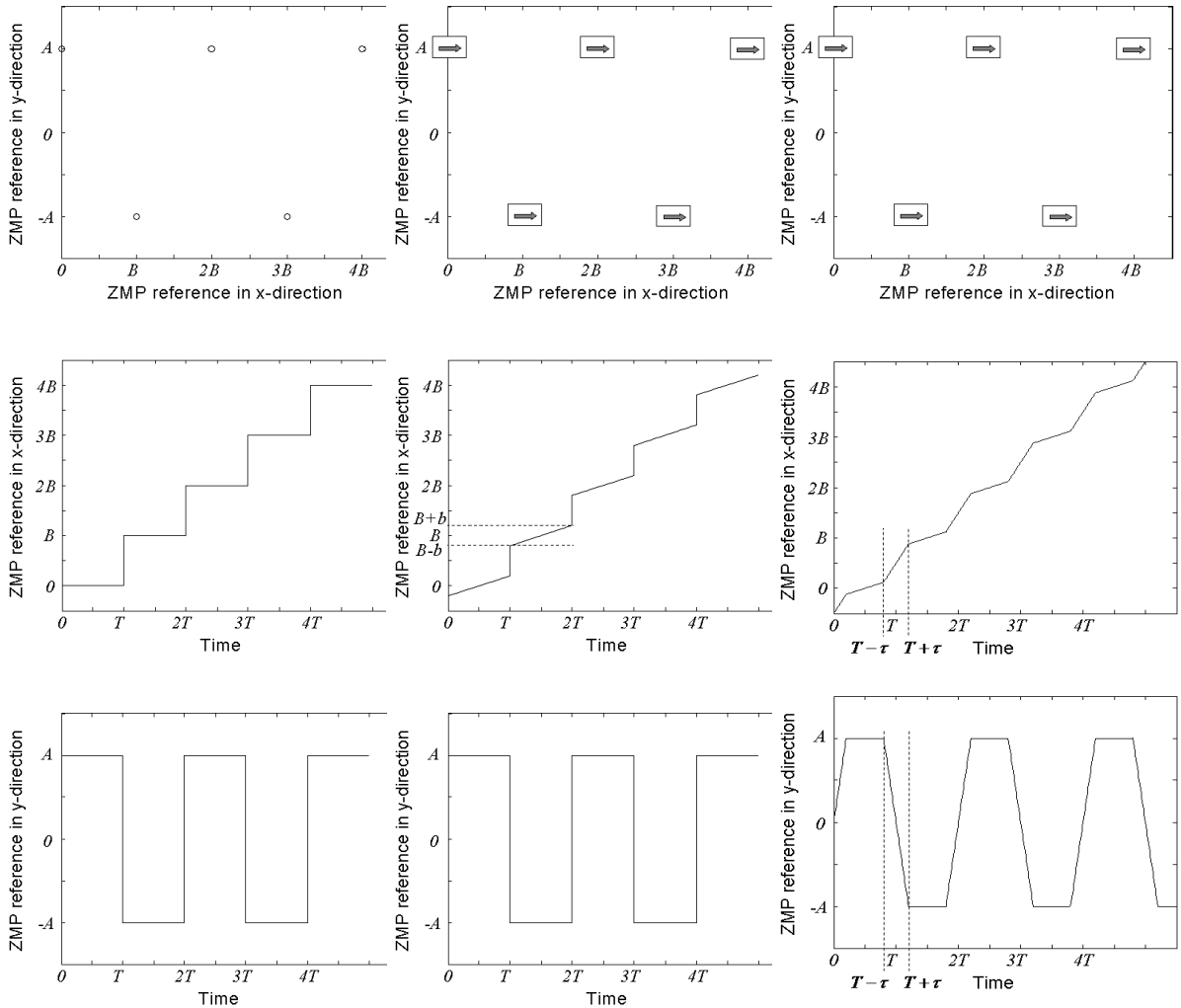


Figure 4.2: Fixed ZMP references.

Figure 4.3: Forward moving ZMP reference

Figure 4.4: Forward moving ZMP references with pre-assigned double support phases.

With this motivation, in [4] and [52], a new ZMP reference trajectory is employed where the double support phase is introduced by using the parameter τ in Figure 4.4. An interpolation interval is inserted around multiples of the half walking period T . The durations of the intervals are equal to 2τ and they correspond to double support periods. The description of the $p_x^{ref}(t)$ in Figure 4.4 is given by

$$p_x^{ref} = (B/T)(t - T/2) + p_x^{*ref} \quad (4.3)$$

where p_x^{*ref} is periodic with period T . p_x^{*ref} is a combination of three line segments on $[0, T]$:

$$p_x^{*ref} = \begin{cases} \Omega_1 + \sigma_1 t & \text{if } 0 \leq t \leq \tau \\ \Omega_2 + \sigma_2 t & \text{if } \tau < t \leq T - \tau \\ \Omega_3 + \sigma_3 t & \text{if } T - \tau < t \leq T \end{cases} \quad (4.4)$$

$$\begin{aligned} \Omega_1 &= 0, & \sigma_1 &= \delta/\tau, & \Omega_2 &= \delta - \tau\sigma_2, & \sigma_2 &= -2\delta/T - 2\tau, \\ \Omega_3 &= -\delta - (T - \tau)\sigma_3, & \sigma_3 &= \sigma_1. \end{aligned} \quad (4.5)$$

with

$$\delta = (T - 2\tau/T)(B/2 - b). \quad (4.6)$$

Note that δ is the magnitude of peak difference between p_x^{ref} and the non-periodic component $(B/T)(t - T/2)$ of p_x^{ref} . $p_y^{ref}(t)$ in Figure 4.4 is expressed as

$$\begin{aligned} p_y^{ref} &= \sum_{k=1}^{\infty} A(-1)^k \{ (2/2\tau)(t - kT)[u(t - (kT - \tau)) - u(t - (kT + \tau))] \\ &\quad + [u(t - (kT + \tau)) - u(t - (kT + T - \tau))] \}, \end{aligned} \quad (4.7)$$

where $u(\cdot)$ represents the unit step function.

Defining $\omega_n \equiv \sqrt{g/z_c}$, we can rewrite (4.1) and (4.2) for the reference variables as follows.

$$\ddot{c}_x^{ref} = \omega_n^2 c_x^{ref} - \omega_n^2 p_x^{ref}, \quad (4.8)$$

$$\ddot{c}_y^{ref} = \omega_n^2 c_y^{ref} - \omega_n^2 p_y^{ref}. \quad (4.9)$$

Note that the y -direction ZMP reference $p_y^{ref}(t)$ is a periodic function with the period $2T$. It is reasonable to assume that $c_y^{ref}(t)$ is periodic too and that it has the same period. Hence, it can be approximated by a Fourier series

$$c_y^{ref}(t) = \frac{a_0}{2} + \sum_{k=1}^{\infty} a_k \cos\left(\frac{2\pi kt}{2T}\right) + b_k \sin\left(\frac{2\pi kt}{2T}\right) \quad (4.10)$$

By (9) and (10), p_y^{ref} can be expressed as

$$\begin{aligned} p_y^{ref}(t) &= c_y^{ref} - \frac{1}{\omega_n^2} \ddot{c}_y^{ref} \\ &= \frac{a_0}{2} + \sum_{k=1}^{\infty} a_k \left(1 + \frac{\pi^2 k^2}{\omega_n^2 T^2}\right) \cos\left(\frac{2\pi kt}{2T}\right) + b_k \left(1 + \frac{\pi^2 k^2}{\omega_n^2 T^2}\right) \sin\left(\frac{2\pi kt}{2T}\right) \end{aligned} \quad (4.11)$$

Noting that this expression is in the form of a Fourier series for $p_y^{ref}(t)$, and since $p_y^{ref}(t)$ is an odd function, we conclude that $a_0/2$ and $a_k(1 + (\pi^2 k^2)/(\omega_n^2 T^2))$ for $k=1,2,3,\dots$ are zero. The coefficients $b_k(1 + (\pi^2 k^2)/(\omega_n^2 T^2))$ are computed by the Fourier integral:

$$b_k \left(1 + \frac{\pi^2 k^2}{\omega_n^2 T^2}\right) = \frac{2}{2T} \int_0^{2T} p_y^{ref} \sin\left(\frac{2\pi kt}{2T}\right) dt \quad (4.12)$$

As a result, after some arithmetical steps (omitted here), the coefficients b_k of $c_y^{ref}(t)$ in (10) can be obtained as

$$b_k = \begin{cases} \frac{\omega_n^2 T^2}{\omega_n^2 T^2 + \pi^2 k^2} \frac{2A}{\pi k} \left\{ \left[\frac{2}{\tau} \left\langle \frac{T}{\pi k} \sin\left(\frac{\pi k \tau}{T}\right) - \tau \cos\left(\frac{\pi k \tau}{T}\right) \right\rangle \right] \right. \\ \quad \left. + \left[\cos\left(\frac{\pi k \tau}{T}\right) - \cos\left(\frac{\pi k (T - \tau)}{T}\right) \right] \right\} & \text{if } k \text{ is odd} \\ 0 & \text{if } k \text{ is even} \end{cases} \quad (4.13)$$

The second step is finding the Fourier series coefficients for c_x^{ref} . In Figure 4.4, p_x^{ref} is not a periodic function. It cannot be expressed as a Fourier series. However, as expressed above, this function is composed of the periodic function p_x^{ref} and the non-periodic function $((B/T)(t - T/2))$. It is again a reasonable assumption that c_x^{ref} has a periodic part and a non-periodic part too. Further, if we suppose that the two non-periodic parts (of $p_x^{ref}(t)$ and c_x^{ref}) are non-equal, then the difference $p_x^{ref}(t) - c_x^{ref}$ will be non-periodic. This is not expected in a continuous walk as the one described in Figure 4.4. Therefore we conclude that the non-periodic parts of the two functions are equal. Note that, the period of the periodic part of $p_x^{ref}(t)$ is T and we can state the same for the period of the periodic part of c_x^{ref} . Finally, c_x^{ref} can be expressed as the sum of the non-periodic part of p_x^{ref} and a Fourier series:

$$c_x^{ref} = \frac{B}{T} \left(t - \frac{T}{2}\right) + \frac{\alpha_0}{2} + \sum_{n=1}^{\infty} \alpha_n \cos\left(\frac{2\pi nt}{T}\right) + \beta_n \sin\left(\frac{2\pi nt}{T}\right) \quad (4.14)$$

With (8) and (14) $p_x^{ref}(t)$ as a Fourier series is

$$p_x^{ref}(t) = c_x^{ref} - (1/\omega_n^2)\ddot{c}_x^{ref} = (B/T)(t-T/2) + \alpha_0/2 + \sum_{n=1}^{\infty} \alpha_k \left(1 + \frac{\pi^2 k^2}{\omega_n^2 T^2}\right) \cos\left(\frac{2\pi kt}{T}\right) + \beta_k \left(1 + \frac{\pi^2 k^2}{\omega_n^2 T^2}\right) \sin\left(\frac{2\pi kt}{T}\right) \quad (4.15)$$

Therefore the Fourier coefficients of $p_x^{ref}(t)$, the periodic part of $p_x^{ref}(t)$, are $\alpha_0/2$, $\alpha_k(1 + \pi^2 k^2/\omega_n^2 T^2)$ and $\beta_k(1 + \pi^2 k^2/\omega_n^2 T^2)$ for $k=1, 2, 3, \dots$. The Fourier coefficients $\alpha_0/2$, $\alpha_k(1 + \pi^2 k^2/\omega_n^2 T^2)$ of $p_x^{ref}(t)$ are zero because this is an odd function. The coefficients for $\beta_k(1 + (\pi^2 k^2)/(\omega_n^2 T^2))$ can be found by

$$\beta_k(1 + \pi^2 k^2/\omega_n^2 T^2) = \frac{2}{T} \int_0^T p_x^{ref}(t) \sin\left(\frac{2\pi kt}{T}\right) dt \quad (4.16)$$

This yields the result

$$\beta_k = \frac{\omega_n^2 T^2}{\pi^2 k^2 + \omega_n^2 T^2} \frac{2}{\pi k} \left\{ \sigma_1 \left[-\tau \cos\left(\frac{2\pi k \tau}{T}\right) + \frac{T}{2\pi k} \sin\left(\frac{2\pi k \tau}{T}\right) \right] + \sigma_2 \left[\tau \cos\left(\frac{2\pi k \tau}{T}\right) - \frac{T}{2} \left(\cos\left(\frac{2\pi k \tau}{T}\right) \right) - \frac{T}{2\pi k} \sin\left(\frac{2\pi k \tau}{T}\right) \right] \right\}. \quad (4.17)$$

The curves obtained for c_x^{ref} and c_y^{ref} are shown in Figure 4.5 together with the corresponding ZMP references defined in Figure 4.4. The infinite sums in (10) and (14) are approximated by finite sums of N terms. $N = 24$ is used in the experiments. N is found by the inspection of the ‘‘Fourier-series-approximated’’ p_y^{ref} and p_x^{ref} curves obtained from (11) and (15) respectively. (These approximated curves are not shown here due to space considerations. These curves, however, are computed, plotted and compared with the ZMP references in Figure 4.4. in order to validate the formulae derived for the Fourier series coefficients. The plots served a secondary purpose of determining a suitable value for N .) We observed that, with $N = 24$, the approximated curves match with the original piecewise continuous ZMP reference curves in Figure 4.4. The matching quality we judged from the reproduction of the sharp corners of the original ZMP reference curves in their approximated versions. With lower values for N the matching quality is deteriorated. In Fig 5, the following parameter values are used: $A = 0.1$ m, $B = 0.1$ m, $b = 0.04$ m, $T = 1$ s and $\tau = 0.2$ s.

In addition to the CoM references, foot position reference trajectories have to be designed. These references are generated for the Denavit-Hartenberg sole frames. (The sole frames replace the tool frames of an industrial manipulator in the legged robot

context.) The x and z -direction components of the foot trajectories used, are shown in Figure. 6. These curves are combinations of sinusoidal and constant function segments. T_d and T_s represent the double and single support periods, respectively. ($T_d = 2\tau$, $T_s = T - \tau$.) B is the step size from Figure 4.4. The y direction trajectories are constant at $-A$ and A for the right and left feet, respectively, where A is half of the foot to foot y direction distance also shown in Figure 4.4. h_s is the step height parameter and h_p is the ground push magnitude. The foot orientation references used in inverse kinematics are computed for feet parallel to the ground for the consideration of flat floor.

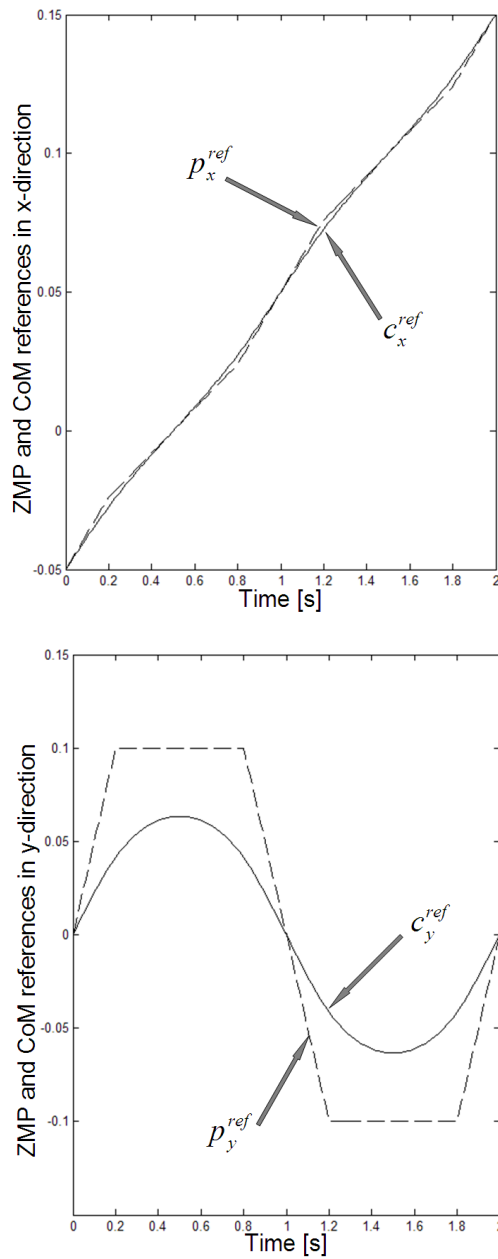


Figure 4.5: x and y -direction CoM and ZMP references

Note that the x -directional CoM references begin with a value less than zero. This is because the body coordinate frame is assumed to be positioned above the world frame in which the coordinates of the CoM are expressed. The CoM is typically at a position off the body coordinate frame center, usually towards the rear of the robot. The vector connecting the body coordinate frame origin to the CoM, as expressed in the body coordinate frame is denoted by s_b^b .

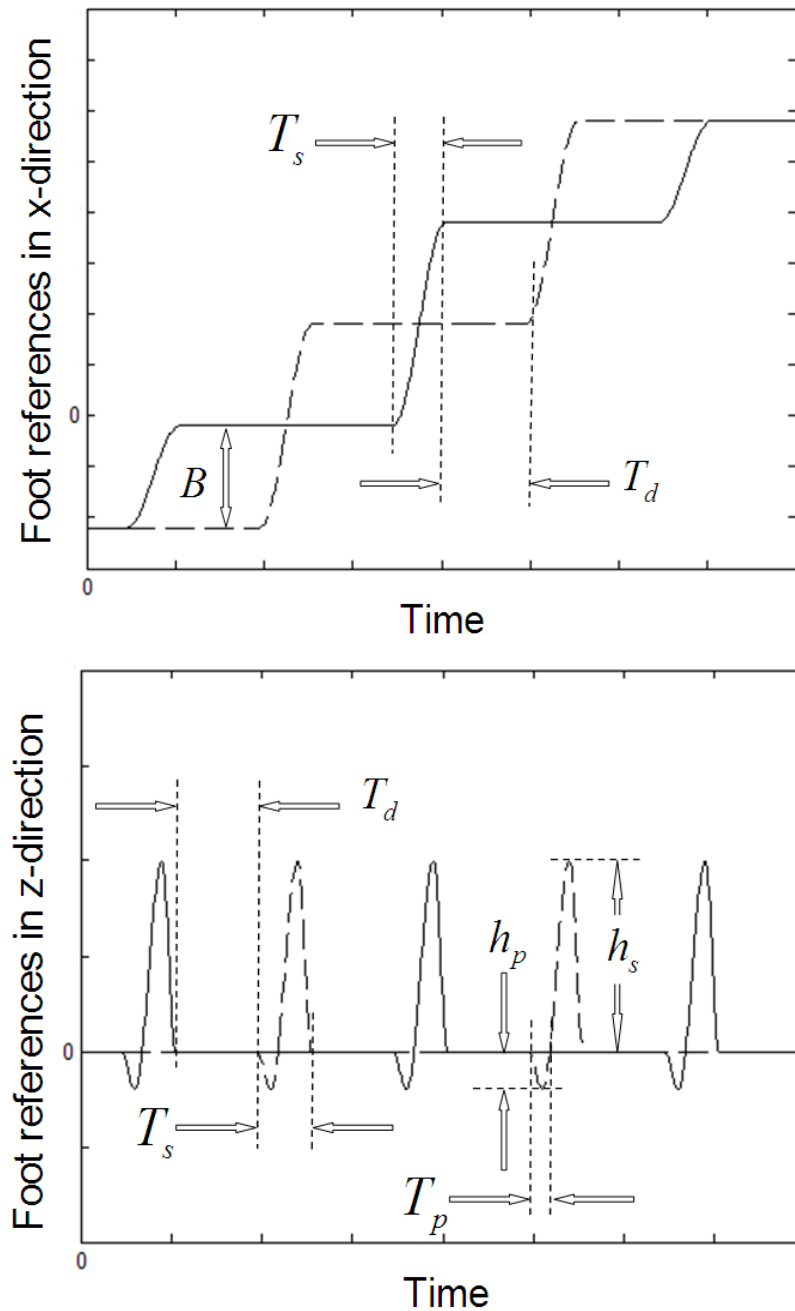


Figure 4.6: x and z -direction foot references as expressed in the world frame. Solid curves belong to the right foot, dashed curves indicate left foot.

The foot sole position references are denoted by $x_R(t), x_L(t), y_R(t), y_L(t), z_R(t)$ and $z_L(t)$ as expressed in the world coordinate frame. x , y and z denote the directions. R and L denote right and left feet, respectively. Note that the x -directional foot references also begin with a value less than zero. This is because feet are in their initial configuration behind the world coordinate frame and body coordinate frame. This is done in order to achieve static balance when the robot does not move. The initial x position of the feet is x_{offset} , which is a negative quantity in Figure 4.6.

4.2. Central Reference Path (CRP)

At this point it is appropriate to discuss reference generation terminology for bipedal robotics.

Reference trajectory:

- a) For a coordinate frame (or for a rigid body with a coordinate frame attached to it) it refers to position and orientation references, as expressed in another coordinate frame, over a specified time interval.
- b) For a point on the robot it refers to a position reference, as expressed in another coordinate frame, over a specified time interval.
- c) It can refer to the reference joint position curves of the robot joints.

Reference path:

- a) It can be used as a synonym for “reference trajectory.”
- b) It may refer to the “average” reference curve on the floor surface, defined as a function of time, over a specified time interval, similar to the path of a wheeled mobile vehicle. The average reference curve on the floor surface planned to be tracked can be defined in various ways. The CoM reference or body fixed coordinate frame origin reference projection on the ground surface can be examples of alternative definitions.

It can be noticed from the considerations above that there is a certain degree of ambiguity in the terminology. In order to disambiguate these definitions, the following specific definition, which is very useful in the derivation of the omnidirectional walking reference generation, is proposed in this thesis:

Central reference path (CRP):

Consider a bipedal humanoid robot with a body fixed coordinate system attached in the middle of the robot in the lateral direction. Suppose that the x -direction of the coordinate frame shows forward, into the walking direction, the z -direction up and the y -direction into the lateral direction to form a right hand frame with the former axes (Figure 4.7). Suppose that the robot is in an initial posture on a flat floor, with right and left feet positioned symmetrically with respect to the body fixed coordinate frame $x-z$ plane. Define the pseudo foot centers on the line where the the body coordinate frame $y-z$ plane intersects the floor level, symmetrically positioned with respect to the body frame $x-z$ plane.

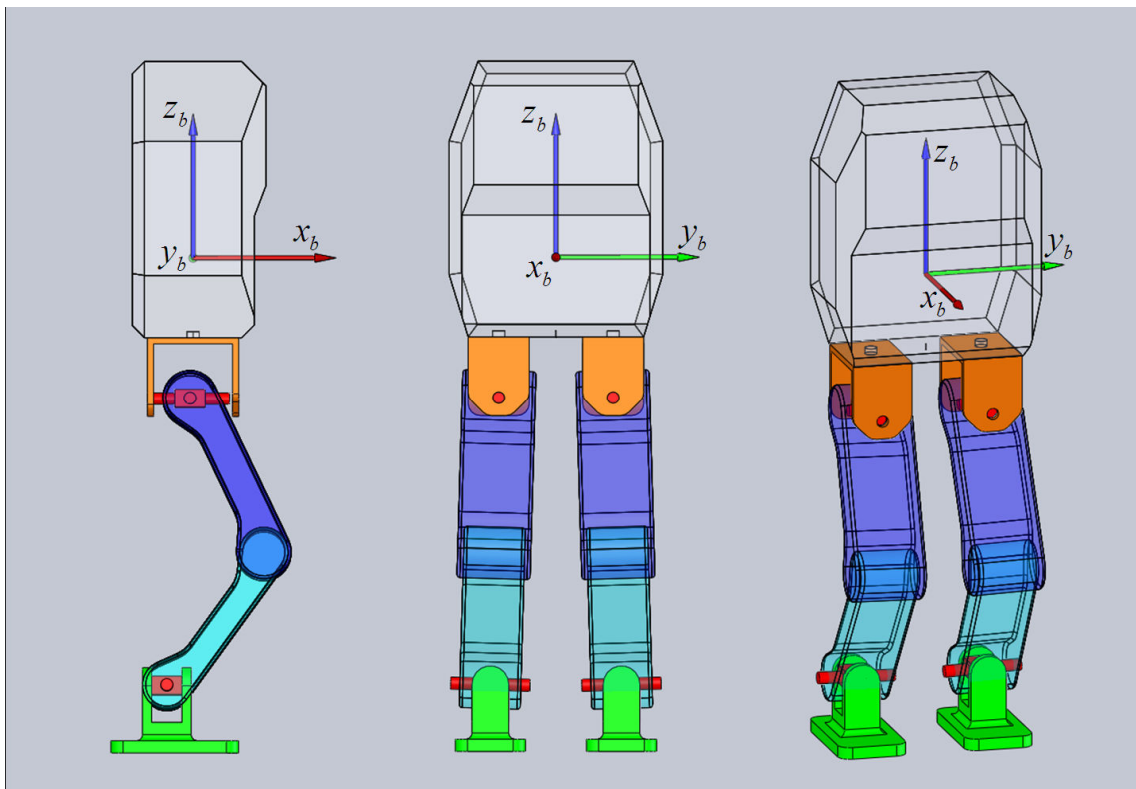


Figure 4.7: Assignment of the body coordinate frame

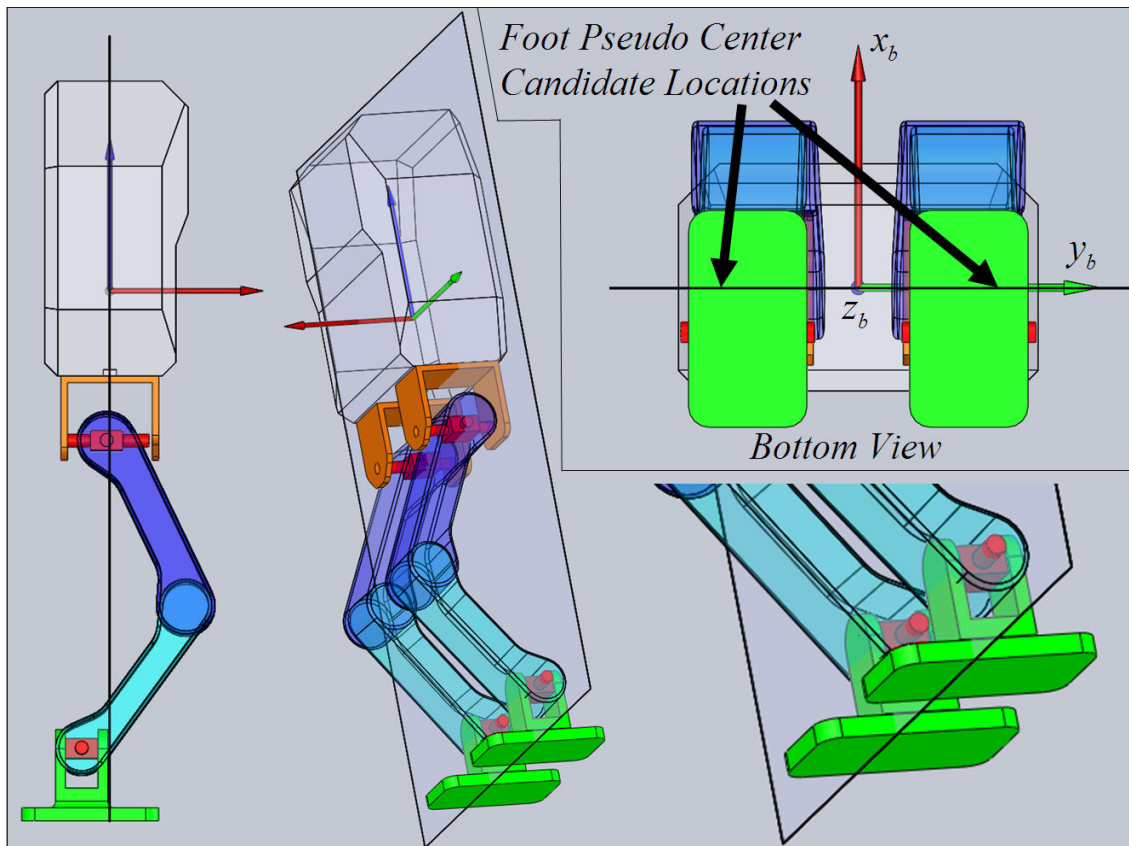


Figure 4.8: The body coordinate frame $y-z$ plane intersects the foot soles. The foot pseudo centers are assigned on this intersection. There are infinitely many candidate locations. Any pair of them can be chosen as long as the right foot pseudo center and left foot pseudo center are assigned symmetrically with respect to the $x-z$ of the body coordinate frame.

This intersection is illustrated in Figure 4.8. For many bipedal robots, if the configuration of the body and the feet is a statically stable one, the pseudo foot centers can be picked within the sole of the robot and not in front or behind the foot. If, however this is not the case, still the definition is valid. Even if the pseudo foot centers

are outside of the foot soles, they should be regarded as “rigidly attached” to the feet, moving with them whenever the feet move.

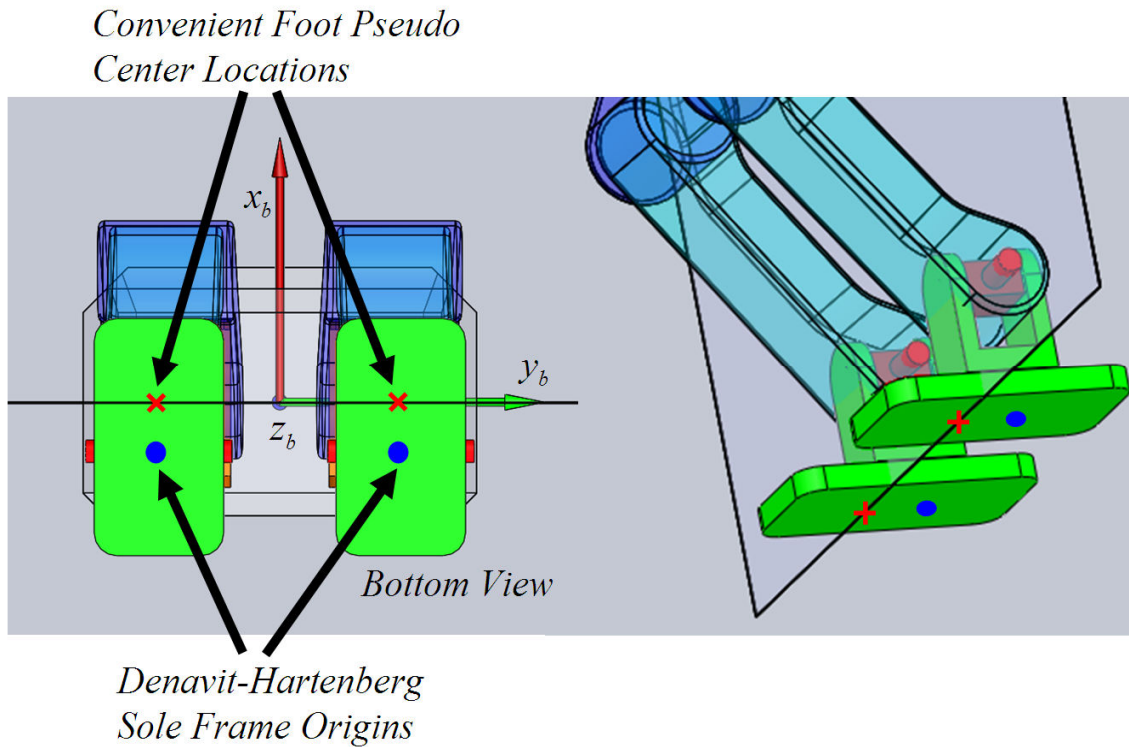


Figure 4.9: Typically convenient locations for the foot pseudo centers, in front of the projections of the ankle frame origins on the on the foot sole.

A convenient location for a foot pseudo center is in front of the Denavit-Hartenberg sole frame center, which in turn is just below the ankle frame center (Figure 4.9). The reason to term the foot pseudo centers so is that they are in general different than the Denavit-Hartenberg sole frame “centers” (that is, sole frame origins). Next, coordinate frames attached at the foot pseudo centers. These frames are oriented fully parallel to the body frame coordinate frame when the robot is in the configuration explained in the above discussion and shown in Figure 4.7. These frames are shown in Figure 4.10. The subscript R_p in this figure stands for “frame attached at the pseudo center of the right foot.” The subscript L_p is similarly employed for the left foot. Also shown in Figure 4.10 are the Denavit-Hartenberg frames at the foot soles. The

subscripts R_6 and L_6 denote these frames. This notation is chosen because SURALP's legs are 6-D.O.F. ones.

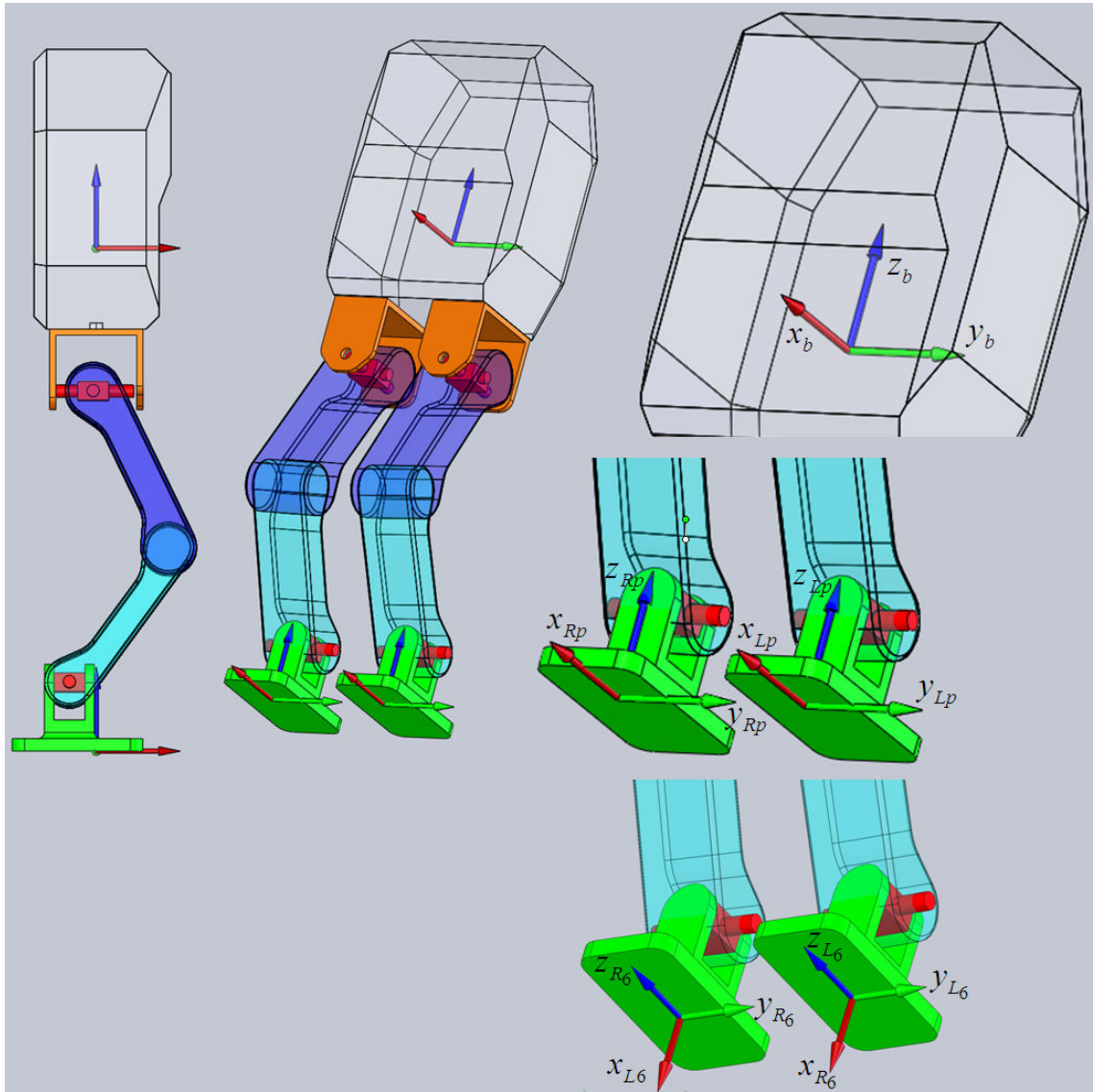


Figure 4.10: Coordinate frames attached at the foot pseudo centers and at the foot sole Denavit-Hartenberg frames

If there is a curve $c(t)$ in the ground level which satisfies the following conditions throughout the walk, we call it a *central reference path*.

- 1) Denoting the half of the distance in the lateral (y_b) direction between the foot pseudo centers, in the initial robot configuration by σ , the first

condition is that at any time t , the distance between the foot pseudo centers and the curve c along the foot pseudo center y -directions must be equal to σ . If the projection of the right foot pseudo center O_{R_p} along y_{R_p} on the curve c is denoted by C_R and the projection of the left foot pseudo center O_{L_p} along y_{L_p} on the curve c is C_L , then this condition can be stated as

$$\left|C_R - O_{R_p}\right| = \left|C_L - O_{L_p}\right| = \sigma \quad \forall t \geq t_0 \quad (4.18)$$

where t_0 is the beginning time of the walk from the initial configuration described above.

- 2) Denoting the unit vectors tangent to the curve c at C_R and C_L , u_{C_R} and u_{C_L} , respectively, the second condition is respective orthogonality of these unit vectors to the foot pseudo center frame y -directional unit vectors at any time:

$$y_{R_p} \perp u_{C_R}, \quad y_{L_p} \perp u_{C_L} \quad \forall t \geq t_0. \quad (4.19)$$

It should be noted that the z-directional foot references are assumed to be zero in the conditions above. If the feet are off the ground, however, their projections on the ground should obey the conditions above.

The two conditions are illustrated in Figure 4.11. A central reference path is illustrated in Figure 4.12. (18) and (19) are conditions for the feet but they do not describe the positions and the orientations of the feet as functions of time. Neither do these conditions impose position and orientation references on the body. Still, a central reference path indicates the main route of the locomotion.

Not all walking references are necessarily generated about central reference paths. However, it can be seen that a central reference path can be fit to a number of walking references in the literature [1, 5, 22, 48, 52]. Surely, the simplest central reference path is a line and the mentioned works in their straight walk do follow a linear central reference path. The straight walk reference reviewed in the previous section does possess a central reference path which is also linear.

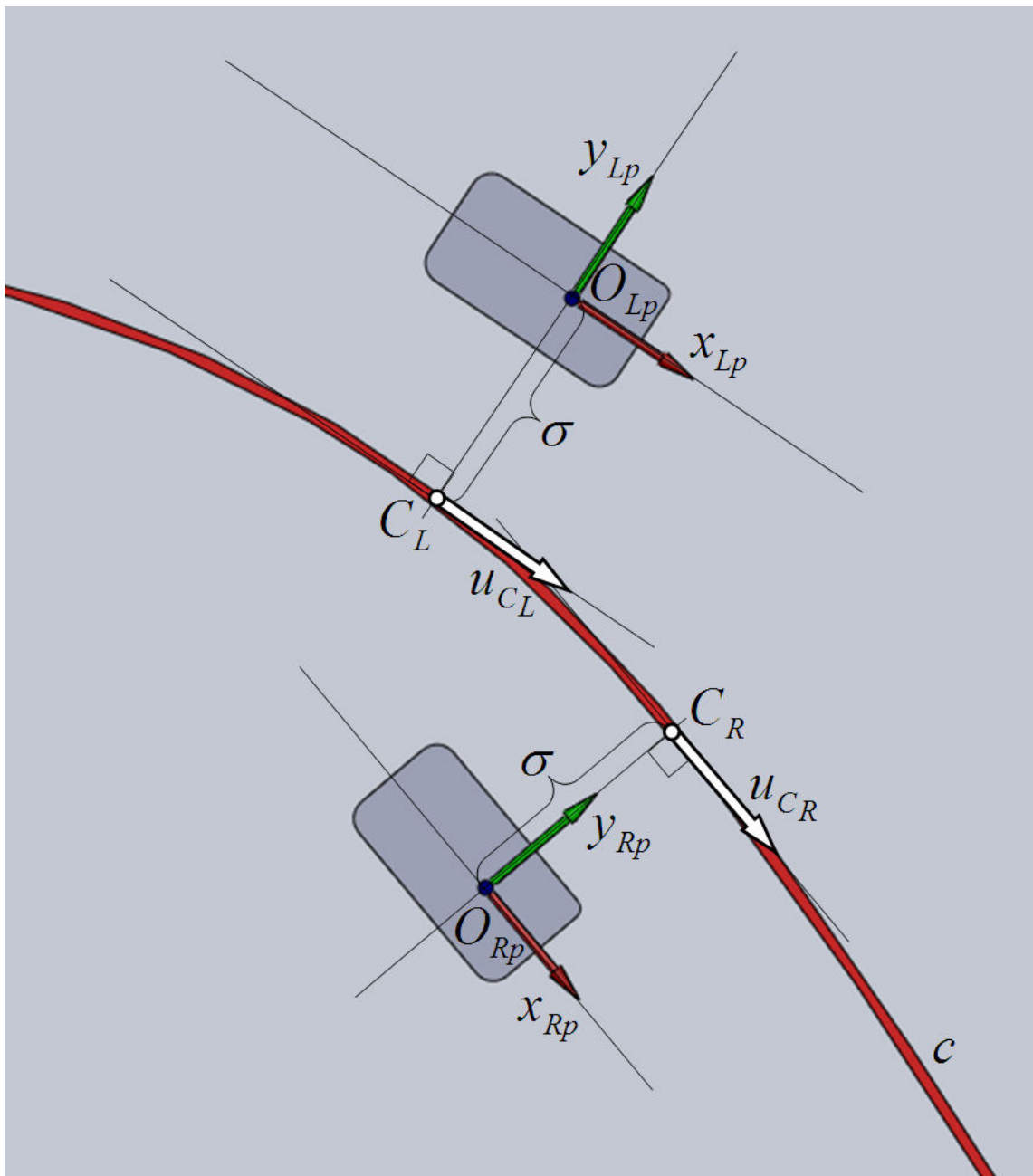


Figure 4.11: Distance and direction conditions on a central reference path.

Foot references defined about a certain central reference path can be mapped onto a walking reference about another central reference path. A procedure for mapping a reference about a Central Reference Path A to a reference about Central Reference Path B is given by Figure 4.12 to Figure 4.25. The procedure is summarized below.

- Define the CRP A.
- For any instant, assign the position and orientation of the right foot about CRP A.
- Define CRP B.
- Extend the right foot pseudo center frame y-axis to intersect CRP A.
- Mark the intersection point.
- Mark the initial point of CRP A.
- Measure the travelled distance between the initial point and the intersection point, and call this distance s .
- Mark the initial point of CRP B.
- Measure the distance travelled along CRP B.
- Mark the ending point of the distance travelled on CRP B.
- Create the normal of CRP B.
- Measure the foot distance on the normal, and place the foot.

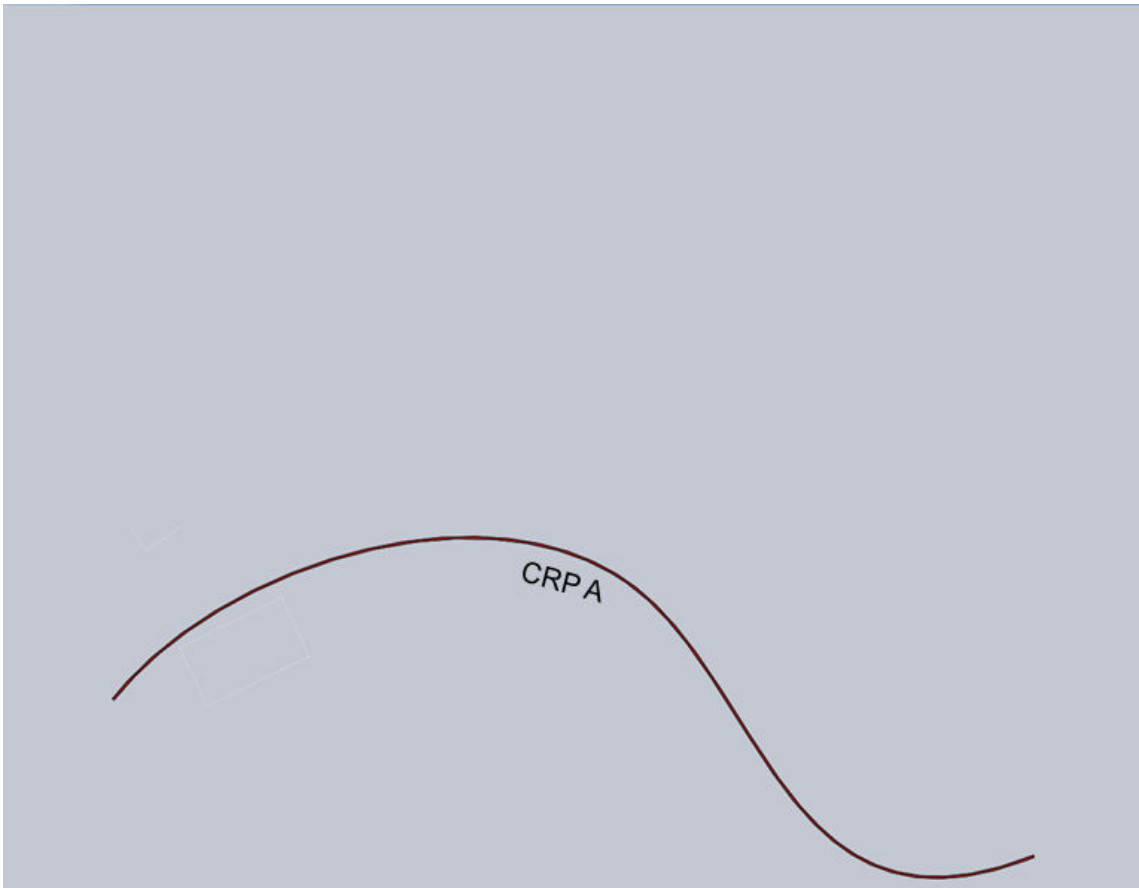


Figure 4.12: Central Reference Path A.

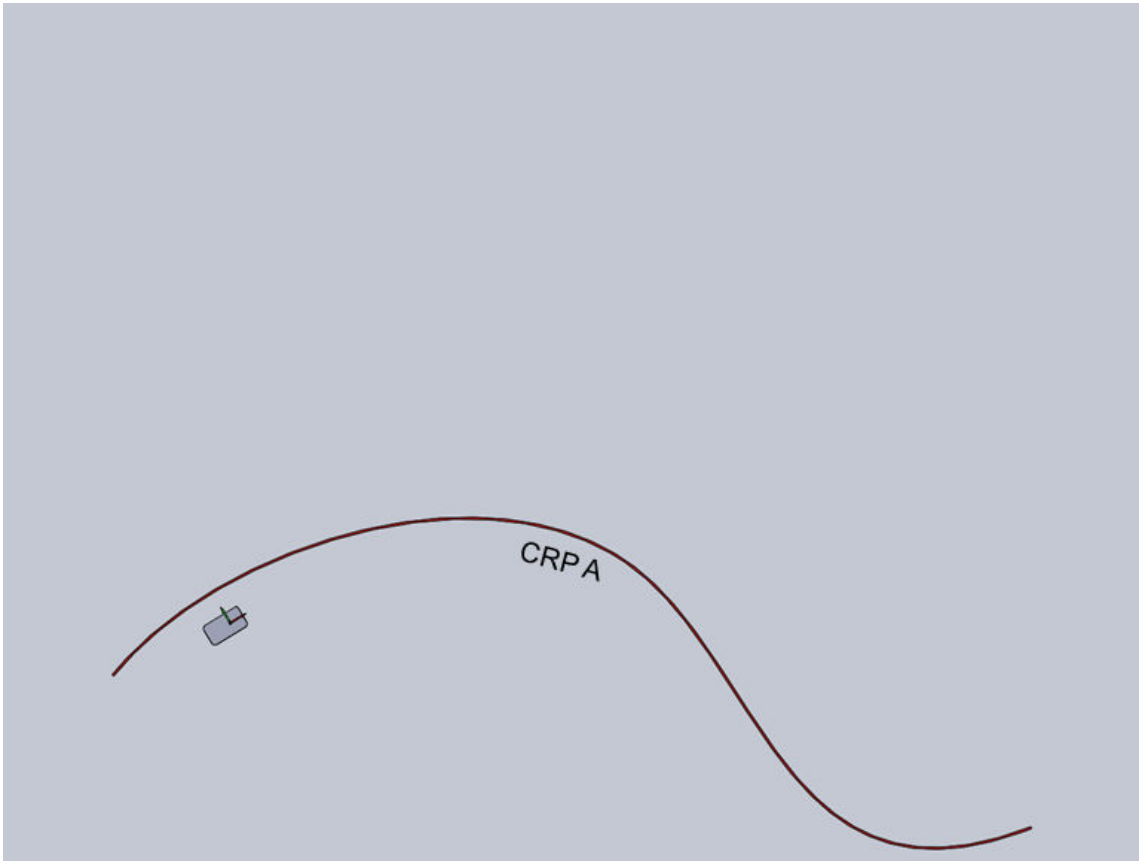


Figure 4.13: Right foot placement with respect to Central Reference Path A.

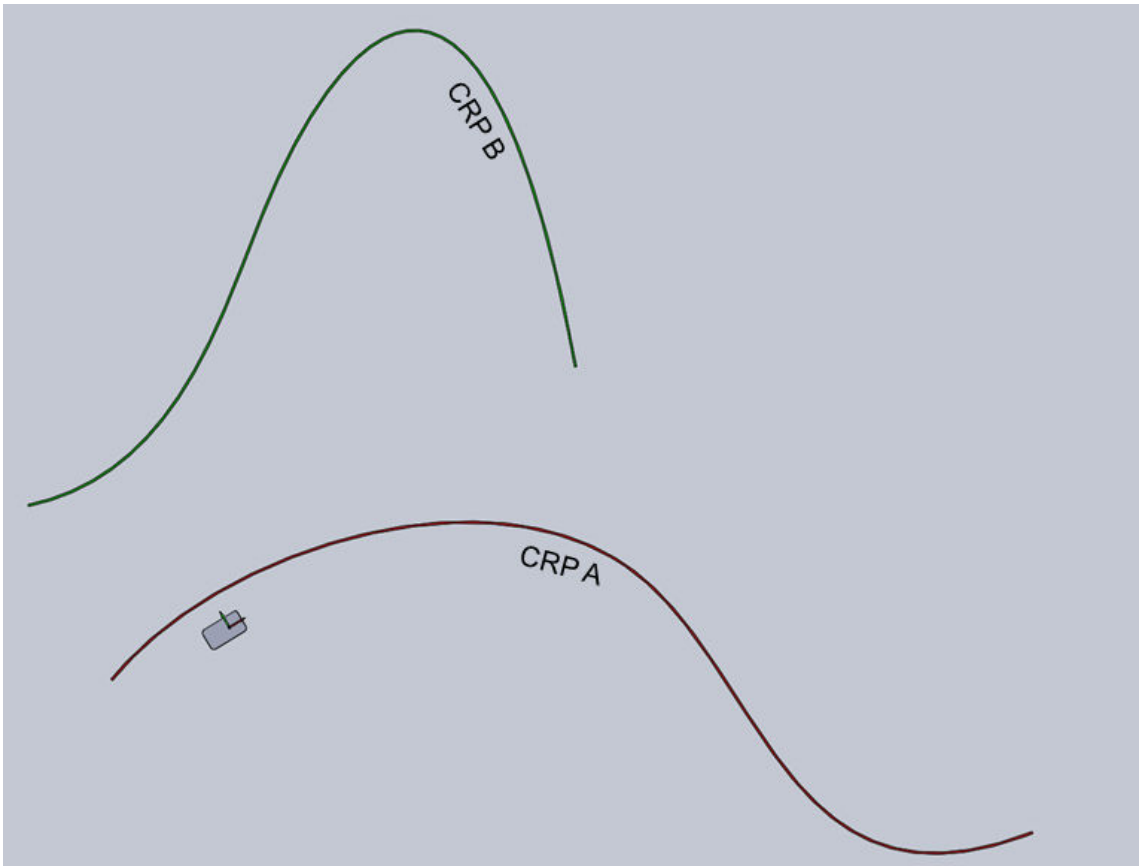


Figure 4.14: Central Reference Path B.



Figure 4.15: Close up view for CRP A and CRP B.



Figure 4.16: Normal of foot pseudo center.



Figure 4.17: Intersection of foot pseudo center normal with CRP A.

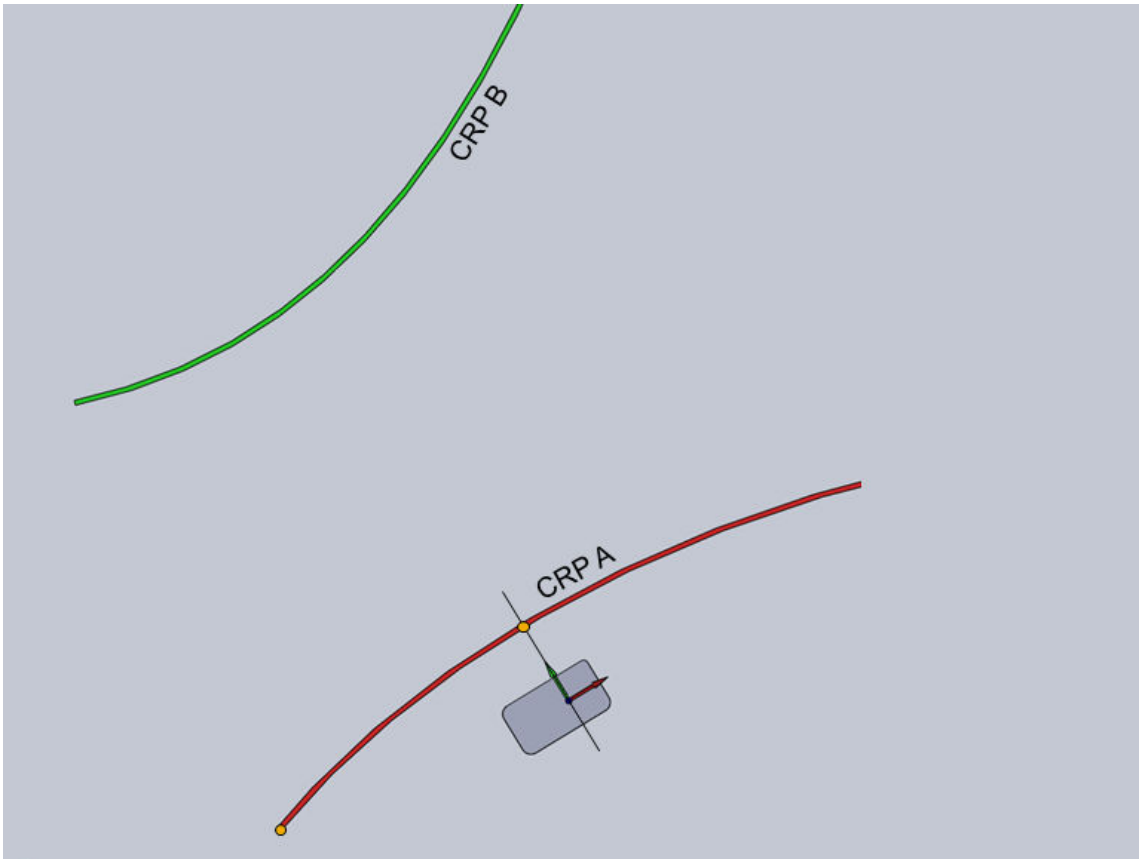


Figure 4.18: Starting point of CRP A.

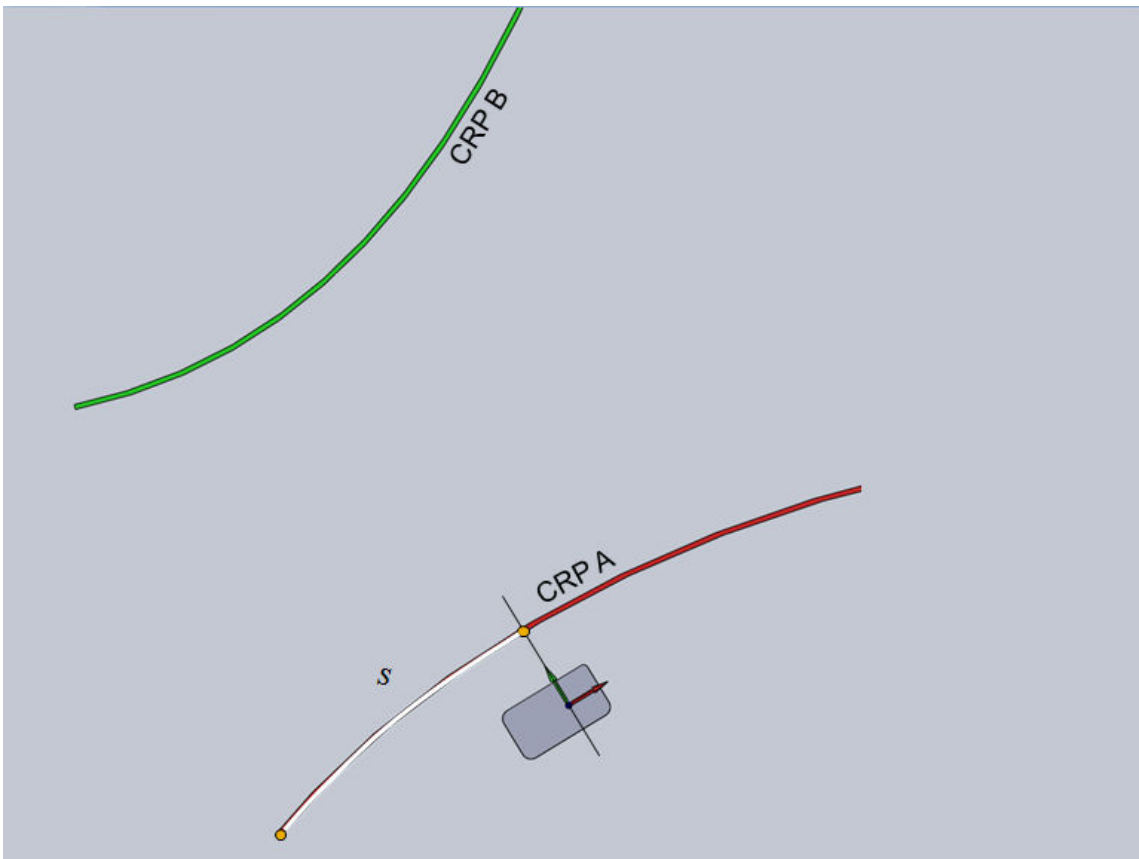


Figure 4.19: Distance s travelled on CRP A.

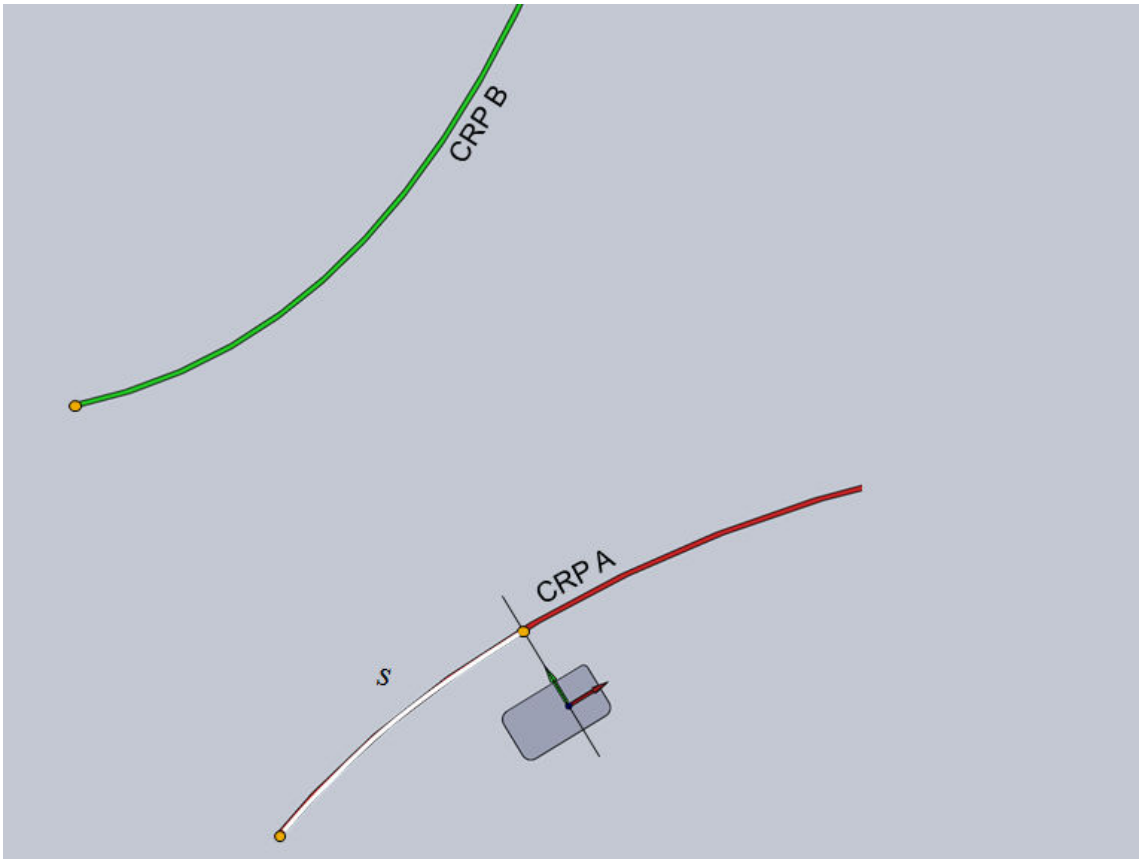


Figure 4.20: Starting point of CRP B.

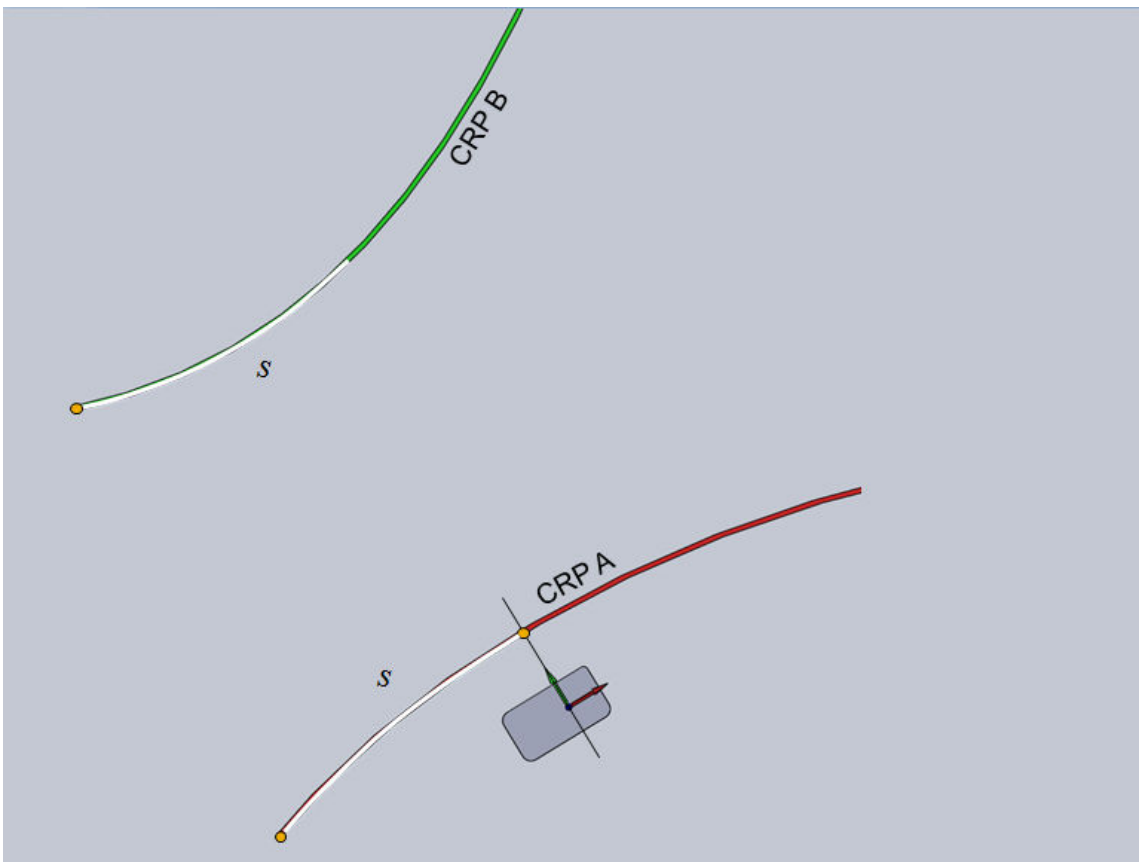


Figure 4.21: Distance s travelled on CRP B.



Figure 4.22: Marking the end point of the travelled distance on CRP B.

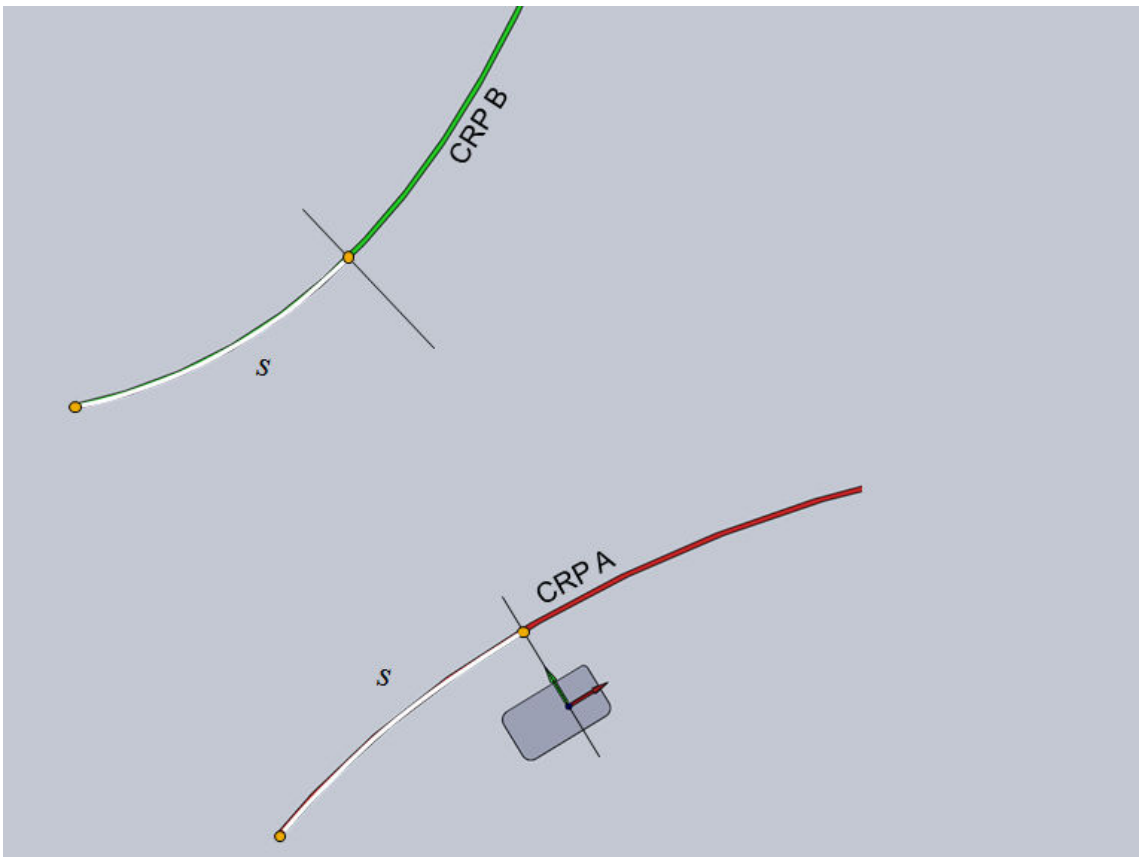


Figure 4.23: Calculating the normal of CRP B at the end point of s .

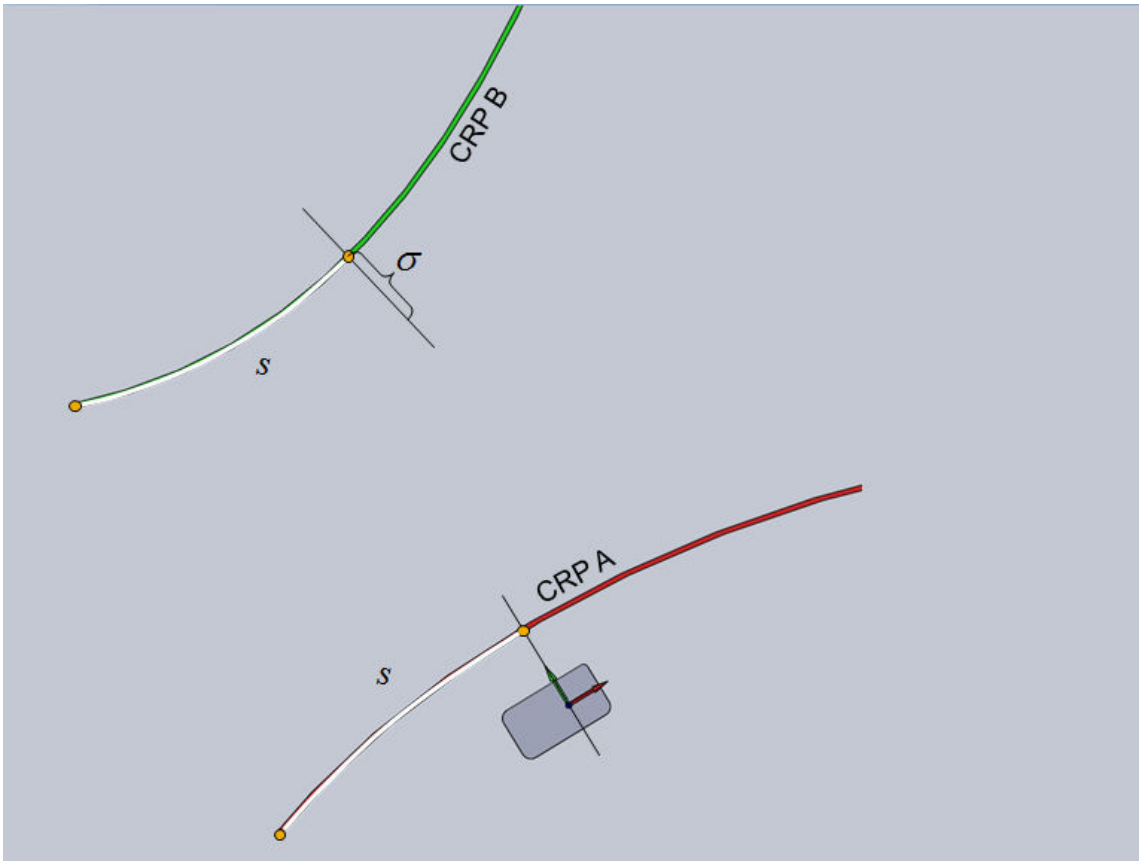


Figure 4.24: σ offset measured on the normal.

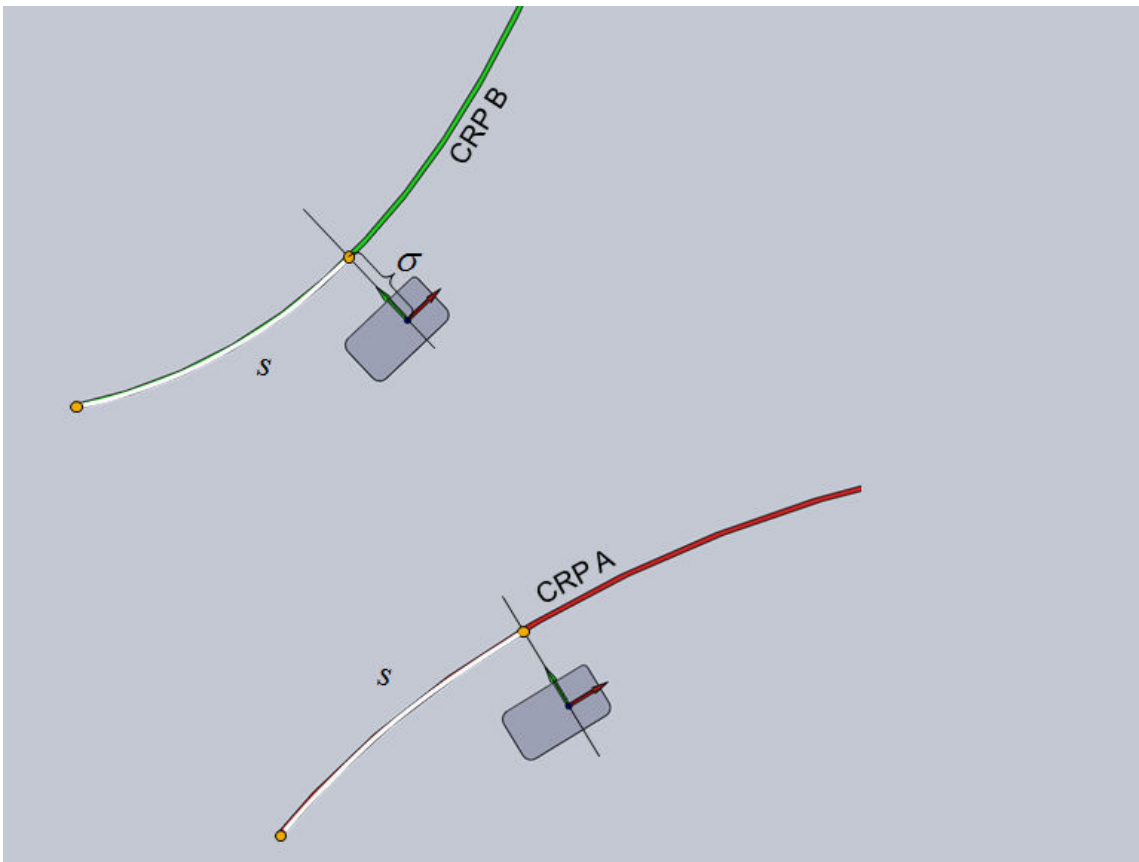


Figure 4.25: Placement of the foot with respect to CRP B.

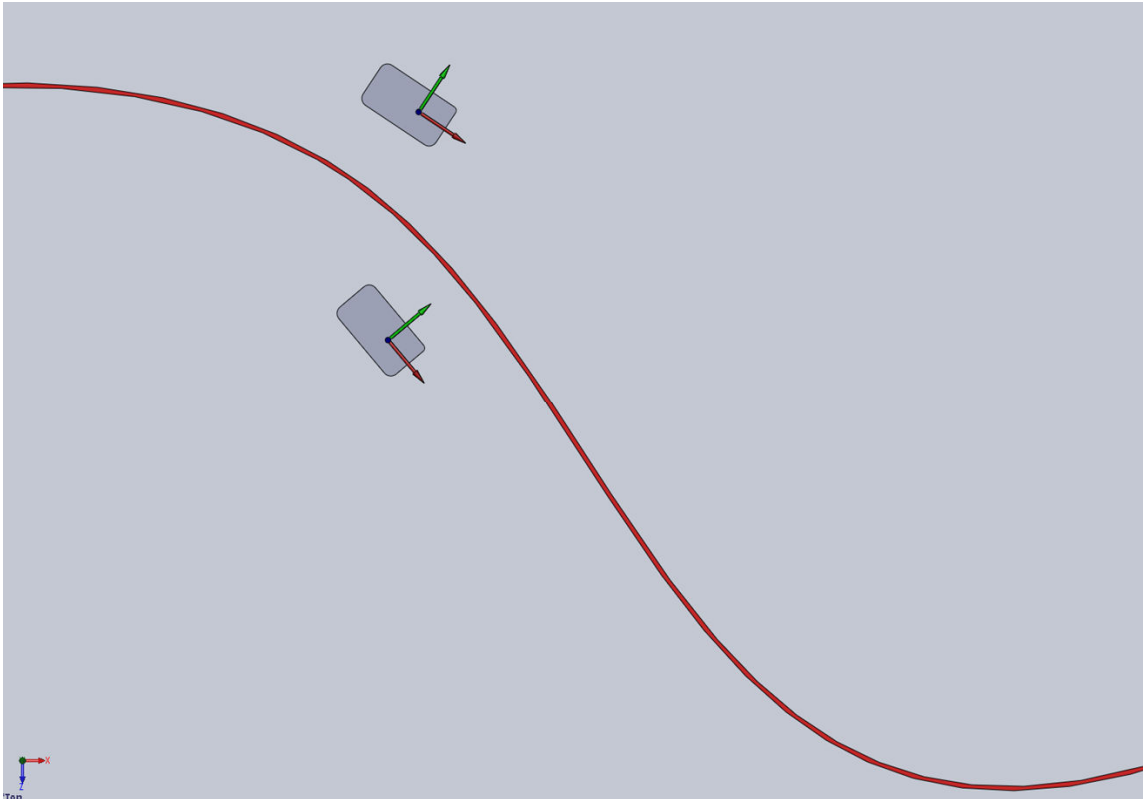


Figure 4.26: A central reference path.

An attractive property of a foot references defined about a certain central reference path is that this reference can easily be mapped onto a walking reference about another central reference path, as is applied in the omnidirectional walking reference design in this thesis.

Among many possible patterns of omnidirectional walk, this thesis concentrates on changing robot walking direction by following a circular arc shaped central reference path. The locomotion capability of a robot which is readily able to walk on straight trajectories can be significantly enriched by mapping the linear central path walk onto a circular arc shaped central reference path walk.

4.3. Mapping a Linear CRP Walk onto a Circular Arc Shaped CRP Walk

Figure 4.27 shows the initial configuration of the robot together with the world coordinate frame. The world coordinate frame is assumed to be below the body

coordinate frame with the z-axes of these two frames coinciding and respective x and y -axes parallelly aligned. The position and orientation references of the feet and the CoM are expressed in the world frame for the straight walk reference described in Section 2.1.

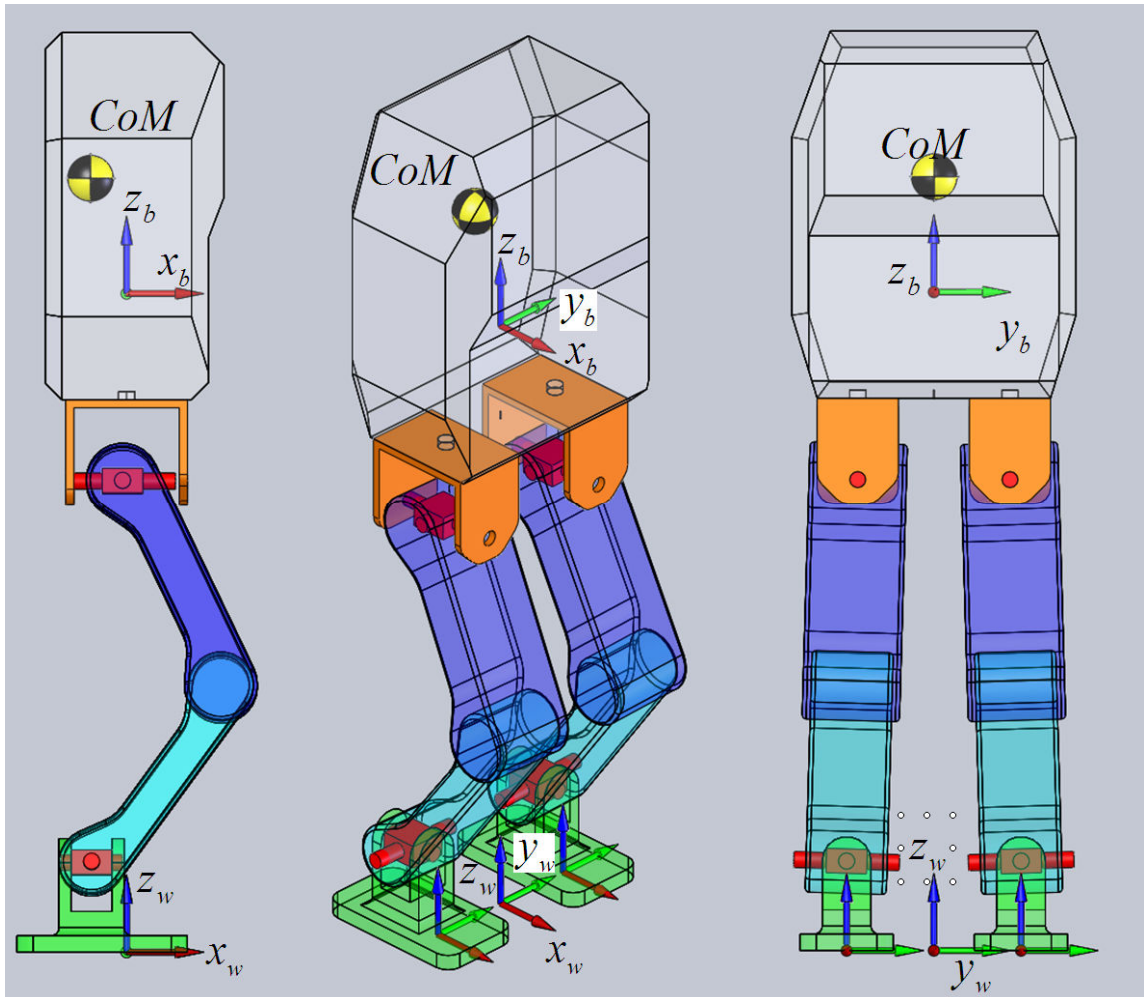


Figure 4.27: The alignment of the world, body right foot pseudo center and left foot pseudo center frames in the initial robot configuration. The axis unit vectors of the pseudo centers are not shown in the figure for the sake of simplicity. The CoM is located off the body coordinate frame center.

In order to obtain a walking reference about a circular arc shaped CRP, the linear CRP walking of Section 4.1 will be exploited. The idea of mapping between linear and arc shaped CRP walking references are illustrated in Figure 4.28. Note from this figure

that the distance $(N - 1)B$ is covered in the linear walk by the body and the foot pseudo centers with this walk where N is the number of swings and B is the step size parameter shown in Figure 4.6. Equivalently, an angle of ψ_{total} is covered at the end of the walk with N swings about the arc shaped CRP. It should also be noted that the initial and final relative configurations of the body frame and the foot pseudo centers are the same. The final position and orientations of the body and foot pseudo centers can be obtained by rotating the body and the feet counterclockwise about the point M located at $[0 \ -r_c \ 0]^T$ by $\psi_{total} \cdot r_c$ is the radius of the arc shaped CRP. The correspondence of the travelled distance and the covered angle has a key role in the linear to arc shaped CRP walk mapping. The following assumptions are made:

- 1) The inputs to the walking reference are the step size parameter B , the number of swings N and the radius r_c .
- 2) The distance traveled on the two CRP's (on the line and or the arc) by the body coordinate frame is the same.

With these assumptions, ψ_{total} can be computed as

$$\psi_{total} = \frac{(N - 1)B}{r_c}. \quad (4.20)$$

Although (20) gives information about the final positions of the body and the feet, it does not produce results for the intermediate references. However, in order to compute them a relation similar to this equation is employed. Before starting their derivation, we should remember which reference variables, as a function of time, and which parameters are readily available from our straight walking reference generation of Section 4.1. (Since only reference variables are considered, the superscript *ref* is dropped for the sake of simplicity in notation.):

- $x_R(t)$: The x -coordinate of the right foot sole Denavit-Hartenberg frame as expressed in the world coordinate frame.
- $x_L(t)$: The x -coordinate of the left foot sole Denavit-Hartenberg frame as expressed in the world coordinate frame.
- $y_R(t)$: The y -coordinate of the right foot sole Denavit-Hartenberg frame as expressed in the world coordinate frame. As indicated in Figure 4.4, this

variable is constant and equal to $-A$, a reference generation parameter which is freely assignable (as long as it is in the leg workspace). Note also that the parameter σ used in the initial robot configuration and CRP definitions is also equal to A . Therefore the identity $y_R(t) = -\sigma$ will be used in the derivations to follow.

$y_L(t)$: The y -coordinate of the left foot sole Denavit-Hartenberg frame as expressed in the world coordinate frame. Similar to the case with $y_R(t)$ the identity $y_L(t) = \sigma$ will be used in the derivations to follow.

$z_R(t)$: The z -coordinate of the right foot sole Denavit-Hartenberg frame as expressed in the world coordinate frame.

$z_L(t)$: The z -coordinate of the left foot sole Denavit-Hartenberg frame as expressed in the world coordinate frame.

$c_x(t)$: The x -coordinate of the CoM as expressed in the world coordinate frame.

$c_y(t)$: The y -coordinate of the CoM as expressed in the world coordinate frame.

$c_z(t)$: The z -coordinate of the CoM as expressed in the world coordinate frame.

This variable is constant at z_c .

s_b^b : The vector from the origin of the body coordinate frame to the CoM, as expressed in the body coordinate frame.

x_{offset} : The initial x -directional position of the foot sole Denavit-Hartenberg frame origins, as expressed in the world coordinate frame.

Also used are the following reference generation parameters:

$p_{R_0}^{R_0}$: The vector from the origin of the body coordinate frame to the origin of the right hip frame, as expressed in the right hip coordinate frame.

$p_{L_0}^{L_0}$: The vector from the origin of the body coordinate frame to the origin of the right left hip frame, as expressed in the left hip coordinate frame.

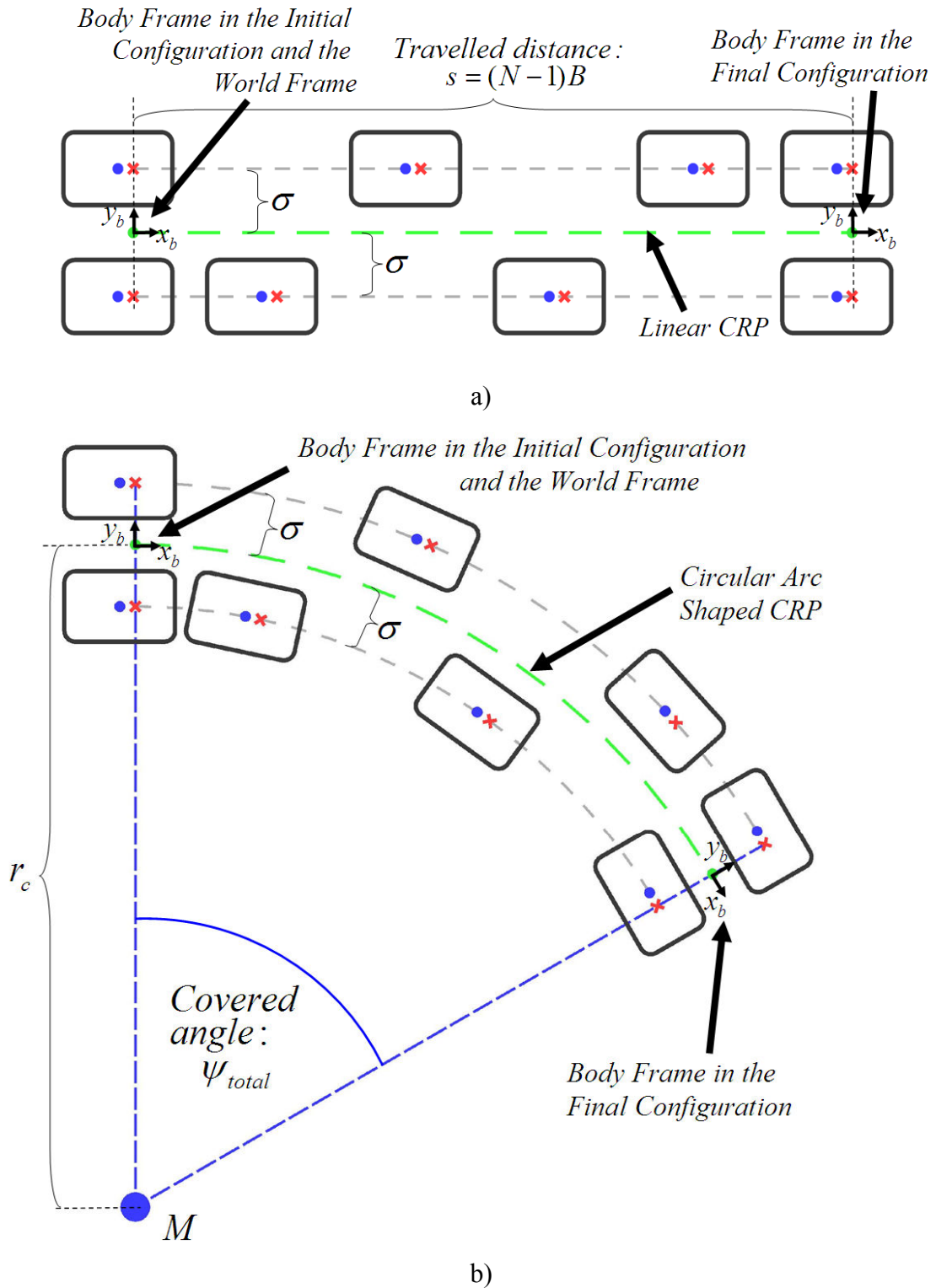


Figure 4.28: Mapping of foot placement locations of a linear CRP walk onto the foot placement locations of a circular arc shaped CRP walk. a) The linear CRP walk b) Circular arc CRP walk.

In the following, the position and orientation references will be obtained for the foot sole Denavit-Hartenberg coordinate frames with respect to the the hip frames. This kind of reference information can easily be converted into joint position references via inverse kinematics.

Firstly, the assumption of projecting linearly travelled distance to the distance travelled on the arc will be exploited to compute instantaneous positions of the body and foot pseudo centers, as expressed in the world coordinate frame. This requires the computation of the linear-walk body position in the x direction:

$$x_b(t) = c_x(t) - s_{b_x}^b. \quad (4.21)$$

The instantaneous angle covered by the body on the arc is then

$$\psi_b(t) = \frac{x_b(t)}{r_c} \quad (4.22)$$

Assuming that the the body keeps its orientation constant and parallel to the world frame, in the linear walk, for a laterally symmetric weight distributed robot the body coordinate frame y -coordinate is the same as that on the CoM:

$$y_b(t) = c_y(t). \quad (4.23)$$

$y_b(t)$ defines the distance to the linear CRP. We keep this definition the same for the arc shaped CRP too. Note also that with the body orientation assumption made above the body x -axis is parallel to the linear CRP at all times. Carrying out this parallelity assumption to the arc shaped CRP walk defines the body orientation in the arc walk. Referring, to Figure 4.29 we have

$$R_{warc}^b = \begin{bmatrix} \cos(-\psi_b) & -\sin(-\psi_b) & 0 \\ \sin(-\psi_b) & \cos(-\psi_b) & 0 \\ 0 & 0 & 1 \end{bmatrix}. \quad (4.24)$$

Here, the subscript *arc* indicates that the orientation matrix is computed for the arc walk. From the same figure, the modified coordinates for the body frame center for the arc walk are then computed as

$$x_{b_{arc}} = [r_c + y_b(t)]\sin(\psi_b(t)) \quad (4.25)$$

and

$$y_{b_{arc}} = [r_c + y_b(t)]\cos(\psi_b(t)) - r_c. \quad (4.26)$$

The z -directional component of the body position can be computed from the CoM position as

$$z_b(t) = c_z(t) - s_{b_z}^b. \quad (4.27)$$

Since the walking direction does not change the body height, we can state that

$$z_{b_{arc}}(t) = z_b(t) \quad (4.28)$$

Defining the three-dimensional body position vector as

$$\mathbf{d}_{warc}^b = \begin{bmatrix} x_{b_{arc}} \\ y_{b_{arc}} \\ z_{b_{arc}} \end{bmatrix}, \quad (4.29)$$

the right hip frame position in the world coordinate frame is obtained by

$$\mathbf{d}_{warc}^{R0} = \mathbf{d}_{warc}^b + R_{warc}^b \mathbf{p}_{R0}^{R0}. \quad (4.30)$$

Similarly the left hip position is

$$\mathbf{d}_{warc}^{L0} = \mathbf{d}_{warc}^b + R_{warc}^b \mathbf{p}_{L0}^{L0} \quad (4.31)$$

The orientations of the hip frames are the same as that of the body frame as the three frames are rigidly and paralelly attached to the robot body:

$$R_{warc}^{R0} = R_{warc}^{L0} = R_{warc}^b. \quad (4.32)$$

Similar to (21), the distance travelled by the right foot pseudo center in the linear walk is

$$x_{Rp} = x_R(t) - x_{offset} \quad (4.33)$$

and the corresponding instantaneous angle covered by it in the arc walk can be computed as

$$\psi_{Rp}(t) = \frac{x_{Rp}(t)}{r_c}. \quad (4.34)$$

Almost identically, the instantaneous angle covered by the left foot in the arc walk is

$$\psi_{Lp}(t) = \frac{x_{Lp}(t)}{r_c}, \quad (4.35)$$

where $x_{Lp}(t)$ is obtained by

$$x_{Lp} = x_L(t) - x_{offset}. \quad (4.36)$$

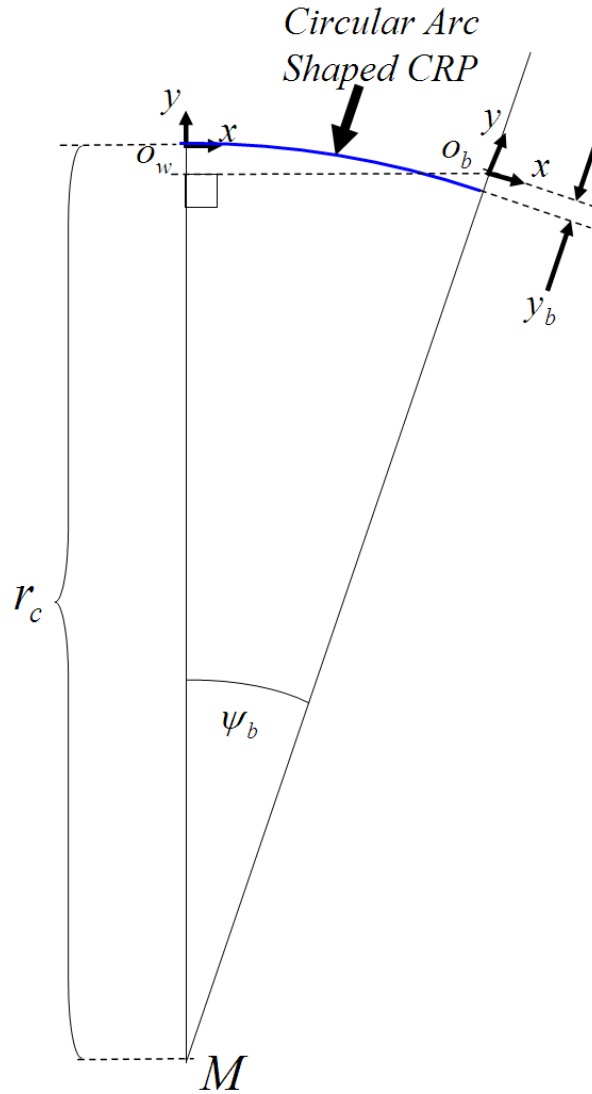


Figure 4.29: Geometry of the computation of the body frame origin position on the arc walk.

Using (34) and Figure 4.30, the right foot pseudo center position is computed as

$$d_{walk}^{Rp} = \begin{bmatrix} [r_c - \sigma] \sin(\psi_{Rp}(t)) \\ [r_c - \sigma] \cos(\psi_{Rp}(t)) - [r_c - \sigma] \\ z_R(t) \end{bmatrix}. \quad (4.37)$$

Note that the z -directional references for the feet do not change when the walking direction changes. This fact is used in (37). The orientation reference for the right foot pseudo center frame with the CRP orientation assumption in the previous section is

$$R_{warc}^{Rp} = \begin{bmatrix} \cos(-\psi_{Rp}) & -\sin(-\psi_{Rp}) & 0 \\ \sin(-\psi_{Rp}) & \cos(-\psi_{Rp}) & 0 \\ 0 & 0 & 1 \end{bmatrix} \quad (4.38)$$

The right foot sole Denavit-Hartenberg frame center position reference is obtained then by

$$d_{warc}^{R6} = d_{warc}^{Rp} + R_{warc}^{Rp} \begin{bmatrix} x_{offset} \\ 0 \\ 0 \end{bmatrix} \quad (4.39)$$

The computation of the left foot pseudo center position as expressed in the world frame is similar to (37) and it uses Figure 4.31:

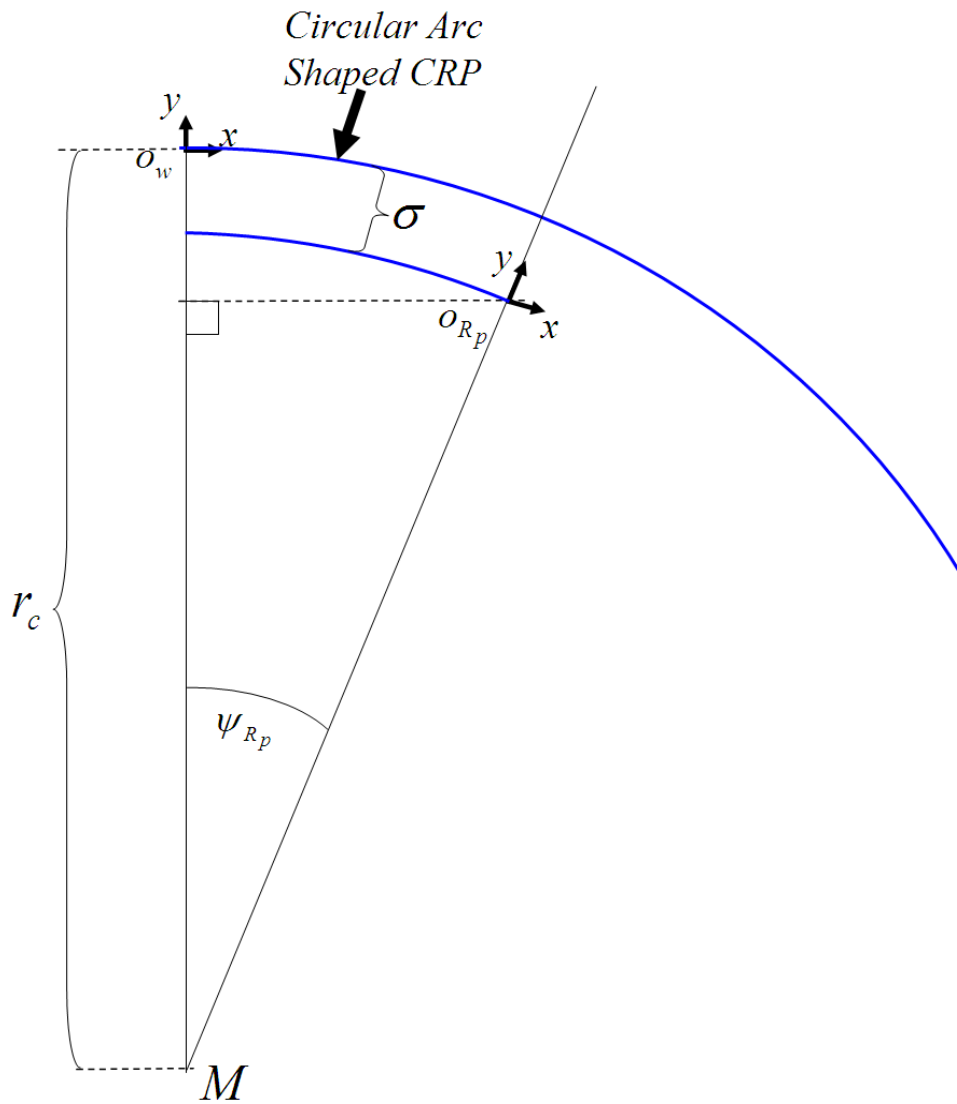


Figure 4.30: Geometry of the computation of the right foot pseudo center position on the arc walk.

$$d_{warc}^{Lp} = \begin{bmatrix} [r_c + \sigma] \sin(\psi_{Lp}(t)) \\ [r_c + \sigma] \cos(\psi_{Lp}(t)) - [r_c + \sigma] \\ z_L(t) \end{bmatrix}. \quad (4.40)$$

The left foot pseudo center frame orientation is

$$R_{warc}^{Lp} = \begin{bmatrix} \cos(-\psi_{Lp}) & -\sin(-\psi_{Lp}) & 0 \\ \sin(-\psi_{Lp}) & \cos(-\psi_{Lp}) & 0 \\ 0 & 0 & 1 \end{bmatrix} \quad (4.41)$$

and the Denavit-Hartenberg frame center at the left foot sole is obtained by

$$d_{warc}^{L6} = d_{warc}^{Lp} + R_{warc}^{Lp} \begin{bmatrix} x_{offset} \\ 0 \\ 0 \end{bmatrix} \quad (4.42)$$

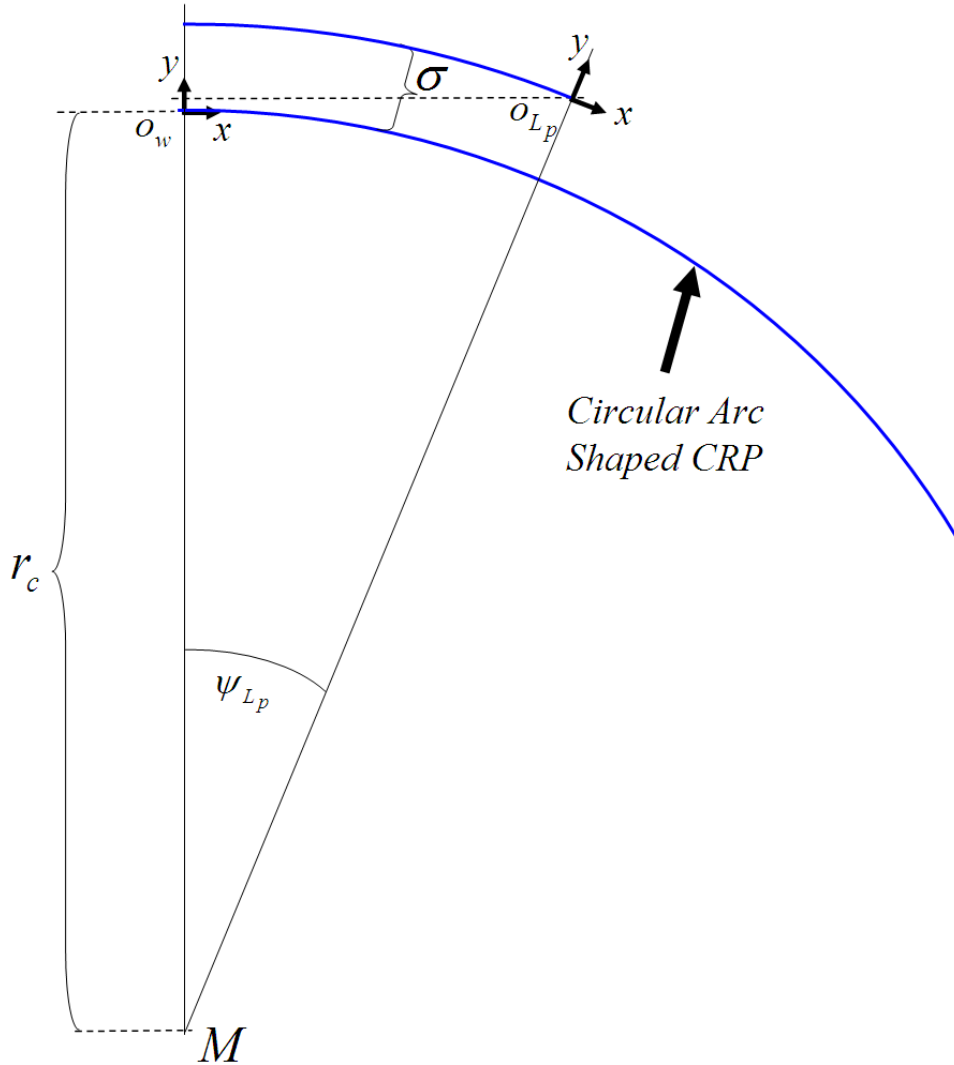


Figure 4.31: Geometry of the computation of the left foot pseudo center position on the arc walk.

Having obtained the hip and sole frame position and orientation references as expressed in the world frame, what is left before inverse kinematics can be employed is the compute the sole references in the hip frames. The position reference for the right foot is

$$d_{R0_{arc}}^{R6} = \left(R_{warc}^{R0} \right)^T \left[d_{warc}^{R6} - d_{warc}^{R0} \right]. \quad (4.43)$$

The left foot position reference is obtained by a similar expression:

$$d_{L0_{arc}}^{L6} = \left(R_{warc}^{L0} \right)^T \left[d_{warc}^{L6} - d_{warc}^{L0} \right] \quad (4.44)$$

The orientation references for the right and left foot sole Denavit-Hartenberg frames are computed by

$$R_{R0_{arc}}^{R6} = \left(R_{warc}^{R0} \right)^T R_{warc}^{R_p} R_{R_p}^{R6} \quad (4.45)$$

and

$$R_{L0_{arc}}^{L6} = \left(R_{warc}^{L0} \right)^T R_{warc}^{L_p} R_{L_p}^{L6} \quad (4.46)$$

With the configuration in Figure 4.10, the matrices are $R_{R_p}^{R6}$ and $R_{L_p}^{L6}$ are

$$R_{R_p}^{R6} = R_{L_p}^{L6} = \begin{bmatrix} 0 & 0 & 1 \\ 0 & 1 & 0 \\ -1 & 0 & 0 \end{bmatrix}. \quad (4.47)$$

This completes the preparation of the position and orientation references for the six-dof-sole coordinate frames. Figure 4.32 shows the model of SURALP on an arc walk.

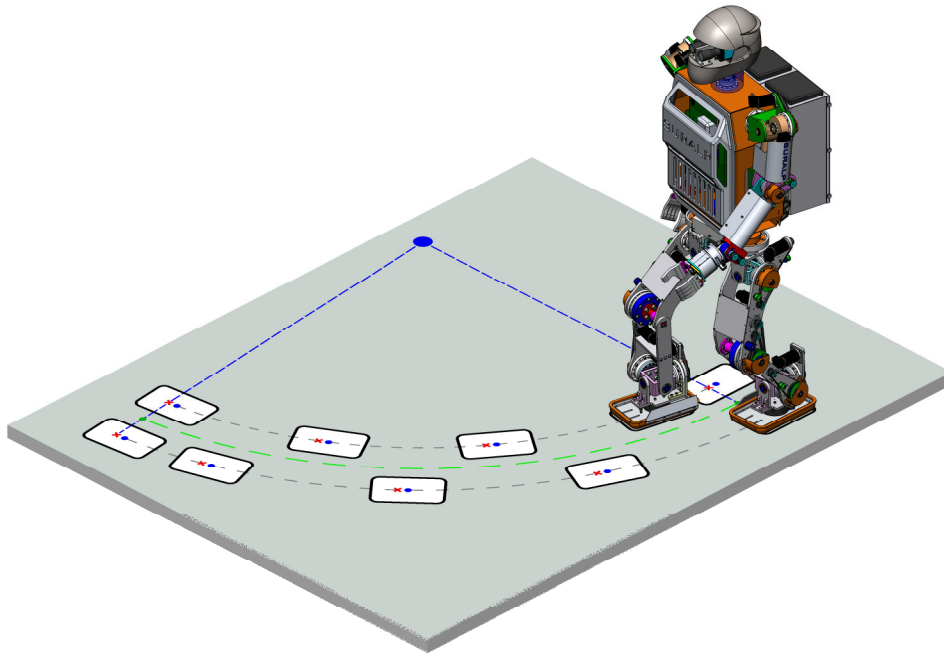


Figure 4.32: SURALP CAD model on a circular arc shaped CRP walking trajectory.

Chapter 5

5. WALKING CONTROL ON INCLINED PLANES WITH FUZZY PARAMETER ADAPTATION

5.1. Straight Walking Control Methods of SURALP

Although, the walking reference trajectory generation is essential for a stable walk in bipedal robots research area, employment of proper controllers is at least as important for the achievement of a stable gait. A number of controller strategies were employed for the stability of SURALP for a straight walking path [52]. In this subsection, these controllers are reviewed for the sake of completeness.

Independent joint PID controllers are employed and the controller gains are obtained via trial and error. The first controller to be reviewed is the foot orientation control. In [22] landing orientation controllers are proposed for the ankle joints. This approach assumes that two joints with coinciding joint axes perpendicular to each other are present at ankles. The scheme computes joint angle reference modifications in such a way that the feet are aligned parallel to the ground when they are in contact with the ground. The reference modification law in [22] is the form of a first order filter applied on the foot to ground contact torques. This method was adopted for our control system too. For the roll axis of the ankle, we employ the following reference modification law in the Laplace domain.

$$\bar{\theta}_{roll}(s) = \theta_{roll}(s) + \frac{K_{roll}}{s + \lambda_{roll}} T_{roll}(s) \quad (5.1)$$

where s is the Laplace variable. θ_{roll} is the roll joint reference angle computed from the inverse kinematics with CoM reference input. $\bar{\theta}_{roll}$ is the reference angle after the

reference modification. T_{roll} is the torque about the roll axis due to the interaction of the foot with the ground. T_{roll} is measured by torque sensors positioned at the ankle. K_{roll} and λ_{roll} are low pass filter constants which are determined by trial and error in our approach. In the digital implementation, the Laplace domain transfer function in (5.1) is approximated by a difference equation. We used Tustin's approximation technique to obtain the difference equation. When the foot is in contact with the ground only with a corner or an edge, a torque is developed and with the application of (5.1), the joint angle references are modified in such a way to turn the ankle to achieve foot orientation parallel to the ground.

Another important problem in achieving stable walking is the impact generated at the landing of the swing foot. As a solution, [23] suggests the application of a shock absorber control law. This control law is activated when the swing foot lands earlier than planned in the reference generation. In effect, a virtual mass-spring-damper system is positioned between the hip and ankle. Inspired by this idea, we employed the ground impact compensation controller, which uses the following second order relation to modify the distance between the hip and sole of the landing foot.

$$\bar{l}(s) = l(s) - \frac{1}{m_l s^2 + b_l s + k_l} F_z(s) \quad (5.2)$$

In (5.2) l represents the hip-to-sole distance reference obtained from Cartesian foot reference trajectories. \bar{l} is its shock absorber modified version. F_z is the z direction component of the ground interaction force acting on the foot. Again, ankle force sensors measure this force. m_l , b_l and k_l are the desired mass, damping and stiffness parameters of the mechanical impedance relation described in (5.2). Our impact compensator is triggered with any landing (not just for the early landing) of the foot. It is deactivated after a certain time specified by the control designer. In our case we used a 0.4 seconds activation time. However, at the end of this activation time the hip-to-sole distance is no more equal to its original value. In order to resume the hip-to-sole distance, which is originally planned in the reference generation process, at the end of the impact compensation phase the following relation is employed:

$$\bar{l}(t) = l(t) - 0.5(l(t_0) - \bar{l}(t_0))(1 + \cos((t_0 - t)\omega_{return})) \quad (5.3)$$

t_0 is the time at the end of the impact compensation phase. By (5.3), beginning with the final \bar{l} value of the impact compensation phase, \bar{l} returns to the original reference value l after a smooth transient behavior. ω_{return} is a parameter which determines the speed of return of \bar{l} to l . As in the case of (5.1), Tustin's approximation of the continuous relation is obtained and applied for (5.2) and (5.3) too. The reference modification laws, (5.1), (5.2) and (5.3) are applied to the two legs independently.

The irregularities and disturbances on the walking surface or the inclination angle of the robot upper body might cause a difference in the landing time for the swing foot from the given reference. This is called an early landing. This case should be analyzed and solved since when a swung foot is on the ground before the planned beginning of the double support phase, it will go on moving forward. At the same time the supporting foot will move backward in a trunk based coordinate system. In effect, the two feet on the ground will try to push the robot trunk in two different directions. The feet will slip, the robot will turn and possibly loose its balance. This condition is spotted when a force value greater than a threshold value is observed in the landing phase of a swing foot by using the force/torque sensors at the ankles. The early landing modification scheme locks the references of the foot in the body coordinate frame keeping them parallel to each other in the early landing situation. The feet will not move forward and the slipping of the robot is blocked.

5.2. Fuzzy Logic Control Methods

One of the most challenging problems in this field is the robust balance of the walk, not only on even floor but on surfaces with irregularities and slopes too. Inclined planes pose a very typical floor condition encountered in human daily life. Usually such planes are a part of the city environment. However, the indoor floors are not perfectly even either. In this thesis, as a second contribution to omnidirectional walking reference generation proposed in the previous chapter, fuzzy logic parameter adaptation control method for biped walking robots is proposed. The proposed controllers are used in both straight and omnidirectional walking patterns. Experimental results indicate that these control techniques enabled SURALP to climb onto an inclined plane with inclination angle of 5.6 degrees. In this chapter, the details of the implemented fuzzy logic controllers are explained.

5.2.1. Fuzzy Adaptive Pitch Tilt Control

Figure 5.1 shows a typical biped robot walking on flat floor and on inclined planes with changing slopes. The motion of the robot is defined in a fixed coordinate frame, called the world frame. The robot walking direction coincides with the x-direction of the world frame. Another frame is attached at the pelvis link of the robot. This link can be considered as a “central” one since the legs and possibly waist links are connected to the pelvis. Initially (before the start of the walk), the pelvis frame axes are aligned parallel with the corresponding world frame axis. However, this parallel alignment changes during the walk due to various effects including gravitational forces, foot to ground interaction, changing slopes and coupling effects between the links.

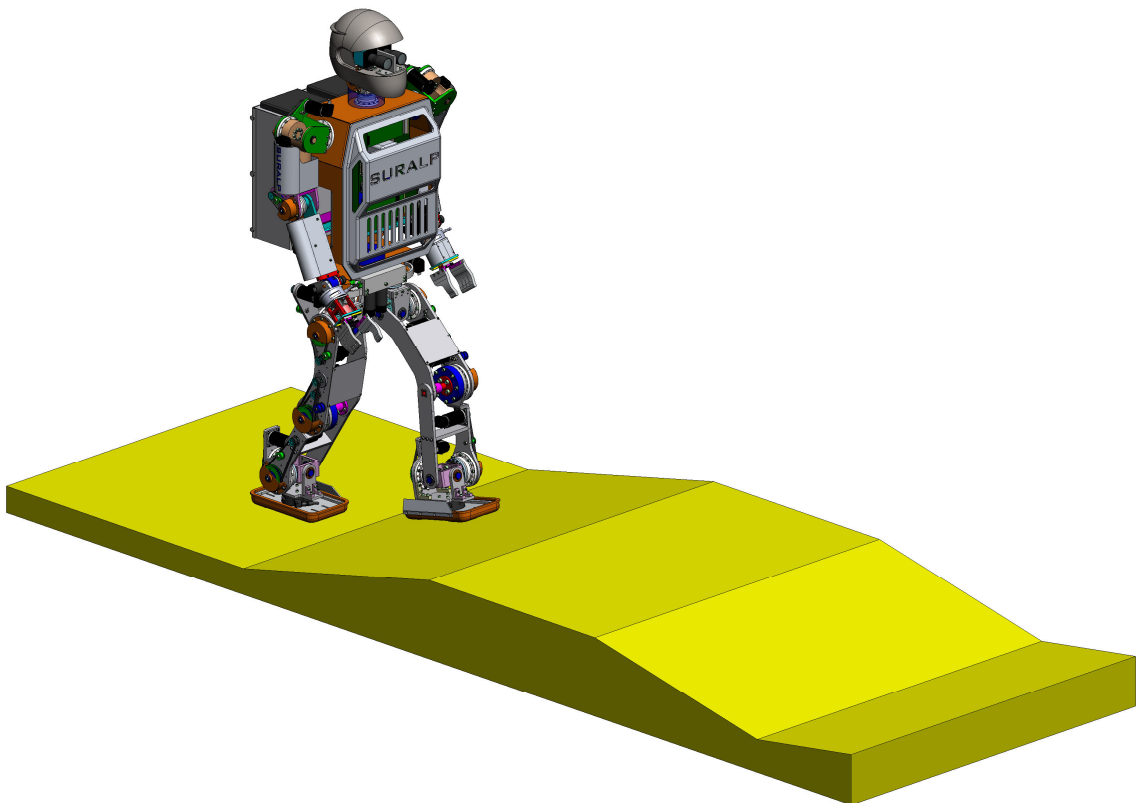


Figure 5.1: Bipedal robot walk on changing slopes

The pelvis pitch angle which is the angle the z-axis of the pelvis frame makes with a vertical line is an indicator of the balance of the walk. Assuming that a gait with zero pelvis pitch angle is planned in the reference generation, the online measurement of this angle can provide feedback indicating whether the robot is following this reference. It can also detect a falling forward or backward. However, our simulation and experimental results suggest that the pelvis pitch angle is oscillating during the walk. Even in a steady and stable walk the pelvis pitch angle trajectory can be in the form of a periodic signal with peak values of a few degrees. Therefore, a single measurement of the angle can be misleading in deciding upon the balance condition of the robot. In order to infer whether the robot goes on with a steady walking pattern or is in the trend of falling, the average rather than the instantaneous value of the pelvis pitch angle is more suitable. Averaging can be done in many different ways. One question to be answered is related to the length of the averaging window. Another concern is the sampling period for the data to be averaged. Usually, joint space controller sampling times of one to ten milliseconds are employed in robotic applications. Using a long averaging window from the current sampling instant back with a low sampling period in the order of the joint control sampling period would require large storage space and consume online computational resources. There is a trade-off in the accuracy of the averaging computation and the efficient use of the computational power. Employing the number of samples N used in the average computation and the pelvis pitch angle sampling period T_p as design parameters, the average value $\bar{\beta}_{pitch}$ of the pelvis pitch angle β_{pitch} in Figure 5.2 is computed as;

$$\bar{\beta}_{pitch}(kT_p) = \frac{1}{N} \sum_{l=0}^{N-1} \beta_{pitch}((k-l)T_p) \quad (5.4)$$

where k is the sampling index. In addition to the average value of β_{pitch} , the frequency and size of the oscillations of this angle are also indicators of the stability of the walk. Measurements during experiments with bipedal robots indicate that the frequency and peak values of the angle change drastically when encountered disturbances like irregularities on the floor, slope changes or external forces applied to the robot body. The following pelvis pitch angle activity indicator (or measure of the oscillatory behavior), inspired from the sliding mode robot position control chattering indicator in [53-55] and denoted by Γ_{pitch} , is suggested in this controller design.

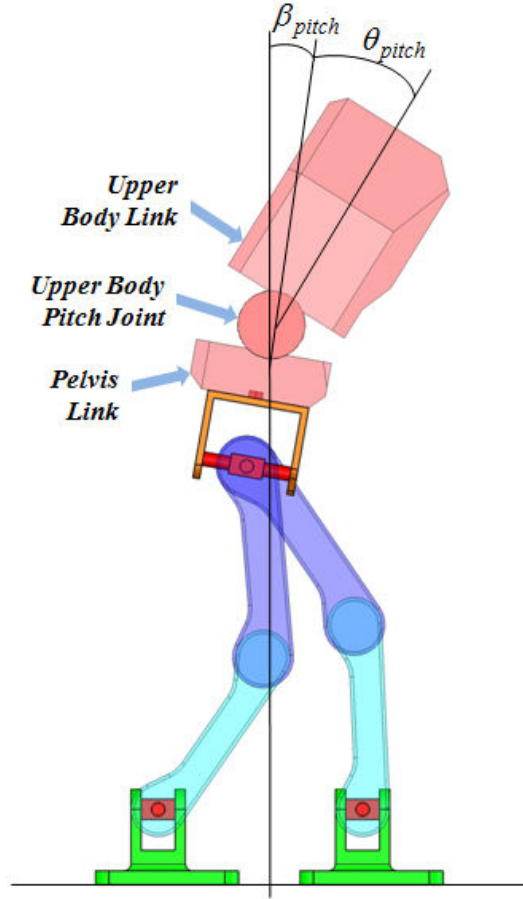


Figure 5.2: Legs, pelvis and the upper body

$$\Gamma_{pitch}(kT_p) = \sum_{l=0}^{N-1} \left| \beta_{pitch}((k-l)T_p) - \beta_{pitch}((k-l-1)T_p) \right| \quad (5.5)$$

In (5.5), $|\cdot|$ signifies the absolute value function.

Among many actions which can enhance the stability during the walk, one of the proposed methods in this thesis is the online adjustment of the body pitch angle (the angle θ_{pitch} shown in Figure 5.2) parameter. Note that, while β_{pitch} is an angle between a link (pelvis) of the robot and the environment (a vertical line), θ_{pitch} is an angle between two links (pelvis and upper body) of the robot. In other words, β_{pitch} is a measured parameter which, due to the underactuation between the robot feet and the ground surface, can only be controlled indirectly, whereas θ_{pitch} can be controlled directly and accurately via a joint position controller. [56] uses this angle as a balance control variable for a 2D (sagittal plane) biped model. One of the benefits of increasing this angle is an addition to the robot moment of inertia about the yaw axis (pelvis frame

z-axis) by moving some percentage of the robot weight far from this axis. In this way, disturbance torques due to foot swing motion and foot-ground interaction have a more diminished effect on the rotary motion about the yaw axis. Yaw moment compensation techniques using this fact are studied in [57]. Bending the body forward or stretching backward moves the CoM of the robot forward and backward, respectively. The location of the CoM with respect to the support polygon determines static stability, whereas the time history of the CoM determines the location of the ZMP, the location of which is a widely used stability criterion for biped robots.

Motivated by these significant effects of the body pitch angle on the balance of the robot, a fuzzy logic system which adjusts this parameter online by evaluating the average $\bar{\beta}_{pitch}$ of the pelvis pitch angle and the activity Γ_{pitch} of this angle as its inputs, is developed.

The main idea of the parameter adaptation system can be summarized as below.

(i) When high levels of pelvis pitch activity Γ_{pitch} is observed, the upper body should be rotated forward (by increasing the body pitch angle θ_{pitch} between the pelvis and the upper body) to counter disturbance effects.

(ii) The body pitch angle θ_{pitch} should be decreased if the pelvis pitch activity Γ_{pitch} is low. This is since, ideally, an upright posture is preferred for the upper body in many tasks. This study regards the upright posture as the default one, and if no disturbing effects are observed the robot should return to its default upper body orientation mode.

The guidelines (i) and (ii) on their own can be used to devise body pitch angle adjustment methods. However, these two guidelines use only the information about the pelvis pitch activity in the system. Another source of valuable information is the average $\bar{\beta}_{pitch}$ of the pelvis pitch angle. The following guidelines describe the role of $\bar{\beta}_{pitch}$ in the body pitch angle adjustment.

(iii) When the average value of pelvis pitch angle is positive, assuming that a flat pelvis trajectory is planned, we can infer that this is a posture inclined to a fall towards front, to the walking direction. In this case, the body pitch angle should be decreased (and even made negative) to compensate for the gravity effect of the forward leaned pelvis link.

(iv) In a similar way to the guideline 3 above, when the average value of pelvis pitch angle is negative, the body pitch angle should be increased to compensate for the gravity effect of the backward leaned pelvis link.

The four guidelines above can be used in various ways to construct a tuning mechanism for θ_{pitch} . An analytic relation between $\bar{\beta}_{pitch}$, Γ_{pitch} and θ_{pitch} could be one of the choices. The method proposed in this thesis employs fuzzy systems for the online tuning of θ_{pitch} . Fuzzy systems are natural choices to exploit verbal descriptions (like the four guidelines above) of the plant or problem to obtain control or adaptation mechanisms. Table 5.1 and Figure 5.3 describe the nine fuzzy rules used in the tuning. In Table 5.1 the subscript “P1” of the rule strength θ_{P1} stands for positive small. “ θ_{P2} ” is also positive and small, however, it is bigger than θ_{P1} . θ_{P3} is bigger than θ_{P2} . Similarly defined are θ_{P4} and θ_{P5} with increasing magnitudes. ZZ symbolizes “zero” and N1 is negative small. The numerical values of the rule strengths and the corner positions of the trapezoidal membership functions in Figure 5.3 are tabulated in the next chapter along with experimental results.

The rules are summarized in Table 5.1. An example for a rule is given below as:

Rule 11: If Γ_{pitch} is small and $\bar{\beta}_{pitch}$ is negative, then θ_{pitch} is positive of grade 3 (θ_{P3}).

Table 5.1: The Fuzzy Rule Base

		Γ_{pitch}		
		Small Γ_{pitch}	Medium Γ_{pitch}	Big Γ_{pitch}
$\bar{\beta}_{pitch}$	Negative $\bar{\beta}_{pitch}$	θ_{P3} <i>Rule 11</i>	θ_{P4} <i>Rule 12</i>	θ_{P5} <i>Rule 13</i>
	Zero $\bar{\beta}_{pitch}$	θ_{P1} <i>Rule 21</i>	θ_{P2} <i>Rule 22</i>	θ_{P4} <i>Rule 23</i>
	Positive $\bar{\beta}_{pitch}$	θ_{N1} <i>Rule 31</i>	θ_{ZZ} <i>Rule 32</i>	θ_{P2} <i>Rule 33</i>

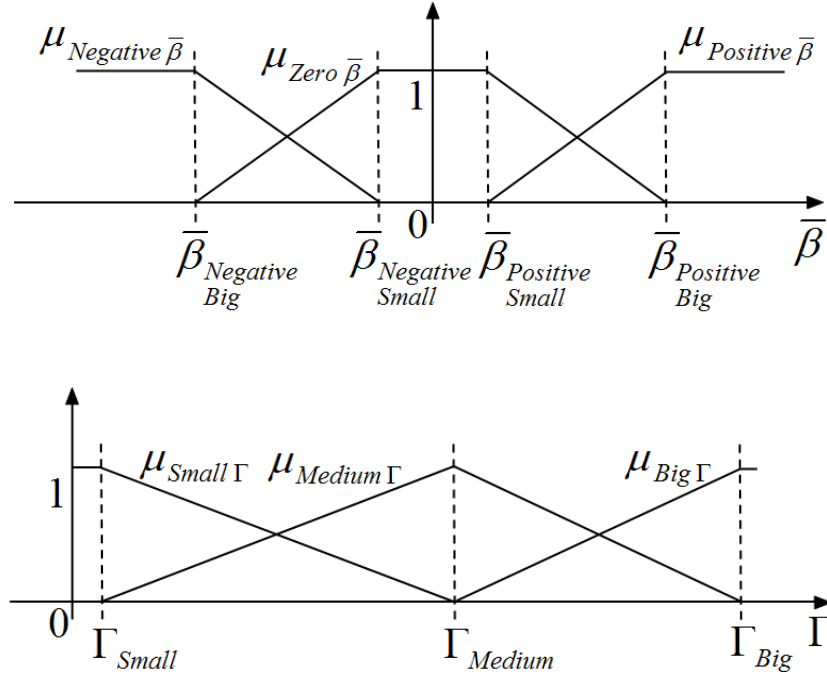


Figure 5.3: The membership functions

The choice of the rule base and the membership functions satisfies the conditions (i) - (iv) above. The truth value of a rule is obtained by multiplying the membership values of Γ_{pitch} and $\bar{\beta}_{pitch}$ fuzzy sets involved in the rule. For example, from Table 5.1, the truth value of Rule 11, denoted by w_{11} , is computed as

$$w_{11} = \mu_{Small \Gamma}(\Gamma_{pitch}) \mu_{Negative \bar{\beta}}(\bar{\beta}_{pitch}) \quad (5.6)$$

In general, the truth value of rule Rule ij is denoted by w_{ij} and computed in a way similar to the computation of w_{11} . Let the rule strength matrix Θ be defined from Table 5.1 as;

$$\Theta = \begin{bmatrix} \theta_{p3} & \theta_{p4} & \theta_{p5} \\ \theta_{p1} & \theta_{p2} & \theta_{p4} \\ \theta_{N1} & \theta_{ZZ} & \theta_{p2} \end{bmatrix} \quad (5.7)$$

Using this matrix, the defuzzification is carried out by the expression

$$\theta_{pitch} = \frac{\sum_{i=1}^3 \sum_{j=1}^3 w_{ij} \Theta_{ij}}{\sum_{i=1}^3 \sum_{j=1}^3 w_{ij}} \quad (5.8)$$

This function characterizes a fuzzy system with singleton fuzzification, product inference rule and center average defuzzifier. As mentioned above the computed θ_{pitch} value is applied as the reference angular position of the joint between the pelvis and upper body links. However there is an important practical consideration: What if the robot does not possess a pitch joint between its pelvis and upper body?

The kinematic arrangement of SURALP does include a waist yaw axis; however no pitch axis is present. There are many other examples of robots which do not feature a pitch joint between the pelvis and the upper body. A method which enables the application of the adaptation mechanism to humanoids without such a joint is introduced. Actually, the method is a general one and can be employed in any control technique which uses the pitch joint between the pelvis and the upper body. The idea of the method is based on the introduction of a virtual pelvis link illustrated in Figure 5.4.

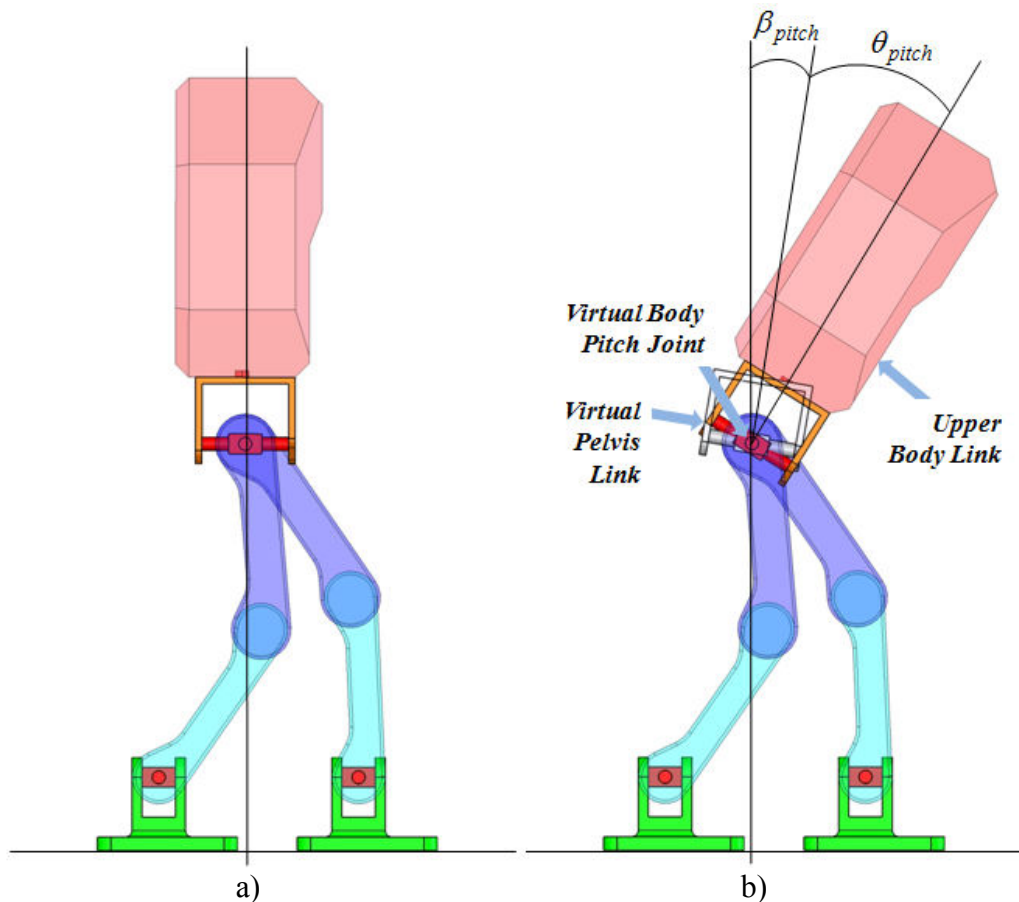


Figure. 5.4: a) Walk with upright upper body posture. b) Upper body leaned forward. Body and virtual pelvis angles are shown.

Consider the robot walk without the pitch motion between the pelvis and upper body. Assume that the position and orientation references of the feet are defined in an upper body-fixed coordinate frame. (If they are defined in another frame, for example in

a world fixed frame then usually it is possible to apply a coordinate transformation and express the foot position references with respect to the body fixed frame.) The position and orientation references can be expressed in the form of a reference homogenous transformation matrix H_r as

$$H_r = \begin{bmatrix} \begin{bmatrix} R_r \\ 0 \ 0 \ 0 \end{bmatrix} & \begin{bmatrix} d_r \\ 1 \end{bmatrix} \end{bmatrix} \quad (5.9)$$

where R_r is the reference orientation matrix and d_r is the reference position of a foot. Suppose that the foot orientation reference matrix R_r is such that the feet are parallel to the upper body. Figure 5.4(a) shows such a walking posture. The body fixed coordinate frame is shown in this figure too. By applying a pure pitch rotation operator on the reference homogenous transformation matrix H_r , new, rotated foot references can be obtained:

$$H_{r_{new}} = \begin{bmatrix} \begin{bmatrix} R_{y,-\theta} \\ 0 \ 0 \ 0 \end{bmatrix} & \begin{bmatrix} 0 \\ 0 \\ 0 \\ 1 \end{bmatrix} \end{bmatrix} H_r \quad (5.10)$$

Here, $R_{y,-\theta}$ is the basic rotation matrix about the y -axis by the angle $-\theta$. The y -axis of the body-fixed coordinated frame in Figure 5.4 points into the page. The reference posture resulting from the rotation of the foot references in Figure 5.4(a) about this axis by the angle $-\theta$ is shown in Figure 5.4(b). Assuming that the feet will keep their contact with the ground, the effect of rotating the feet with respect to the body fixed coordinate frame is to rotate the body by the angle θ . Hence, upper body pitch motion can be generated by planning a rotated version of the upright body references, even for robots without a pitch joint at the waist.

Note that the angle θ in equation 5.10 can be used as the adapted pitch angle θ_{pitch} in equation 5.8. However, the adaptation mechanism, requires the pelvis pitch angle β_{pitch} as its input and this angle, different from the upper body pitch angle, is yet to be defined for robots without a waist pitch joint. Actually for such robots the pelvis and the upper body links can be considered to be the same. However, if we measure the pitch orientation angle of the robot by an inertial measurement system mounted at the upper

body of the robot and subtract from it the rotation angle θ explained above, we can find an offset angle which can be considered as the pitch orientation angle of a virtual pelvis link:

$$\beta_{pitch} = \beta_{body} - \theta \quad (5.11)$$

Here β_{body} is the pitch angle measured by the inertial measurement system at the upper body. The virtual pelvis link is shown in Figure 5.4(b). The experimental results achieved by the employment of this fuzzy adaptive pitch tilt controller are given in Chapter 6.

5.2.3. Fuzzy Adaptive Roll Tilt Control

The same approach, introduced in the previous subsection, is used for the realization of fuzzy adaptive roll tilt control.

Similarly defined, the pelvis roll angle is the angle the z-axis of the pelvis frame makes with a vertical line. This angle can also be utilized to detect if there is any falling left or right situation. However, a single measurement of the angle is again misleading as in the case of pelvis pitch angle since there are also oscillations in roll direction during the walk. The average value $\bar{\beta}_{roll}$ of the pelvis roll angle β_{roll} in Figure 5.5 is computed as;

$$\bar{\beta}_{roll}(kT_p) = \frac{1}{N} \sum_{l=0}^{N-1} \beta_{roll}((k-l)T_p) \quad (5.12)$$

where k is the sampling index, N is the number of samples used in the average computation and T_p is the sampling period.

The frequency and size of the oscillations, denoted by Γ_{roll} is computed as;

$$\Gamma_{roll}(kT_p) = \sum_{l=0}^{N-1} \left| \beta_{roll}((k-l)T_p) - \beta_{roll}((k-l-1)T_p) \right| \quad (5.13)$$

In (5.13), $|\cdot|$ signifies the absolute value function.

Online adjustment of the body roll angle (the angle θ_{roll} shown in Figure 5.5) parameter is done by a fuzzy logic system by evaluating the average $\bar{\beta}_{roll}$ of the pelvis roll angle and the activity Γ_{roll} of this angle as its inputs.

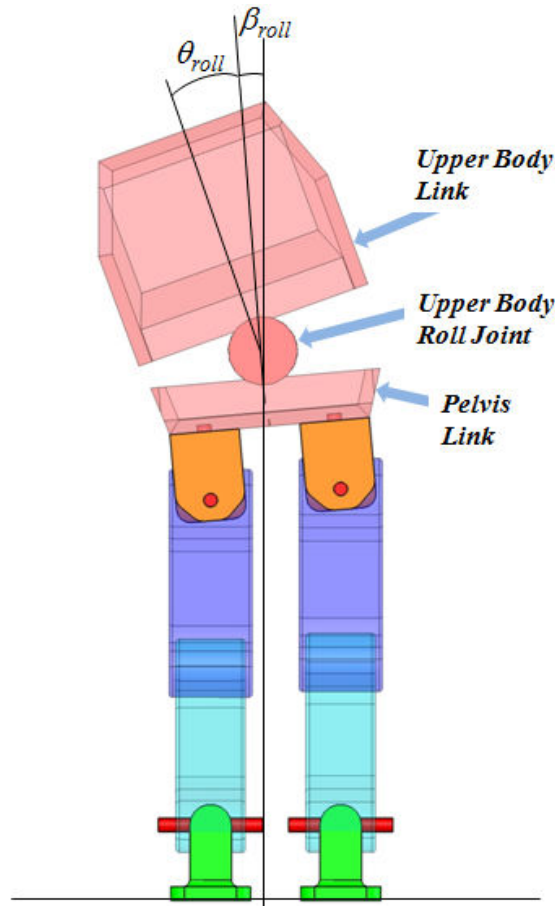


Figure 5.5: Legs, pelvis and the upper body in roll axis

The main idea of the parameter adaptation system can be summarized as below.

(i) When the average value of pelvis roll angle is positive, we can infer that the robot is in a posture inclined to fall to its right side. In this case the body should be rotated to the left by decreasing the body roll angle.

(ii) In a similar way, if the average value of the body roll angle is negative the trunk should be rotated to the right to compensate for the left leaning upper body.

(iii) When high levels of pelvis roll activity is observed, the body should be rotated more in accordance with (i) and (ii)

(iv) In a similar way to the guideline 3 above, when the pelvis roll activity is low the body roll angle should be taken to zero for the compensation of gravity effect of the left or right leaned pelvis link.

Table 5.2 and Figure 5.3 describe the nine fuzzy rules used in the tuning. The same symbolization used for constructing Table 5.1 is considered here too. The numerical values of the rules are given in the experimental results chapter.

An example of the rules summarized in Table 5.2 is given below as:

Rule 11: If Γ_{roll} is big and $\bar{\beta}_{roll}$ is negative, then θ_{roll} is positive of grade 3 (θ_{N3}).

Table 5.2: The Fuzzy Rule Base Roll

		Γ_{roll}		
		Small Γ_{roll}	Medium Γ_{roll}	Big Γ_{roll}
$\bar{\beta}_{roll}$	Negative $\bar{\beta}_{roll}$	θ_{P1} <i>Rule 11</i>	θ_{P2} <i>Rule 12</i>	θ_{P3} <i>Rule 13</i>
	Zero $\bar{\beta}_{roll}$	θ_{ZZ} <i>Rule 21</i>	θ_{ZZ} <i>Rule 22</i>	θ_{ZZ} <i>Rule 23</i>
	Positive $\bar{\beta}_{roll}$	θ_{N1} <i>Rule 31</i>	θ_{N2} <i>Rule 32</i>	θ_{N3} <i>Rule 33</i>

The truth value of a rule is obtained using the same calculations for fuzzy pitch tilt controller. These calculations are summarized below for the sake of completeness.

The truth value of Rule 11, denoted by w_{11} , is computed as

$$w_{11} = \mu_{Small \Gamma}(\Gamma_{roll}) \mu_{Negative \bar{\beta}}(\bar{\beta}_{roll}) \quad (5.14)$$

The rule strength matrix Θ be defined from Table 5.2 as;

$$\Theta = \begin{bmatrix} \theta_{P1} & \theta_{P2} & \theta_{P3} \\ \theta_{ZZ} & \theta_{ZZ} & \theta_{ZZ} \\ \theta_{N1} & \theta_{N2} & \theta_{N3} \end{bmatrix} \quad (5.15)$$

Using this matrix, the defuzzification is carried out by the expression

$$\theta_{roll} = \frac{\sum_{i=1}^3 \sum_{j=1}^3 w_{ij} \Theta_{ij}}{\sum_{i=1}^3 \sum_{j=1}^3 w_{ij}} \quad (5.16)$$

The computed θ_{roll} value is applied as the reference angular position of the joint between the pelvis and upper body links. However, since SURALP only possesses a waist yaw axis, the same method explained in the previous section is used to make use of a virtual pelvis link in roll axis as shown in Figure 5.6.

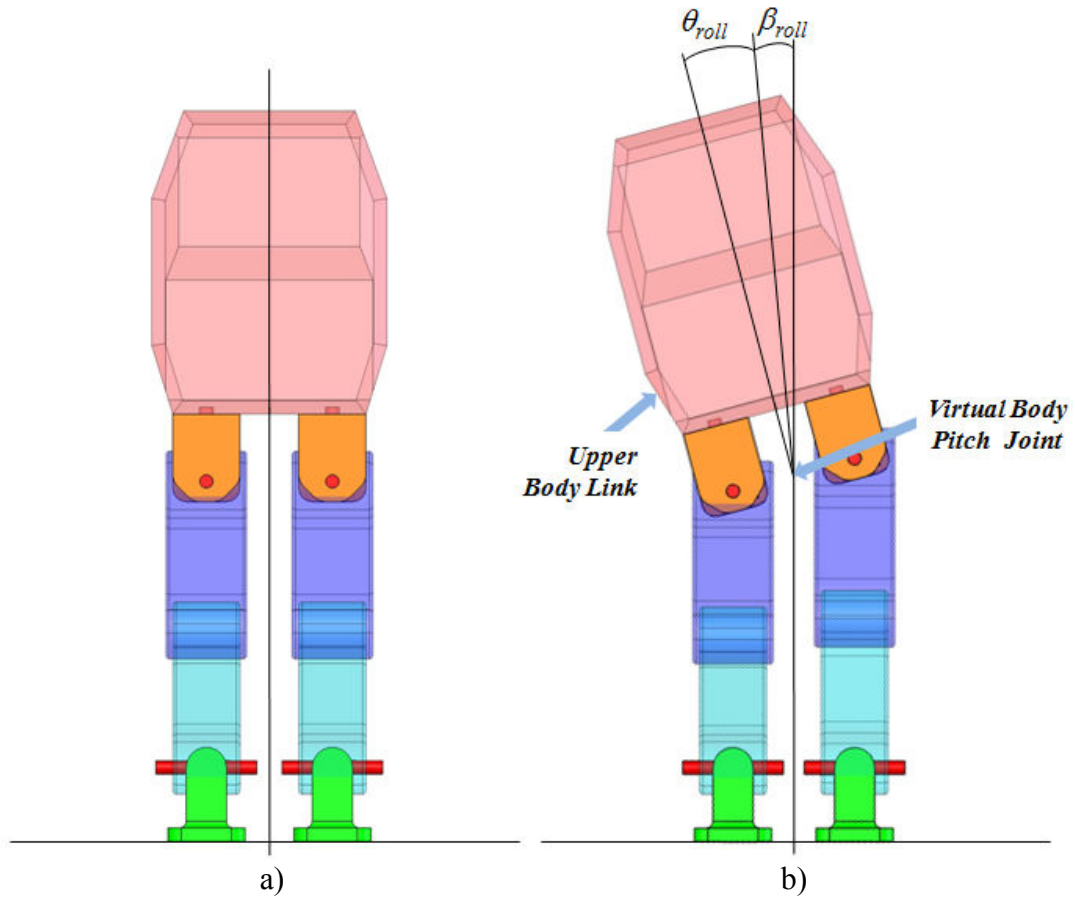


Figure 5.6: a) Walk with upright upper body posture. b) Upper body leaned right. Body and virtual pelvis angles are shown.

The same procedure introduced in the previous subsection is used to rotate the trunk of the robot to utilize a virtual pelvis link in the roll axis. The experimental results achieved by the employment of this fuzzy adaptive roll tilt controller are given in Chapter 6.

Chapter 6

6. EXPERIMENTAL RESULTS

In this chapter, experimental results obtained with the proposed omnidirectional walking reference trajectory generation method and the fuzzy logic parameter adaptation system, are presented. Omnidirectional walking experiments and proposed control techniques are implemented on the humanoid robot SURALP.

Figure 6.1 shows the roll and pitch angles of the upper body of SURALP during an omnidirectional walking. The walking parameters are given in Table 6.1. The maximum and minimum values of the oscillations are +1.9 and -1.9 degrees in the roll direction, respectively. The oscillations of the trunk are quite low in the pitch direction with maximum and minimum values of +0.9 and -1.4 degrees, respectively. The resulting roll and pitch angles show that a stable omnidirectional walk is achieved.

Table 6.1: Reference Generation Parameters 1

Single Support Time	1 s
Double Support Time	0.9 s
Arc Radius	50 cm
Step size	10 cm

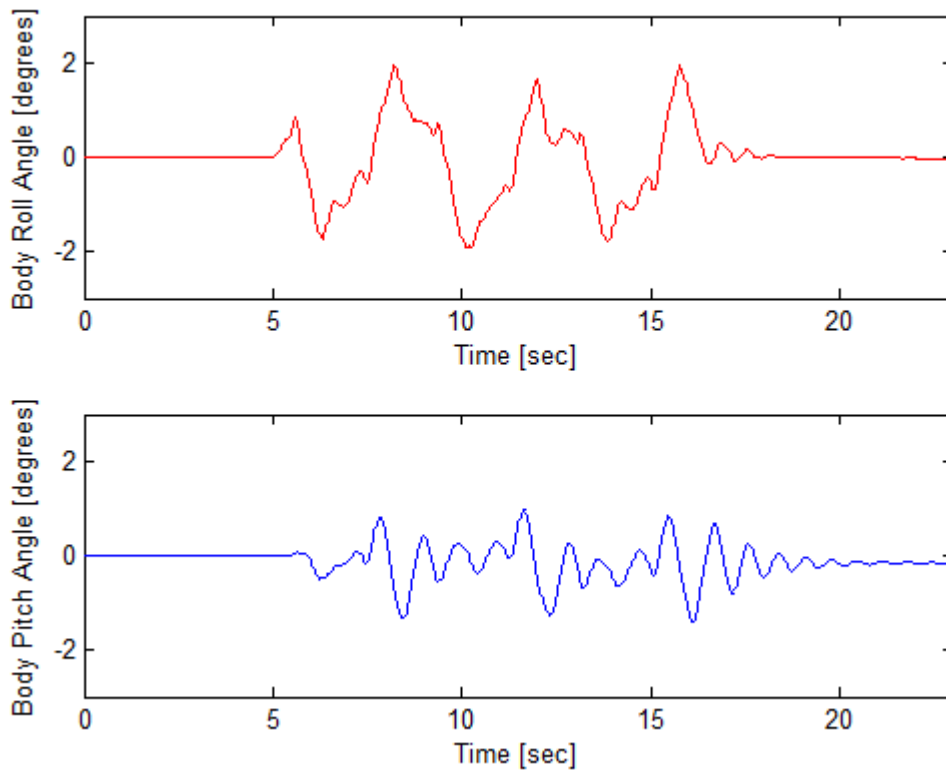


Figure 6.1: Body Roll and Body Pitch Angles

Another omnidirectional walking experiment result is presented in Figure 6.2. In this experiment, the walk on the arc is employed with a larger radius. The values of the parameters of the walk are given in Table 6.2. These results also indicate that the omnidirectional walking reference trajectory is successfully applied, with peak values +1.8 and -1.9 degrees for the roll and also +1 and -1.2 degrees for the pitch angles.

Table 6.2: Reference Generation Parameters 2

Single Support Time	1 s
Double Support Time	0.9 s
Arc Radius	75 cm
Step size	10 cm

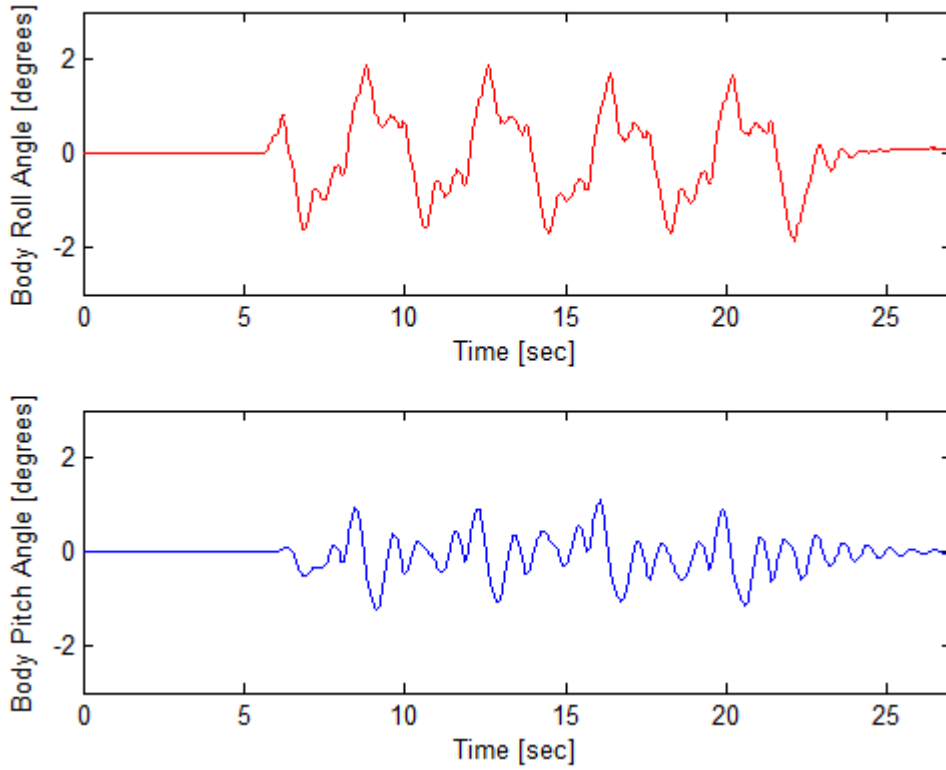


Figure 6.2: Body Roll and Body Pitch Angles for another experiment

As a second contribution after omnidirectional walking reference generation, the proposed fuzzy adaptive controllers are also tested with biped robot SURALP. Experimental results indicate that the fuzzy logic system is successful in obtaining a stable walk in the transition from a horizontal plane onto an inclined one with a slope of 5.6 degrees.

The experimental results obtained with the fuzzy parameter adaptation systems are shown in Figures 6.3 and 6.4. In Figure 6.3 fuzzy pitch tilt input parameters $\bar{\beta}_{pitch}$, Γ_{pitch} , calculated control input θ_{pitch} and virtual pelvis pitch angle are shown in order. In Figure 6.4 the same order is given for $\bar{\beta}_{roll}$, Γ_{roll} , θ_{roll} and virtual pelvis roll angle during the inclined climb are shown. The walking surface of the experiment environment contains two parts: An even surface and a plane inclined with 5.6 degrees (10% grade). Initially, the experiment starts with the robot in upright posture at a distance to the inclined plane. The robot starts walking on the even surface, reaches and steps on to the inclined plane and continues walking on the inclined plane until the walking ends.

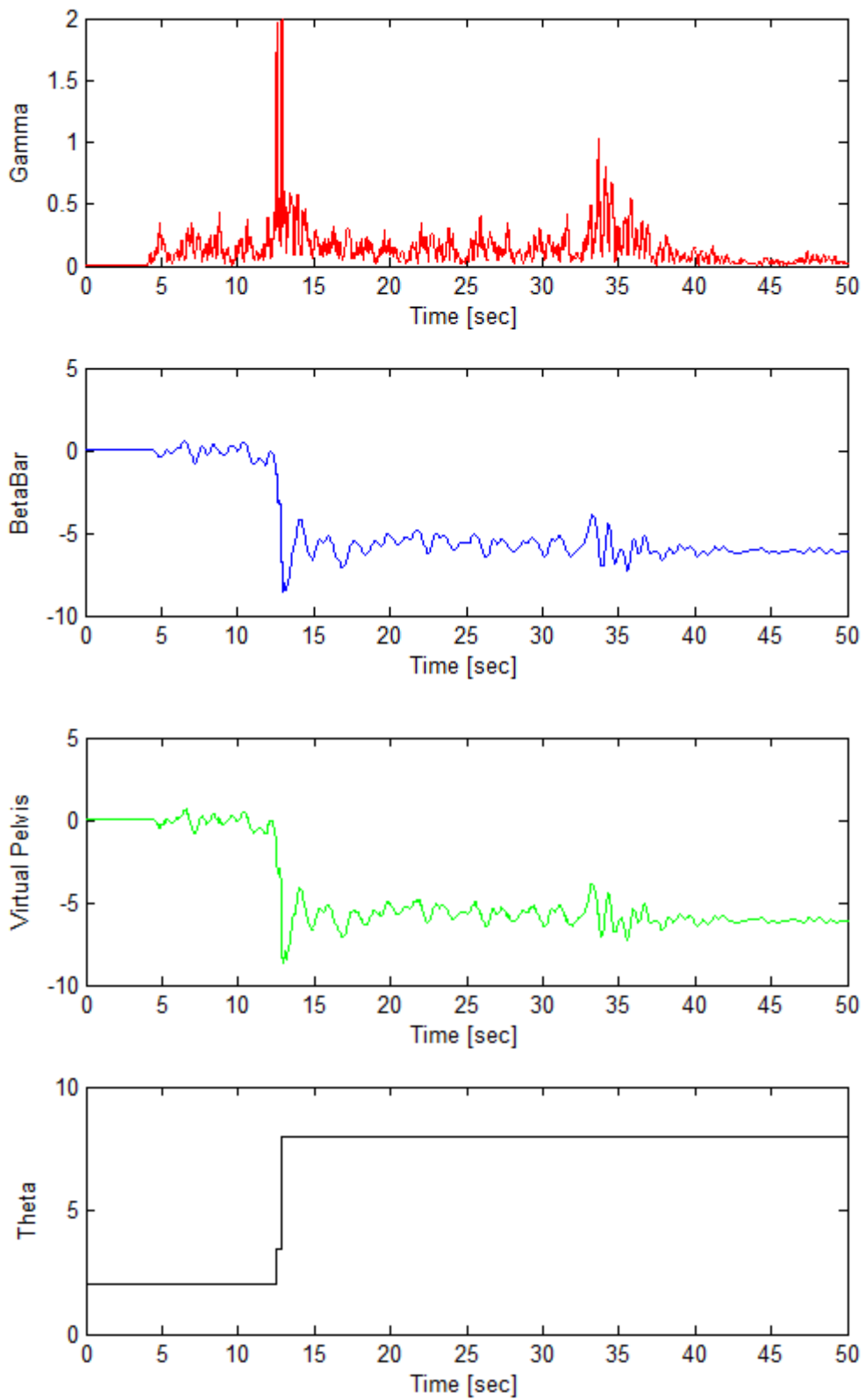


Figure 6.3: $\bar{\beta}_{pitch}$, Γ_{pitch} , θ_{pitch} and virtual pelvis pitch angle (from top to bottom)

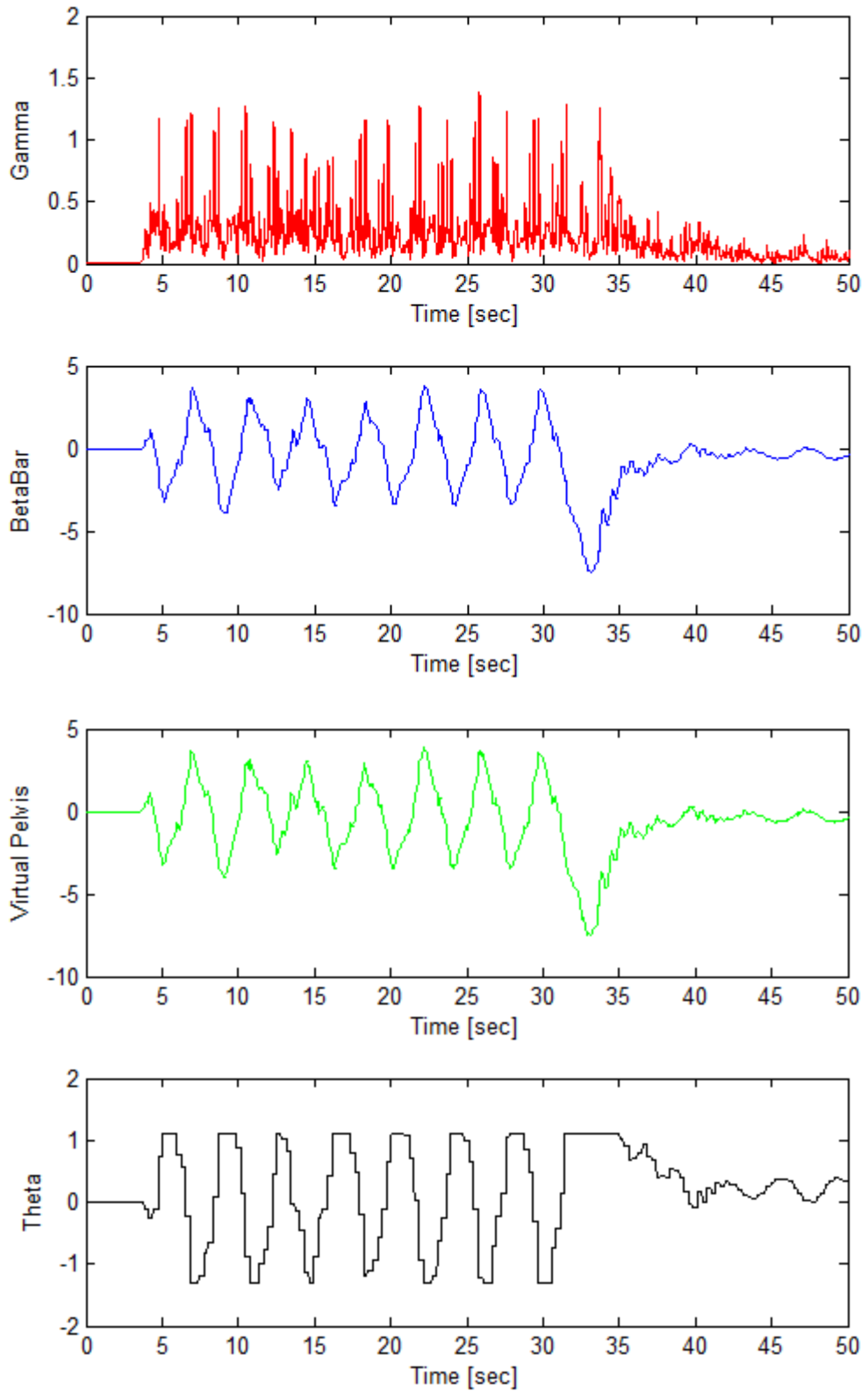


Figure 6.4: $\bar{\beta}_{roll}$, Γ_{roll} , θ_{roll} and virtual pelvis roll angle (from top to bottom)

It can be observed from Figure 6.3 that the robot reaches the inclined plane after approximately 10 seconds is elapsed from the start of the walk. The $\bar{\beta}_{pitch}$ graph shows

that the average oscillation of the upper body of the robot is small during this period. After the feet establish contact with the inclined plane $\bar{\beta}_{pitch}$ and Γ_{pitch} parameters start indicating an increasing activity of the pelvis pitch angle. The fuzzy parameter adaptation system acts according to the fuzzy rule base and finds the appropriate θ_{pitch} angle. This angle is first increased as a response to the activity Γ_{pitch} and kept high due to the increasing magnitude of the average pelvis pitch angle $\bar{\beta}_{pitch}$. It can be noted from Figure 6.3 that the generated curve for θ_{pitch} is in the form of a staircase. This is because of the slower update rate of the fuzzy system when compared with the implementation cycle time. The staircase-like change in this parameter, although beneficial for an efficient usage of computational resources, is not very suitable for reference generation purposes. In order to avoid step changes in the joint position references (obtained via the inverse kinematics relations which use the angle θ as one of its inputs) the obtained values for θ_{pitch} and θ_{roll} are then low pass filtered. This avoids abrupt changes in the pelvis pitch angle which would cause balance problems. Experimental studies are carried out with the same control method by deactivating the fuzzy adaptation too. It is observed that the robot fails to climb onto the inclined plane and falls without the fuzzy adaptation algorithms. Table 6.3 and Table 6.4 shows the parameters used for fuzzy pitch tilt and fuzzy roll tilt calculations respectively.

Table 6.3. Rule Strengths and Membership Function Corner Locations Fuzzy Pitch Tilt

Rule Strength	Numeric Value	Corner	Numeric Value
$\theta_{pitch_b_{N1}}$	-1	$\bar{\beta}_{NegativeBig}$	-5
$\theta_{pitch_b_{ZZ}}$	0	$\bar{\beta}_{NegativeSmall}$	-0.25
$\theta_{pitch_b_{P1}}$	1	$\bar{\beta}_{PositiveSmall}$	0.25
$\theta_{pitch_b_{P2}}$	4	$\bar{\beta}_{PositiveBig}$	5
$\theta_{pitch_b_{P3}}$	5	Γ_{Small}	1
$\theta_{pitch_b_{P4}}$	6	Γ_{Medium}	5
$\theta_{pitch_b_{P5}}$	8	Γ_{Big}	10

Table 6.4. Rule Strengths and Membership Function Corner Locations Fuzzy Roll Tilt

Rule Strength	Numeric Value	Corner	Numeric Value
$\theta_{roll_b\ N1}$	-1	$\bar{\beta}_{NegativeBig}$	-2
$\theta_{roll_b\ N2}$	-2	$\bar{\beta}_{NegativeSmall}$	-0.1
$\theta_{roll_b\ N3}$	-3	$\bar{\beta}_{PositiveSmall}$	0.1
$\theta_{roll_b\ ZZ}$	0	$\bar{\beta}_{PositiveBig}$	2
$\theta_{roll_b\ P1}$	1	Γ_{Small}	1
$\theta_{roll_b\ P2}$	2	Γ_{Medium}	2
$\theta_{roll_b\ P3}$	3	Γ_{Big}	5

The controller cycle time employed is 1 milliseconds. The cycle time of the fuzzy adaptation routine is, however, set to 200 milliseconds. The sampling of β and the computation of $\bar{\beta}$ and Γ , are also carried out with this cycle time. The value of the number of samples, N , in these equations equals to 10. The sampling time and the number of samples for the computations are chosen to cover a history corresponding to two past walking steps without causing significant computational burden.

Also the snapshots taken from an omnidirectional walking pattern are given in Figure 6.5. in the following page.

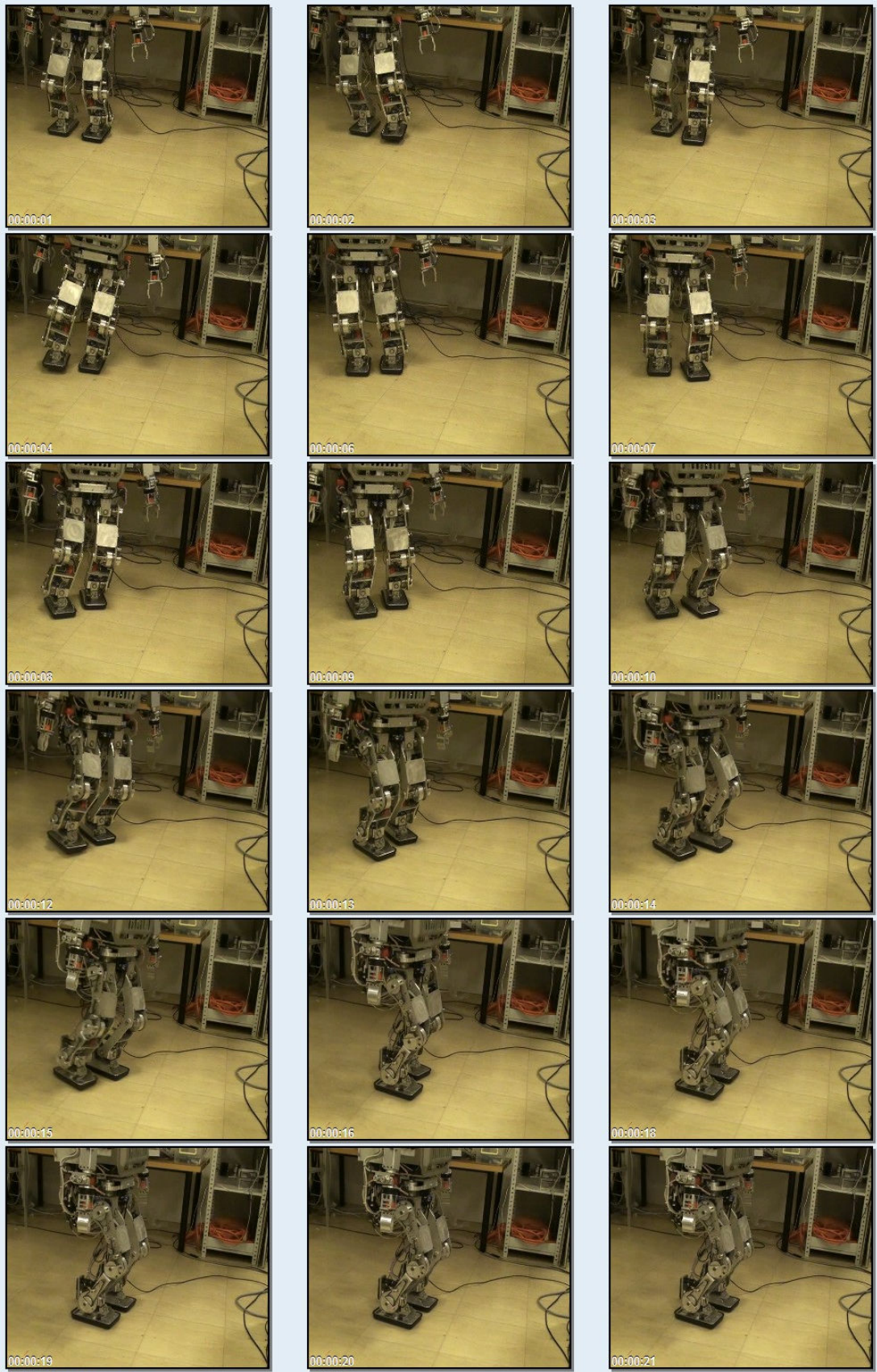


Figure 6.5: Snapshot taken during an omnidirectional walk

Chapter 7

7. CONCLUSION

Stable reference generation is a vital part in humanoid robot locomotion. In many studies various straight walk trajectories are generated. Being able to change the direction of the walk, however, increases the capacity of the robot dramatically. In this thesis, a Zero Moment Point based omnidirectional bipedal robot walking reference is proposed.

The design begins with a Zero Moment Point based straight walking trajectory generation. As a novelty, the central reference path is defined and mapping of the straight walk reference onto a reference about a central reference path is considered. The specific case where the central reference path is a circular arc is studied in more detail. The motion about the arc shaped central reference path is employed to change the direction of the robot.

A significant problem faced in legged robotics research is the walking surface irregularities. Inclined planes are among the most common surface irregularities encountered. With the omnidirectional walk the slope changes of the walking surfaces are even more pronounced because of the changing walk direction after the first robot homing process which tunes the robot initial posture for the initial surface slope. As another contribution of the thesis, two fuzzy logic based controllers, which enhance the balance of the walk by the use of orientation data obtained from inertial measurement units, are designed. These two controllers are for the body pitch and roll angle corrections, respectively. The controllers use the average of the respective body inclination angle and a rotation activity indicator which is newly introduced in this thesis as the input variables for the fuzzy systems.

The performances of the omnidirectional walking reference generation and fuzzy control methods are tested via experimental studies on the humanoid robot SURALP.

Experimental results indicate that the omnidirectional walking reference is followed stably to change the walking direction of the robot. Also a transition from flat floor to slopes with 10 percent grade is achieved by the use of fuzzy pitch and roll angle correction controllers. As future research efforts, increasing the slope to which the robot can climb, may be considered. The omnidirectional walk capabilities are planned to be extended on central reference paths other than the linear and circular arc shaped ones are also among future research plans.

REFERENCES

- [1] Kajita, S., Kanehiro, F., Kaneko, K., Fujiwara, K., Harada, K., Yokoi, K. and Hirukawa, H., "Biped Walking Pattern Generation by using Preview Control of Zero-Moment Point", *Proceedings of the 2003 IEEE International Conference on Robotics & Automation*, pp. 1620-1626, Taipei, Taiwan, September 2003.
- [2] Choi, Y., You, B. J. and Oh, S. R., "On the Stability of Indirect ZMP Controller for Biped Robot Systems", *Proceedings of the 2004 IEEE/RSJ International Conference on Intelligent Robots and Systems*, pp. 1966–1971, Sendai, Japan, October 2004
- [3] Erbatur, K. and Kurt, O., "Natural ZMP Trajectories for Biped Robot Reference Generation", *IEEE Transactions on Industrial Electronics*, vol. 56, no. 3, pp. 835-845, March 2009.
- [4] Erbatur, K., Koca O., Taşkıran E., Yılmaz M. and Seven, U. "ZMP Based Reference Generation for Biped Walking Robots", *ICICRA'09, Int. Conf. Intelligent Control, Rob. and Aut.*, Venice, Italy, Oct. 2009.
- [5] Taskiran, E., Yilmaz, M., Koca, O., Seven U. and Erbatur, K. (2010). "Trajectory Generation with Natural ZMP References for the Biped Walking Robot SURALP," In *Proc. 2010 IEEE International Conference on Robotics and Automation, ICRA, Alaska, USA*.
- [6] <http://www.anatomy.tv/StudyGuides/StudyGuide.aspx?guideid=9&NextID=0&customer=primal>
- [7] Wang, J. W., Xiong, W. L., Liu, H. and Ma, H., "Locomotion Planning Research for a Humanoid Robot Based on the ZMP", *Proceedings of the 2003 IEEE International Conference on Robotics, Intelligent Systems and Signal Processing*, pp. 942-947, Changsha, China, October 2003.
- [8] Feng, S. and Sun, Z., "A Simple Trajectory Generation Method for Biped Walking", *Proceedings of the 2008 10th International Conference on Control, Automation, Robotics and Vision*, pp. 2078-2082, Hanoi, Vietnam, December 2008.
- [9] Villeda, L. L., Frisoli, A. and Vega, V. P., "A Mechatronic Analysis and Synthesis of Human Walking Gait", *Proceedings of the 2009 IEEE International Conference on Mechatronics*, pp. 1-6, Malaga, Spain, April 2009.
- [10] Ha, S., Han, Y. and Hahn, H., "Natural Gait Generation of Biped Robot based on Captured Human Motion Image", *Proceedings of the 2008 IEEE International Conference on Multisensor Fusion and Integration for Intelligent Systems*, pp. 522-525, Seoul, Korea, August 2008.
- [11] http://www.laboratorium.dist.unige.it/~piero/Teaching/Gait/Malanga%20and%20DeLisa%20Clinical%20Observation_files/mala-f01.jpg

- [12] Seven, U., “Linear Inverted Pendulum Model and Swing Leg Dynamics in Biped Robot Walking Trajectory Generation”, Thesis (MS), Department of Mechatronics Engineering of the Graduate School of Engineering and Natural Sciences of Sabanci University, July 2007.
- [13] Vukobratovic, M., Borovac, B., Surla, D., Stokic, “Biped Locomotion: Dynamics, Stability, Control and Application”, Springer-Verlag, 1990.
- [14] Takanishi, A., Lim, H., “Biped walking robots created at Waseda University: WL and Wabian family”, *Philosophical Transactions of the Royal Society, Series A*, 365 (1850), pp. 49-64, 2007.
- [15] Takanishi, A., Ishida, M., Yamazaki, Y., Kato, I., “The realization of dynamic walking by the biped walking robot WL-10RD”, *Proceedings of International Conference on Advanced Robotics*, pp. 459-466, Tokyo, Japan, September 1985.
- [16] Raibert, M., “Legged Robots That Balance”, MIT Press, Cambridge, MA, 1986
- [17] Takanishi, A., Lim H., “Waseda Biped Humanoid Robots Realizing Human-like Motion”, *Proceedings of the International Workshop on Advanced Motion Control*, pp. 525-530, Nagoya, Japan, March 2000.
- [18] <http://world.honda.com/ASIMO/>
- [19] Hirose, M., Ogawa, K., “Honda humanoid robots development”, *Philosophical Transactions of the Royal Society, Series A*, 365 (1850), pp. 11-19, 2007.
- [20] Nishiwaki, V., Sugihara, T., Kagami, S., Kanehiro, F., Inaba, M., Inoue, H., “Design and Development of Research Platform for Perception-Action Integration in Humanoid Robot: H6”, *Proceedings of the 2000 IEEE/RSJ International Conference on Intelligent Robots and Systems*, vol.3, pp. 1559-1564, Takamatsu, Japan, October 2000.
- [21] Nishiwaki, V., Kuffner, J., Kagami, S., Kanehiro, F., Inaba, M., Inoue, H., “The experimental humanoid robot H7: a research platform for autonomous behavior”, *Philosophical Transactions of the Royal Society, Series A*, 365 (1850), pp. 79-107, 2007.
- [22] Oh, J.-Y., Kim, J.-H., “Realization of dynamic walking for the humanoid robot platform KHR-1” *Advanced Robotics*, vol. 18, no. 7, pp. 749-768, 2004.
- [23] Kim, J.-Y., Park, I.-W., Oh, J.-H., “Walking Control Algorithm of Biped Humanoid Robot on Uneven and Inclined Floor” *Journal of Intelligent and Robotic Systems*, vol. 48, no. 4, pp. 457-484, April 2007.
- [24] Park, I.-W., Kim, J.-Y., Lee, J., Oh, J.-H., “Online Free Walking Trajectory Generation for Biped Humanoid Robot KHR-3 (KAIST Humanoid Robot-3: HUBO)” *2006 6th IEEE-RAS International Conference on Humanoid Robots*, pp. 398-403, Genova, Italy, December 2006.

- [25] Hirose, M., Ogawa, K., "Walking biped humanoids that perform manual labour", *Philosophical Transactions of the Royal Society, Series A*, 365 (1850), pp. 65-77, 2007.
- [26] Kaneko, K., Harada, K., Kanehiro, F., Miyamori, G., Akachi, K., "Humanoid Robot HRP-3" *Proceedings of 2008 IEEE/RSJ International Conference on Intelligent Robots and Systems*, pp. 2471-2478, Nice, France, September 2008
- [27] Kaneko, K.; Kanehiro, F.; Morisawa, M.; Miura, K.; Nakaoka, S.; Kajita, "Cybernetic human HRP-4C," *Humanoid Robots, 2009. Humanoids 2009. 9th IEEE-RAS International Conference on* , vol., no., pp.7-14, 7-10 Dec. 2009
- [28] Gouaillier, D., Hugel, V., Blazevic, P., Kilner, C., Monceaux, J., Lafourcade, P., Marnier, B., Serre, J., and Maisonnier, B. 2009. *Mechatronic design of NAO humanoid*. In *Proceedings of the 2009 IEEE international Conference on Robotics and Automation (Kobe, Japan, May 12 - 17, 2009)*. IEEE Press, Piscataway, NJ, 2124-2129.
- [29] http://en.wikipedia.org/wiki/RoboCup_Standard_Platform_League
- [30] Lim, S. H. and Kim, J. G., "Adaptive Gait Algorithm for IWR Biped Robot", *Proceedings of the 1995 International Conference on Power Electronics and Drive Systems*, pp. 438-443, February 1995.
- [31] Zhang, Y., Wang, Q. and Fu, P., "A New Method of Desired Gait Synthesis in Biped robot", *Proceedings of the 3rd World Congress on Intelligent Control and Automation*, pp. 1300-1304, Hefei, China, June-July 2000.
- [32] Kajita, S., Kanehiro, F., Kaneko, K., Fujiwara, K., Yokoi, K. and Hirukawa, H., "A Realtime Pattern Generator for Biped Walking", *Proceedings of the 2002 IEEE International Conference on Robotics & Automation*, pp. 31-37, Washington, USA, May 2002.
- [33] Lim, H. O., Kaneshima, Y. and Takanishi, A., "Online Walking Pattern Generation for Biped Humanoid Robot with Trunk", *Proceedings of the 2002 IEEE International Conference on Robotics & Automation*, pp. 3111-3116, Washington, USA, May 2002.
- [34] Sugihara, T., Nakamura, Y. and Inoue, H., "Realtime Humanoid Motion Generation through ZMP Manipulation based on Inverted Pendulum Control", *Proceedings of the 2002 IEEE International Conference on Robotics & Automation*, pp. 1404-1409, Washington, USA, May 2002.
- [35] Harada, K., Kajita, S., Kaneko, K. and Hirukawa, H., "An Analytical Method on Real-time Gait Planning for a Humanoid Robot", *Proceedings of the 2004 IEEE/RAS International Conference on Humanoid Robots*, pp. 640-655, November 2004.
- [36] Nishiwaki, K., Kagami, S., Kuffner, J. J., Inaba, M. and Inoue, H., "Online Humanoid Walking Control System and a Moving Goal Tracking Experiment", *Proceedings of the 2003 IEEE International Conference on Robotics & Automation*, pp. 911-916, Taipei, Taiwan, September 2003.

- [37] Tanaka, T., Takubo, T., Inuoe, K. and Arai, T., “Emergent Stop for Humanoid Robots”, Proceedings of the 2006 IEEE/RSJ International Conference on Intelligent Robots and Systems, pp. 3970-3975, Beijing, China, October 2006.
- [38] Verrelst, B., Stasse, O., Yokoi, K. and Vanderborght, B., “Dynamically Stepping Over Obstacles by the Humanoid Robot HRP-2”, Proceedings of the 2006 IEEE/RAS International Conference on Humanoid Robots, pp. 117-123, December 2006.
- [39] Nishiwaki, K. and Kagami, S., “High Frequency Walking Pattern Generation based on Preview Control of ZMP”, Proceedings of the 2006 IEEE International Conference on Robotics & Automation, pp. 2667-2672, Florida, USA, May 2006.
- [40] Huang, W., Chew, C. M., Zheng, Y. and Hong, G. S., “Pattern Generation for Bipedal Walking Slopes and Stairs”, Proceedings of the 2008 IEEE/RAS International Conference on Humanoid Robots, pp. 205-210, Daejeon, Korea, December 2008.
- [41] Kim, J. Y., Park, I. W. and Oh, J. H., “Experimental Realization of Dynamic Walking of the Biped Humanoid Robot KHR-2 Using Zero Moment Point Feedback and Inertial Measurement”, Proceedings of the 2006 International Conference on Advanced Robotics, pp. 707-736, 2006.
- [42] Sven Behnke. Online trajectory generation for omnidirectional biped walking. In Proceedings of IEEE International Conference on Robotics and Automation, pages 1597–1603, Orlando, Florida, 2006.
- [43] Strom J., Slavov G., and Chown E., “Omnidirectional walking using ZMP and preview control for the nao humanoid robot,” in RoboCup 2009: Robot Soccer World Cup XIII
- [44] S. Hong, Y. Oh, Y. H. Chang, and B. J. You, “An Omni-directional Walking Pattern Generator Method for Humanoid Robots with Quartic Polynomials,” in Proc. of IEEE/RSJ Int. Conf. on Intelligent Robots and Systems, pp.4207-4213, 2007.
- [45] Y. Xu and Y. Tan, “Layered omnidirectional walking controller for the humanoid soccer robot,” in 2007 IEEE International Conference on Robotics and Biomimetics, Sanya, China.
- [46] Erbatur, K. and Seven, U., “An Inverted Pendulum based Approach to Biped Trajectory Generation with Swing Leg Dynamics”, Proceedings of the 2007 IEEE/RAS International Conference on Humanoid Robots, pp. 216-221, November 2007.
- [47] Dasgupta, A. and Nakamura, Y., “Making Feasible Walking Motion of Humanoid Robots from Human Motion Capture Data” *Proceedings of the 1999 IEEE International Conference on Robotics and Automation*, pp. 1044-1049, Detroit, Michigan, May 1999.
- [48] Erbatur, K., Okazaki, A., Obiwa, K., Takahashi, T. and Kawamura, A., “A Study on the Zero Moment Point Measurement for Biped Walking Robots,”

Proceedings of the AMC 2002, 7th International Workshop on Advanced Motion Control, pp. 431-436, Maribor, Slovenia, July 2002.

- [49] C. Zhu, Y. Tomizawa, X. Luo, and A. Kawamura “Biped walking with variable ZMP, frictional constraint, and inverted pendulum model”, IEEE Int. Conf. on Robotics and Biomimetics, pp: 425 – 430, Shenyang, China Aug 2004.
- [50] A. Takanishi, H. Lim, M. Tsuda and I. Kato. “Realization of dynamic biped walking stabilized by trunk motion on a sagittally uneven surface,” IEEE/RJS Int. Conf. on Intelligent Rob. and Syst., 1990.
- [51] Erbatur, K., Seven U., Taşkıran E., Koca Ö., Kızıldağ G., Ünel M., Sabanovic A. and Onat A., “SURALP-L, The Leg Module of a New Humanoid Platform,” Proceedings of the 2008 IEEE/RAS International Conference on Humanoid Robots, pp. 168-173, Daejeon, Korea, December 2008.
- [52] Erbatur, K., Seven, U., Taskiran, E., Koca, O., Unel, M., Kiziltas, G., Sabanovic, A., and Onat, A., “SURALP: A New Full-Body Humanoid Robot Platform”, *In the Proceedings of the 2009 IEEE/RSJ International Conference on Intelligent Robots and Systems*, Missouri, USA, October 2009.
- [53] Erbatur, K., Kaynak, O., Sabanovic, A., Rudas, I. (1996). Fuzzy Adaptive Sliding Mode Control of a Direct Drive Robot. *Robotics and Autonomous Systems*, Vol. 19, No, pp. 215-227:
- [54] Erbatur, K., Calli, B. (2009). “Adaptive Fuzzy Boundary Layer Tuning for Sliding Mode Controllers and Its Application on a Direct Drive Robot”, *Soft Computing - A Fusion of Foundations, Methodologies and Applications*, Volume 13, Number 11, pp. 1099-1111, September.
- [55] Erbatur, K., Kaynak, O. (2001). Adaptive Fuzzy Systems in Chattering Free Sliding Mode Control for Robotic Manipulators. *IEEE/ASME Transactions of Mechatronics*, Vol 6, No 4, pp 474-482
- [56] Park, J. H., (2003). "Fuzzy-Logic Zero-Moment-Point Trajectory Generation for Reduced Trunk Motions of Biped Robots," *Fuzzy Sets and Systems*, Vol. 134, No. 1, pp. 189-203.
- [57] Fujimoto, Y. and Kawamura, A. (1998). “Simulation of an autonomous biped walking robot including environmental force Interaction”, *IEEE Robotics and Automation Magazine*, pp. 33-42, June.
- [58] Taşkıran, E., “Walking Trajectory Generation and Control of a Humanoid Robot: SURALP”, Thesis (MS), Department of Mechatronics Engineering of the Graduate School of Engineering and Natural Sciences of Sabanci University, August 2009.
- [59] Bebek, O., and Erbatur, K., "A Fuzzy System for Gait Adaptation of Biped Walking Robots," *Proceedings of the 2003 IEEE Conference on Control Applications*, pp. 669-673, June 2003.